

Feshbach resonances in cold atomic gases

Citation for published version (APA):

Kempen, van, E. G. M. (2006). *Feshbach resonances in cold atomic gases*. [Phd Thesis 1 (Research TU/e / Graduation TU/e), Applied Physics and Science Education]. Technische Universiteit Eindhoven.
<https://doi.org/10.6100/IR609975>

DOI:

[10.6100/IR609975](https://doi.org/10.6100/IR609975)

Document status and date:

Published: 01/01/2006

Document Version:

Publisher's PDF, also known as Version of Record (includes final page, issue and volume numbers)

Please check the document version of this publication:

- A submitted manuscript is the version of the article upon submission and before peer-review. There can be important differences between the submitted version and the official published version of record. People interested in the research are advised to contact the author for the final version of the publication, or visit the DOI to the publisher's website.
- The final author version and the galley proof are versions of the publication after peer review.
- The final published version features the final layout of the paper including the volume, issue and page numbers.

[Link to publication](#)

General rights

Copyright and moral rights for the publications made accessible in the public portal are retained by the authors and/or other copyright owners and it is a condition of accessing publications that users recognise and abide by the legal requirements associated with these rights.

- Users may download and print one copy of any publication from the public portal for the purpose of private study or research.
- You may not further distribute the material or use it for any profit-making activity or commercial gain
- You may freely distribute the URL identifying the publication in the public portal.

If the publication is distributed under the terms of Article 25fa of the Dutch Copyright Act, indicated by the "Taverne" license above, please follow below link for the End User Agreement:

www.tue.nl/taverne

Take down policy

If you believe that this document breaches copyright please contact us at:

openaccess@tue.nl

providing details and we will investigate your claim.

Feshbach Resonances in Cold Atomic Gases

PROEFSCHRIFT

ter verkrijging van de graad van doctor aan de
Technische Universiteit Eindhoven, op gezag van de
Rector Magnificus, prof.dr.ir. C.J. van Duijn, voor een
commissie aangewezen door het College voor
Promoties in het openbaar te verdedigen
op woensdag 28 juni 2006 om 16.00 uur

door

Eric Gerard Marie van Kempen

geboren te Sittard

Dit proefschrift is goedgekeurd door de promotoren:

prof.dr. B.J. Verhaar

en

prof.dr. H.C.W. Beijerinck

Copromotor:

dr.ir. S.J.J.M.F. Kokkelmans

Druk: Universiteitsdrukkerij Technische Universiteit Eindhoven

CIP-DATA LIBRARY TECHNISCHE UNIVERSITEIT EINDHOVEN

Kempen, Eric Gerard Marie van

Feshbach resonances in cold atomic gases / by Eric Gerard Marie van
Kempen. - Eindhoven : Technische Universiteit Eindhoven, 2006. -
Proefschrift.

ISBN-10: 90-386-2541-3

ISBN-13: 978-90-386-2541-6

NUR 924

Trefwoorden: atoombotsingen / Bose-Einstein-condensatie / atomen;
wisselwerking / Feshbach resonanties / alkalimetalen

Subject headings: atom-atom collisions / interatomic potentials / Feshbach
resonances / alkali metals / rubidium / lithium / Bose-Einstein condensation

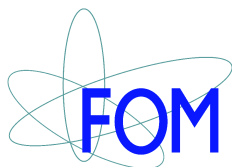
aan mijn ouders

Eric van Kempen
Group for Atomic Physics and Quantum Technology
Department of Physics
Eindhoven University of Technology
P.O. Box 513
5600 MB Eindhoven
The Netherlands

Cover: Rubidium molecules created from a Bose-Einstein condensate, using a Feshbach resonance, are placed in a magnetic-field gradient. Their magnetic moment depends on the magnetic-field strength, causing them to oscillate around the position in space where the magnetic moment changes sign.

Images: Images courtesy of MPQ research team, Garching, Germany. See also Stephan Dürr, Thomas Volz, Andreas Marte, and Gerhard Rempe, “*Observation of Molecules Produced from a Bose-Einstein Condensate*”, *Phys. Rev. Lett.* **92**, 20406 (2004).

Cover design: Jan-Willem Luiten.



The work described in this thesis has been carried out at the Physics Department of the Eindhoven University of Technology, and is part of the research program of the ‘Stichting voor Fundamenteel Onderzoek der Materie’ (FOM), which is financially supported by the ‘Nederlandse Organisatie voor Wetenschappelijk Onderzoek’ (NWO).

Contents

1	Introduction	3
1.1	General	3
1.2	The scattering length	4
1.3	Manipulating the scattering length	6
1.4	This thesis	8
2	Interaction and scattering of pairs of alkali atoms	13
2.1	One particle Hamiltonian	13
2.2	Two particle Hamiltonian	14
2.3	Accumulated phase method	17
2.4	Mass scaling	19
2.5	Adiabatic accumulated phase method	22
2.6	Resonances	25
3	Inter-isotope determination of ultracold rubidium interactions from three high-precision experiments	37
3.1	Introduction	37
3.2	Analysis of recent high-precision experiments	38
3.3	Predictions of Rb scattering properties	40
3.4	Extended analysis	42
3.5	Conclusions	43
4	Feshbach resonances in rubidium 87: Precision measurement and analysis	47
4.1	Introduction	47
4.2	Experimental method	48
4.3	Theoretical perspective on the 43 Feshbach resonances	49
4.4	Fine-tuning the interaction parameters	50
4.5	Discussing the experimental results	51
4.6	Conclusions	52
5	Radio-Frequency Spectroscopy of Ultracold Fermions	57
5.1	Introduction	57
5.2	Experimental techniques	58
5.3	Absence of clock shift	59

5.4	Measurement of $a_{12} - a_{13}$	60
5.5	Role of unitarity	65
5.6	Conclusions	66
6	P-wave Feshbach resonances of ultracold ${}^6\text{Li}$	69
6.1	Introduction	69
6.2	Identification of the resonance-inducing state	70
6.3	Experimental method	71
6.4	Trap losses	72
6.5	Formation of molecules using a Feshbach resonance	75
7	Formation of fermionic molecules via interisotope Feshbach resonances	79
7.1	Introduction	79
7.2	The interaction model	80
7.3	Application of the interaction model	81
7.4	Analytic resonance model	83
7.5	Creating fermionic molecules	85
	Summary	88
	Samenvatting	90
	Dankwoord	92
	Curriculum Vitae	93

1

Introduction

1.1 General

Bose-Einstein condensation is the macroscopic occupation of the lowest energy state in a system of bosons. The phenomenon, a form of quantum degeneracy, was predicted in the 1920's by Einstein to occur in a sample of bosonic atoms [1]. This type of condensation occurs when the thermal de Broglie wavelength, Λ_{dB} , becomes of the same order of magnitude as the mean interparticle separation, $\mathcal{O}(n^{-1/3})$, with n the particle density. Differently formulated, when the phase-space density \mathcal{D} is on the order of unity

$$\mathcal{D} = n\Lambda_{dB}^3 = n(2\pi\hbar^2/mk_B T)^{3/2} \geq 2.61, \quad (1.1)$$

with \hbar Planck's constant divided by 2π , m the mass of an atom, k_B Boltzmann's constant, and T the temperature.

Bose-Einstein condensates in a dilute gas of alkali atoms have been created at temperatures on the order of 1 nK to 1 μ K for densities between 10^{14} cm^{-3} and 10^{15} cm^{-3} . Systems at these low temperatures closely resemble the ideal situation for which this type of condensation was predicted to occur. BEC-like phenomena can also occur in systems resembling less an ideal gas, i.e. systems in the non-dilute regime or embedded in an external medium, at considerably higher temperatures. Indeed superfluidity of liquid helium is ascribed to Bose-Einstein condensation [2] and superconductivity is ascribed to BEC of Cooper pairs [3], which are effectively composite bosons constituted by electrons in a bulk conductor. These systems are far from being a noninteracting gas and the relatively strong interactions between the constituents greatly complicate the theoretical analysis.

In 1995 the first experimental realizations of BEC in the low density regime were demonstrated in dilute gases of the alkali atoms rubidium [4], sodium [5], and lithium [6]. Soon the condensation of other elements followed. Nowadays all alkali elements [7, 8], hydrogen [9], metastable helium [10, 11], ytterbium [12], and chromium [13] have been Bose-Einstein condensed. Since this phenomenon is a result of Bose statistics it is not limited to samples of (bosonic) atoms, also dilute gases of bosonic molecules are able to form a BEC. Condensation to a molecular BEC has been observed for the composite bosons $^6\text{Li}_2$ [14, 15] and $^{40}\text{K}_2$ [16, 17].

Almost all of the low density BEC's mentioned before are created by employing laser cooling [18] and evaporative cooling [19] to reach the low temperatures necessary [20]. The most common approach for making a BEC is to start by loading a magneto-optical trap (MOT) with atoms. Such a trap is a combination of an inhomogeneous magnetic field and a light field consisting of two counter-propagating near-resonant laser beams for each trapping dimension (normally six beams in total). The loading usually takes place via atom capture from a background vapor, or by atom capture from a beam of slow atoms. Typical temperatures for atoms in a MOT are $100 \mu\text{K}$ to 1 mK and densities between 10^{10} cm^{-3} to 10^{11} cm^{-3} . The temperature in the MOT is limited by the Doppler temperature, although sub-Doppler cooling (with the associated recoil temperature as temperature limit) might occur in the center of the MOT. The next step towards BEC is to transfer the atoms from the MOT into a magnetic trap (MT), or into an optical trap in which the atoms can be cooled down further by means of evaporative cooling, until the regime of quantum degeneracy is reached.

During evaporative cooling, the hottest atoms (tail of the Boltzmann distribution) of the sample are continuously being removed. In a MT this is achieved by means of an rf-field causing the hottest atoms to spin-flip, changing their state to untrapped ones causing them to leave the trap. In an optical trap, the hottest atoms are removed by lowering the intensity of the trapping laser and therefore changing the trap depth. Since the hottest atoms have an energy exceeding the average energy per atom, removing them will effectively reduce the average energy per atom of the atoms remaining in the trap.

Provided the energy is redistributed among the atoms, i.e. the tail of the Boltzmann distribution will continuously be replenished, the sample equilibrates to a new energy distribution with a lower temperature. The redistribution of the energy among the atoms is governed by elastic, *good*, collisions. Inelastic two- and three-body collisions, leading to atom loss, are called *bad* collisions. For efficient evaporative cooling, the number of *good* collisions has to considerably outweigh the number of *bad* collisions, which requires a large elastic cross section.

1.2 The scattering length

For the temperatures under consideration only a few partial waves contribute to collisions. The regime in which only the lowest partial wave ($l=0$ for bosons) is relevant is indicated as the ultracold regime. For these so-called ultracold collisions only *s*-wave scattering is important (for bosons), since higher partial waves cannot pass the centrifugal barrier $\hbar^2 l(l+1)/(mr^2)$, with r the interatomic separation and l the relative angular momentum quantum number.

At near zero energy the *s*-wave radial wavefunction at long range is proportional

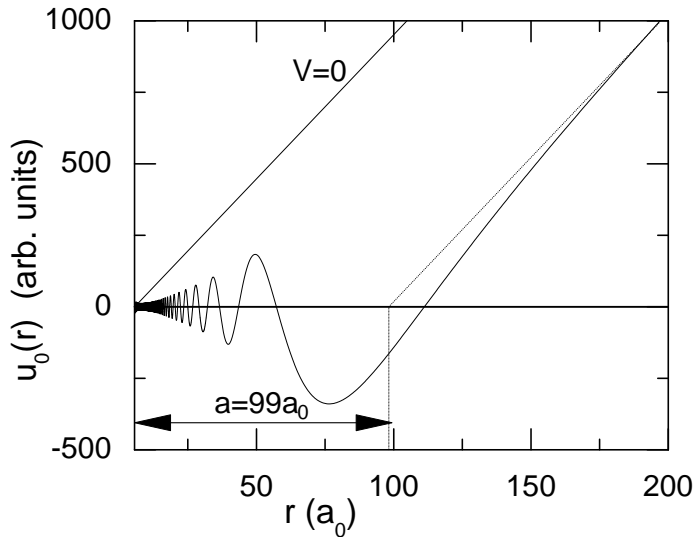


Figure 1.1 Scattering wavefunction times r in the zero temperature limit, for triplet ^{87}Rb and interactionless atoms ($V=0$). When extrapolating the wavefunction at long range to short distances, the r -axis is crossed at a distance equal to the scattering length.

to a sine

$$u_0 \sim \sin(kr + \delta_0) \approx \sin k(r - a), \quad (1.2)$$

with k the wavenumber, δ_0 the s -wave phaseshift, and

$$a = -\lim_{k \downarrow 0} \frac{1}{k} \tan(\delta_0) \quad (1.3)$$

the scattering length. Figure 1.1 illustrates the radial wavefunction for two different situations: for two interactionless atoms and for triplet scattering ($S=1$) of two ground state ^{87}Rb atoms, with valence electron spin $\frac{1}{2}$. At long range these wavefunctions are equal except for a displacement a , due to the interaction potential governing the collision at short range. The same shift would be obtained when the interatomic interaction potential would be replaced with one of a hard sphere of diameter a . The elastic scattering cross section for a pair of bosonic atoms in a spin-polarized gas in the zero temperature limit becomes

$$\sigma = 8\pi a^2, \quad (1.4)$$

which is larger by a factor of 2 as compared to the cross section for non-identical particles.

For temperatures below the critical temperature a Bose Einstein condensate will form. In the limit of weak interactions ($na^3 \ll 1$), one can use a mean field approximation in which the atomic interaction potentials are replaced by the zero-range

pseudopotential $\frac{4\pi\hbar^2 a}{m}\delta(\vec{r}_i - \vec{r}_j)$, yielding a condensate self-energy

$$U|\phi|^2 = \frac{4\pi\hbar^2 a}{m}|\phi|^2, \quad (1.5)$$

with ϕ the condensate wavefunction, normalized such that $|\phi|^2 = n$. The behavior of the condensate can then be described by the Gross-Pitaevskii equation

$$i\hbar\dot{\phi} = \left(-\frac{\hbar}{2m}\nabla^2 + V^{\text{trap}}(\vec{r}) + U|\phi|^2 \right) \phi, \quad (1.6)$$

with V^{trap} the (usually harmonic) trapping potential used for confining the atoms.

Large condensates require a positive scattering length, i.e. effectively repulsive interactions, for stability. The effectively attractive interactions that correspond to a negative scattering length lead to instability for large condensates, ending in a collapse. Although a negative a inhibits the creation of large condensates, it is possible to have stable condensates for a small number of atoms. ^7Li has such a negative scattering length [21, 22], but the creation of a Bose-Einstein condensate with this isotope of lithium is still possible [6].

Clearly, knowledge of the scattering length, is needed for understanding the behavior of samples of ultracold dilute gases. Via the elastic scattering cross section, a determines the time needed for evaporative cooling and an unfavorably sized scattering length can even render an attempt to create a BEC impossible [23]. Its value is sensitive to the specific interactions between the scattering atoms (see figure 1.1 and section 2.6) and it does not only vary between the kinds of atoms which scatter but also between different isotopic variants, or specific spin states of the same isotope. Therefore it is important to understand the relevant interactions if one wants to predict the magnitude or behavior of a .

1.3 Manipulating the scattering length

In the past several techniques for manipulating the scattering properties of atoms have been proposed. By far the most important one is the use of a magnetically tunable Feshbach resonance (see figure 1.2). The application of these resonances in cold-atom physics has been suggested in 1992 [24] and the existence of this type of resonance was first demonstrated experimentally in 1998 [25]. Since then many experiments have been performed making use of Feshbach resonances and in fact most contemporary (ultra)cold-atom experiments make use of them. A striking example is the realization of a Bose Einstein condensate in a sample of ^{85}Rb [26], which was possible despite the negative scattering length ($a=-443a_0$ for both atoms in the commonly used $|f = 2, m_f = -2\rangle$ state [27]) at magnetic fields far from a resonance preventing the creation of a large stable BEC. Feshbach resonances also allow to switch from a positive

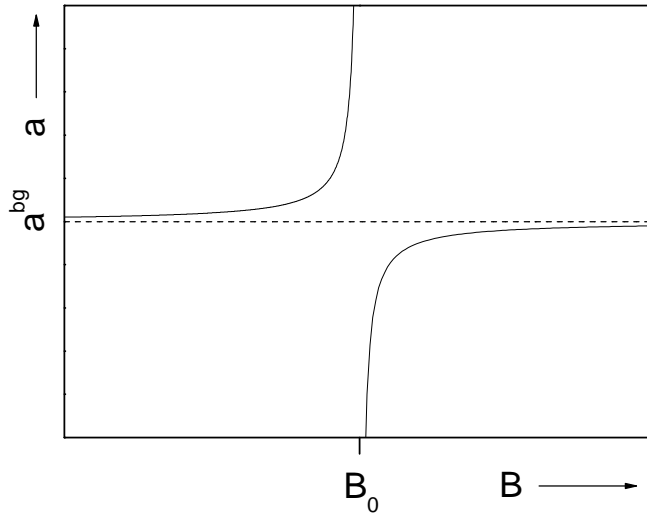


Figure 1.2 Typical behavior of the scattering length a versus magnetic field B in the vicinity of a magnetically tunable Feshbach resonance at B_0 . For a magnetic field far from B_0 the scattering length approaches a background value a^{bg} . The dashed line indicates the value of the scattering length without the presence of the Feshbach resonance. A more detailed description of Feshbach resonances can be found in section 2.6.

scattering length to a negative one. The group of Hulet demonstrated the formation and propagation of matter-wave solitons in a quasi-one-dimensional ${}^7\text{Li}$ BEC with a small negative a [28]. When the scattering length is switched from a positive value to a negative value one expects the ejection of a fraction of the atoms, a phenomenon first observed at JILA [29], where this spectacle was given the name “Bosenova”. In the 1970’s Efimov predicted a universal set of bound trimer states to appear for three identical bosons with resonant two-body interactions [30] (i.e., a very large scattering length). The experimental control over the scattering length also makes it possible to increase its magnitude into the regime for which Efimov states are predicted to exist. Only very recently, more than 30 years after the prediction, evidence for the existence of Efimov States was obtained in an experiment which could not have been performed without control over the scattering length [31]. By sweeping a magnetic field across a Feshbach resonances, it is possible to “trap” scattering atoms permanently in the (“Feshbach”) molecular state [32]. This method has become a standard technique for making ultracold molecules [33] and is at the basis of molecular BEC’s.

It was already mentioned before that magnetically tunable Feshbach resonances are not the only method to change the interaction properties of cold atoms. Other techniques have been proposed to alter a , but their use until now is limited to a

proof-of-principle experiment for one of them. This method uses laser light to drive a transition between two free atoms and an electronically excited molecular state. In this scenario the scattering length is a function of the laser light's detuning with respect to the aforementioned transition. Fedichev *et al.* proposed this method in 1996 [34] and the effect was experimentally demonstrated in 2005 [35]. Another technique is the application of a dc electric field across a sample of cold atoms [36]. Fields on the order of 10^5 V/cm could be needed before changes to the interaction properties become apparent.

The counterpart of BEC in a sample of fermionic atoms is the BCS transition in which two atoms couple together in momentum space. It is worth noting that a magnetic field sweep over a Feshbach resonance can convert a sample of fermionic atoms into a sample of bosonic molecules and reversal of the sweep will recover the fermionic atoms. In other words a simple sweep of a magnetic field can change completely the statistics obeyed by the constituents of a sample; be it Fermi statistics with a BCS transition on the “atomic” side of the resonance, or Bose statistics with the BEC transition on the “molecular” side of the resonance [37]. In the crossover regime, which is the part of the sweep close to resonance where the scattering length diverges, the sample is no longer a weakly interacting gas since na^3 becomes much larger than 1 and only a many-body theory can describe the properties of the sample correctly. Recently superfluidity in the crossover regime was unambiguously demonstrated experimentally [38]. This cross-over regime is not yet fully understood and research is ongoing.

1.4 This thesis

In this thesis a theoretical method is developed which enables one to describe the interaction and scattering of (ultra)cold atoms to unprecedented precision. It is also unparalleled in comprehensiveness: it allows the prediction of a large and varied set of experimental data for all isotopes of the same element. The method relies on the extraction of a few parameters which completely summarize the behavior of the atoms in the (ultra)cold regime. The method is presented in chapter 2 and in chapter 3 it is applied to the “workhorses” of cold-atom physics: the atomic species ^{85}Rb and ^{87}Rb . We extract these few parameters to a very high precision from several recent high-precision experiments, allowing us to predict e.g. the ^{87}Rb spinor condensate to be ferromagnetic: a prediction for which the scattering length has to be calculated with a precision better than 1%. We also predict Feshbach resonances at experimentally accessible magnetic field strengths; resonances searched for and found by the experimental group of Rempe. In close collaboration with his group we “fine-tune” the interaction parameters found previously, by making use of only one of the observed resonances. We then obtain agreement with 42 out of the observed 43 resonance field strengths and

are able to identify bound states inducing the Feshbach resonances at these locations. Chapter 4 describes the results of this collaboration.

With a thorough understanding of the rubidium interactions, we then switch to lithium which has a fermionic (${}^6\text{Li}$) and a bosonic (${}^7\text{Li}$) isotope. Both are being used in cold-atom experiments. In chapter 5 we evaluate the interaction parameters for lithium allowing us to predict magnetic field strengths for which a sample of fermionic ${}^6\text{Li}$ atoms can be regarded as strongly interacting. Furthermore, a three-level method for measuring mean-field shifts, based on radio-frequency techniques, is introduced. For weak interactions we find proportionality of resonance shifts to interaction strengths. In the strongly interacting regime, however, these shifts become very small reflecting the quantum unitarity limit and many-body effects. Most interesting is the fact that in this regime the shifts are small both for large positive a and for large negative a , likely reflecting the universality of the interaction energy.

In chapters 6 and 7 the interactions between lithium atoms are reinvestigated, making use of newly available experimental data and with the updated interaction parameters special attention is paid to locating field strengths at which magnetically tunable Feshbach resonances occur in the scattering of lithium atoms. In chapter 7, the isotopes under investigation are the fermionic ${}^6\text{Li}$ and the bosonic ${}^7\text{Li}$. Molecules created by magnetically sweeping over these resonances will have a fermionic character. One magnetic field strength is predicted at which two different fermionic molecules can be created simultaneously. Furthermore, parameters for an analytic model describing the scattering phase $\delta(B, E)$ (with B the magnetic field strength and E the collision energy) proximate to a Feshbach resonance are determined from coupled channels calculations. Chapter 6 results from a collaboration with the experimental group of Salomon: p -wave Feshbach resonances were searched for and found.

References

- [1] A. Einstein, “*Quantentheorie des einatomigen idealen Gases*”, Sitzungsber. Kgl. Preuss. Akad. Wiss. **1924**, 261 (1924); *ibid.* **1925**, 3 (1925).
- [2] *Bose-Einstein condensation*, Eds.: A. Griffin, D. W. Snoke, and S. Stringari, (Cambridge University Press, Cambridge, 1995).
- [3] Vitaly L. Ginzburg, *On Superconductivity and Superfluidity*, (Nobel lecture, 2003).
- [4] M.H. Anderson, J.R. Ensher, M.R. Matthews, C.E. Wieman, and E.A. Cornell, “*Observation of Bose-Einstein Condensation in a Dilute Atomic Vapor.*”, Science **269**,198 (1995).
- [5] K. B. Davis, M. -O. Mewes, M. R. Andrews, N. J. van Druten, D. S. Durfee, D. M. Kurn, and W. Ketterle., “*Bose-Einstein Condensation in a Gas of Sodium Atoms*”, Phys. Rev. Lett. **75**, 3969 (1995).

- [6] C.C. Bradley, C.A. Sackett, J.J. Tollet, and R.G. Hulet., “*Evidence of Bose-Einstein Condensation in an Atomic Gas with Attractive Interactions*”, Phys. Rev. Lett. **75**, 1687 (1995).
- [7] G. Modugno, G. Ferrari, G. Roati, R. J. Brecha, A. Simoni, and M. Inguscio, “*Bose-Einstein Condensation of Potassium Atoms by Sympathetic Cooling*”, Science **294**, 1320 (2001).
- [8] Tino Weber, Jens Herbig, Michael Mark, Hanns-Christoph Nägerl, and Rudolf Grimm, “*Bose-Einstein Condensation of Cesium*”, Science **299**, 232 (2003).
- [9] Thomas C. Killian, Dale G. Fried, Lorenz Willmann, David Landhuis, Stephen C. Moss, Thomas J. Greytak, and Daniel Kleppner, “*Cold Collision Frequency Shift of the 1S-2S Transition in Hydrogen*”, Phys. Rev. Lett. **81**, 3807 (1998); Dale G. Fried, Thomas C. Killian, Lorenz Willmann, David Landhuis, Stephen C. Moss, Daniel Kleppner, and Thomas J. Greytak, “*Bose-Einstein Condensation of Atomic Hydrogen*”, Phys. Rev. Lett. **81**, 3811 (1998).
- [10] A. Robert, O. Sirjean, A. Browaeys, J. Poupard, S. Nowak, D. Boiron, C. I. Westbrook, and A. Aspect, “*A Bose-Einstein Condensate of Metastable Atoms*”, Science **292**, 461 (2001).
- [11] F. Pereira Dos Santos, J. Lonard, Junmin Wang, C. J. Barrelet, F. Perales, E. Rasel, C. S. Unnikrishnan, M. Leduc, and C. Cohen-Tannoudji, “*Bose-Einstein Condensation of Metastable Helium*”, Phys. Rev. Lett. **86**, 3459 (2001).
- [12] Yosuke Takasu, Kenichi Maki, Kaduki Komori, Tetsushi Takano, Kazuhito Honda, Mitsu-taka Kumakura, Tsutomu Yabuzaki, and Yoshiro Takahashi, “*Spin-Singlet Bose-Einstein Condensation of Two-Electron Atoms*”, Phys. Rev. Lett. **91**, 040404 (2003).
- [13] Axel Griesmaier, Jörg Werner, Sven Hensler, Jürgen Stuhler, and Tilman Pfau, “*Bose-Einstein Condensation of Chromium*”, Phys. Rev. Lett. **94**, 160401 (2005).
- [14] S. Jochim, M. Bartenstein, A. Altmeyer, G. Hendl, S. Riedl, C. Chin, J. Hecker Denschlag, and R. Grimm, “*Bose-Einstein Condensation of Molecules*”, Science **302**, 2101 (2003).
- [15] M. W. Zwierlein, C. A. Stan, C. H. Schunck, S. M. F. Raupach, S. Gupta, Z. Hadzibabic, and W. Ketterle, “*Observation of Bose-Einstein Condensation of Molecules*”, Phys. Rev. Lett. **91**, 250401 (2003).
- [16] Cindy A. Regal, Christopher Ticknor, John L. Bohn, Deborah S. Jin, “*Creation of ultra-cold molecules from a Fermi gas of atoms*”, Nature **424** 47 (2003).
- [17] Markus Greiner, Cindy A. Regal, Deborah S. Jin, “*Emergence of a molecular BoseEinstein condensate from a Fermi gas*”, Nature **426**, 537 (2003).
- [18] T. W. Hänsch and A. L. Schawlow, “*Cooling of gases by laser radiation*”, Opt. Commun. **13**, 68 (1975); Nobel lectures Nobelprize for physics 1997, available at <http://nobelprize.org/physics/laureates/1997/index.html>.
- [19] Greytak, T.J. and Kleppner, D., in *New Trends in Atomic Physics*, edited by G. Grynberg and R. Stora, Les Houches Summer School 1982 (North-Holland, Amsterdam, 1984) p. 1125.
- [20] Harold J. Metcalf and Peter van der Straten, *Laser Cooling and Trapping*, (Springer-Verlag, New York, 1999).

- [21] A. J. Moerdijk, W. C. Stwalley, R. G. Hulet, and B. J. Verhaar, “*Negative scattering length of ultracold ${}^7\text{Li}$ gas*”, Phys. Rev. Lett. **72**, 40 (1994).
- [22] A. J. Moerdijk and B. J. Verhaar, “*Prospects for Bose-Einstein Condensation in Atomic ${}^7\text{Li}$ and ${}^{23}\text{Na}$* ”, Phys. Rev. Lett. **73**, 518 (1994).
- [23] V.P. Mogendorff, *Cold Ne^* collision dynamics*, Ph.D. thesis, (Eindhoven University of Technology, 2004).
- [24] E. Tiesinga, A. J. Moerdijk, B. J. Verhaar, and H. T. C. Stoof, “*Conditions for Bose-Einstein condensation in magnetically trapped atomic cesium*”, Phys. Rev. A **46**, R1167 (1992); E. Tiesinga, B. J. Verhaar, and H. T. C. Stoof, “*Threshold and resonance phenomena in ultracold ground-state collisions*”, Phys. Rev. A. **47**, 4114 (1993).
- [25] Ph. Courteille, R. S. Freeland, D. J. Heinzen, F. A. van Abeelen and B. J. Verhaar, “*Observation of a Feshbach Resonance in Cold Atom Scattering*”, Phys. Rev. Lett. **81**, 69 (1998).
- [26] S. L. Cornish, N. R. Claussen, J. L. Roberts, E. A. Cornell, and C. E. Wieman, “*Stable ${}^{85}\text{Rb}$ Bose-Einstein Condensates with Widely Tunable Interactions*”, Phys. Rev. Lett. **85**, 1795 (2000).
- [27] N. R. Claussen, S. J. J. M. F. Kokkelmans, S. T. Thompson, E. A. Donley, E. Hodby, and C. E. Wieman, “*Very-high-precision bound-state spectroscopy near a ${}^{85}\text{Rb}$ Feshbach resonance*”, Phys. Rev. A **67**, 060701 (2003).
- [28] Kevin E. Strecker, Guthrie B. Partridge, Andrew G. Truscott, Randall G. Hulet, “*Formation and propagation of matter-wave soliton trains*”, Nature **417**, 150 (2002).
- [29] J. L. Roberts, N. R. Claussen, S. L. Cornish, E. A. Donley, E. A. Cornell, and C. E. Wieman, “*Controlled Collapse of a Bose-Einstein Condensate*”, Phys. Rev. Lett. **86**, 4211 (2001).
- [30] Efimov, V., “*Energy levels arising from resonant two-body forces in a three-body system*”, Phys. Lett. **33B**, 563 (1970); Efimov V., “*Weakly-bound states of three resonantly-interacting particles*”, Sov. J. Nucl. Phys. **12**, 589 (1971).
- [31] T. Kraemer, M. Mark, P. Waldburger, J. G. Danzl, C. Chin, B. Engeser, A. D. Lange, K. Pilch, A. Jaakkola, H.-C. Naegerl, and R. Grimm, “*Evidence for Efimov quantum states in an ultracold gas of cesium atoms*”, arXiv:cond-mat/0512394 (2005), *to appear in Nature*.
- [32] F. A. van Abeelen and B. J. Verhaar, “*Time-Dependent Feshbach Resonance Scattering and Anomalous Decay of a Na Bose-Einstein Condensate*”, Phys. Rev. Lett. **83**, 1550 (1999).
- [33] Elizabeth A. Donley, Neil R. Claussen, Sarah T. Thompson, Carl E. Wieman, “*Atom molecule coherence in a Bose Einstein condensate*”, Nature **417**, 529 (2002); Cheng Chin, Andrew J. Kerman, Vladan Vuletić, and Steven Chu, “*Sensitive Detection of Cold Cesium Molecules Formed on Feshbach Resonances*”, Phys. Rev. Lett. **90**, 33201 (2003); Cindy A. Regal, Christopher Ticknor, John L. Bohn, Deborah S. Jin, “*Creation of ultracold molecules from a Fermi gas of atoms*”, Nature, **424**, 47 (2003); Stephan Dürr, Thomas Volz, Andreas Marte, and Gerhard Rempe, “*Observation of Molecules Produced from a Bose-Einstein Condensate*”, Phys. Rev. Lett. **92**, 20406 (2004).

-
- [34] P. O. Fedichev, Yu. Kagan, G. V. Shlyapnikov, and J. T. M. Walraven, “*Influence of Nearly Resonant Light on the Scattering Length in Low-Temperature Atomic Gases*”, Phys. Rev. Lett. **77**, 2913 (1996).
- [35] Gregor Thalhammer, Matthias Theis, Klaus Winkler, Rudolf Grimm, and Johannes Hecker Denschlag, “*Inducing an optical Feshbach resonance via stimulated Raman coupling*”, Phys. Rev. A **71**, 33403 (2005).
- [36] M. Marinescu and L. You, “*Controlling Atom-Atom Interaction at Ultralow Temperatures by dc Electric Fields*”, Phys. Rev. Lett. **81**, 4596 (1998).
- [37] M. Holland, S. J. J. M. F. Kokkelmans, M. L. Chiofalo, and R. Walser, “*Resonance Superfluidity in a Quantum Degenerate Fermi Gas*”, Phys. Rev. Lett. **87**, 120406 (2001).
- [38] M. W. Zwierlein, J. R. Abo-Shaeer, A. Schirotzek, C. H. Schunck, W. Ketterle, “*Vortices and superfluidity in a strongly interacting Fermi gas*”, Nature **435**, 1047 (2005).

2

Interaction and scattering of pairs of alkali atoms

2.1 One particle Hamiltonian

We consider the electronic ground state of the alkali atoms. The valence electron has spin $s=\frac{1}{2}$ while the nucleus has spin i which equals e.g. 1 for ${}^6\text{Li}$, $\frac{3}{2}$ for ${}^7\text{Li}$ and ${}^{87}\text{Rb}$ and $\frac{5}{2}$ for ${}^{85}\text{Rb}$. These spins combine to a total angular momentum $\vec{f} = \vec{s} + \vec{i}$ with each f -state $(2f + 1)$ -fold degenerate in the absence of an external field. In total there are $2(2i + 1)$ possible ‘ground states’ for an alkali atom, split over two different f -states. Note that lower case characters are used to indicate single atom properties while we reserve capitals for two-atom systems.

The above mentioned degeneracy for alkali atoms is lifted by interactions both within the atom and with external fields. The nuclear spin interacts with the valence electron spin, leading to the hyperfine splitting for an atom j ,

$$V_j^{\text{hf}} = \frac{a^{\text{hf}}}{\hbar^2} \vec{s}_j \cdot \vec{i}_j \quad (2.1)$$

with a^{hf} the hyperfine constant. Note that our spin vectors \vec{s} and \vec{i} have the dimension of an angular momentum (include a factor \hbar), so the a^{hf} has the dimension of energy.

Atom j placed in a magnetic field \vec{B} experiences a Zeeman energy

$$V_j^Z = \left(\gamma_{e,j} \vec{s}_j - \gamma_{n,j} \vec{i}_j \right) \cdot \vec{B}, \quad (2.2)$$

where $\gamma_{e,j}$ and $\gamma_{n,j}$ are the electronic and nuclear gyromagnetic ratios. The behavior of the valence electron in alkali atoms is influenced by the electrons filling the inner shells causing the gyromagnetic ratio $\gamma_{e,j}$ to be slightly different from that of a free electron. While s and i have the same order of magnitude, the ratio γ_e/γ_n is of order 10^3 .

Equations (2.1) and (2.2) lead to the familiar graphs for the energy of the hyperfine states as a function of the magnetic field $B\hat{z}$ (see figure 2.1). We will label these one atom hyperfine states by $|f, m_f\rangle$ even though f is only a good quantum number for $B = 0$.

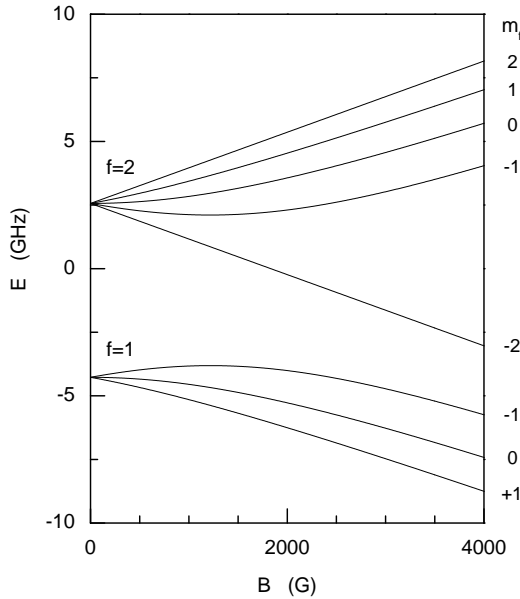


Figure 2.1 Hyperfine diagram of ground-state ^{87}Rb . The energy curves of the hyperfine states are labeled by their $B=0$ quantum numbers. Except for a scaling to the appropriate values of a^{hf} and $\gamma_{e,j}, \gamma_{n,j}$, ^7Li has the same diagram; as have all atoms with nuclear spin $i=3/2$.

2.2 Two particle Hamiltonian

Two alkali atoms experience in the first instance a mutual central interaction. This central interaction can be written as

$$V^{\text{cen}} = V_S(r)P_S + V_T(r)P_T, \quad (2.3)$$

with $P_{S,T}$ the projection operators on the singlet and triplet subspaces and r the interatomic separation. The singlet ($S=0$) and triplet ($S=1$) potentials differing by twice the exchange energy V^{exch} , are given by

$$V_{S,T} = V^{\text{disp}} - (-1)^S V^{\text{exch}}, \quad (2.4)$$

with the dispersion energy V^{disp} described by

$$V^{\text{disp}} = - \left(\frac{C_6}{r^6} + \frac{C_8}{r^8} + \frac{C_{10}}{r^{10}} + \frac{C_{11}}{r^{11}} + \frac{C_{12}}{r^{12}} + \dots \right), \quad (2.5)$$

at larger distances, in which C_n are dispersion coefficients determined by electric multipole-multipole interactions in second order, except for C_{11} , which arises in third order and is negative (*i.e.*, repulsive).

An analytic asymptotic expression for the exchange energy in Eq. (2.4) has been derived by Smirnov and Chibisov [1]:

$$V^{\text{exch}} = Jr^{\frac{7}{2\alpha}-1}e^{-2\alpha r}. \quad (2.6)$$

In Eq. (2.6), $-\alpha^2/2$ is the atomic ionization energy and J is a normalization constant; r and α in atomic units. It is difficult to calculate J from first principles. The most reliable values come from Hartree-Fock calculations for the diatom system which, however, lead to a somewhat different radial behavior.

Leaving out the center of mass kinetic energy and including the above interactions the total effective Hamiltonian for two colliding ground-state alkali atoms becomes

$$H = \frac{\vec{p}^2}{2\mu} + \sum_{j=1}^2 (V_j^{\text{hf}} + V_j^{\text{Z}}) + V^{\text{cen}}, \quad (2.7)$$

in which the first term represents the kinetic energy with μ the reduced mass of the atoms and \vec{p} the relative momentum operator.

For collisions of two identical atoms the hyperfine term can be written as the sum of two parts with different symmetry with respect to the exchange of the electron or nuclear spins,

$$V^{\text{hf}} = \frac{a^{\text{hf}}}{2\hbar^2}(\vec{s}_1 + \vec{s}_2) \cdot (\vec{i}_1 + \vec{i}_2) + \frac{a^{\text{hf}}}{2\hbar^2}(\vec{s}_1 - \vec{s}_2) \cdot (\vec{i}_1 - \vec{i}_2) \equiv V^{\text{hf}+} + V^{\text{hf}-}. \quad (2.8)$$

The convenience of this splitting arises from the fact that $V^{\text{hf}-}$, being antisymmetric in \vec{s}_1 and \vec{s}_2 , is the only term coupling singlet and triplet states.

For the interactions mentioned up to now the system of two colliding atoms is invariant under independent rotations of the spin system and of the orbital system around the axis through the overall center of mass parallel to the magnetic field. Therefore the projection of the total spin angular momentum $\vec{f}_1 + \vec{f}_2 \equiv \vec{F}$ and of the orbital angular momentum \vec{l} along this axis are separately conserved during the collision. Since V^{cen} only depends on r and not on $\hat{r} = \vec{r}/r$, \vec{l} is even conserved as a 3D vector. As a consequence, m_F and the rotational quantum numbers l and m_l are good quantum numbers.

Two other interactions are present which are much weaker than the above-mentioned effects, but nevertheless can play a significant role for interpreting cold atom experiments (see chapter 4). The first one is a direct interaction between the spins of the electrons via their magnetic moment. This very weak interaction is given by

$$V^\mu(\vec{r}) = \mu_0 \frac{\vec{\mu}_1 \cdot \vec{\mu}_2 - 3(\vec{\mu}_1 \cdot \hat{r})(\vec{\mu}_2 \cdot \hat{r})}{4\pi r^3}, \quad (2.9)$$

with $\mu_0 = 4\pi \cdot 10^{-7} \text{Hm}^{-1}$ and $\vec{\mu}_j$ the electron magnetic dipole moment of atom j . We leave out the much weaker magnetic dipole interactions in which the nuclear magnetic

moments are involved. Second, the spin-orbit interaction V^{so} of the spins of the valence electrons is given by a complicated expression [2] that contains contributions from the magnetic fields generated by the orbital currents of electrons and nuclei. For interatomic distances larger than 13 to 14 a_0 this complicated expression reduces for one valence electron outside closed shells in both alkali atoms to the well-known sum of two effective atomic spin-orbit couplings:

$$V^{\text{fs}} = \sum_{j=1}^2 \frac{2E^{\text{fs}}}{3\hbar^2} \vec{\ell}_j \cdot \vec{s}_j, \quad (2.10)$$

with $\vec{\ell}_j$ the valence electron orbital angular momentum of atom j , and E^{fs} the fine-structure splitting.

Separate ground state alkali atoms ($^2S_{1/2}$) have valence electron orbital angular momentum $\ell = 0$ and therefore contributions of (2.10) vanish in this case. However, for small interatomic separations the electron clouds overlap and an important additional contribution arises as a second order effect in V^{so} via an intermediate coupling to electronically excited molecular states [2, 3].

In total, we thus have a spin-spin interaction V^{ss} between the valence electrons, consisting of two parts:

$$V^{\text{ss}} = (V^{\text{ss}})^{\mu} + (V^{\text{ss}})^{\text{so}}, \quad (2.11)$$

a magnetic dipole part and a part arising from V^{so} in second order. The dipole part, when expressed in the spin vectors \vec{s}_i is given by

$$(V^{\text{ss}})^{\mu} = \frac{\mu_0 \gamma_e^2}{4\pi r^3} [\vec{s}_1 \cdot \vec{s}_2 - 3(\vec{s}_1 \cdot \hat{r})(\vec{s}_2 \cdot \hat{r})]. \quad (2.12)$$

The part $(V^{\text{ss}})^{\text{so}}$ has effectively the same spin-angle structure (the factor between square brackets), but is multiplied by a different radial factor. This factor has been calculated via an *ab initio* electronic structure calculation by Mies et al. [4] and can be approximated as an exponentially decaying form $f(r)$ for increasing r .

The total V^{ss} apparently has the structure of a scalar product of two irreducible spherical tensors of rank 2:

$$V^{\text{ss}} = f(r) [(\vec{s}_1, \vec{s}_2)_2 \cdot (\hat{r}, \hat{r})_2]. \quad (2.13)$$

As a consequence, it is invariant under the simultaneous 3D rotations of the internuclear vector \vec{r} and the spin degrees of freedom, thus conserving the total molecular angular momentum. On the other hand, it is not invariant under independent rotations of \vec{r} and the spin degrees of freedom. It therefore obeys triangle type S and l selection rules for a second rank tensor: it couples only spin triplet states and it couples for instance the $l = 0$ and 2 rotational states of the two atom system.

As mentioned before, the spin-spin interaction is rather weak and it does not conserve l, m_l, F, m_F and therefore couples many states. In most cases these interactions can safely be neglected. That these interactions cannot always be neglected is illustrated by the observation of Feshbach resonances in ^{133}Cs [5] and ^{87}Rb [6] in which colliding ultracold atoms, approaching each other in an s -wave, resonate with an $l=2$ or even $l=4$ (quasi-)bound state coupled via the spin-spin interaction to the entrance channel (in the $l=4$ case this interaction is needed twice: s -wave \leftrightarrow d -wave \leftrightarrow g -wave).

2.3 Accumulated phase method

Cold collision phenomena are extremely sensitive to very small changes of the short-range part of the central interatomic interaction. As a consequence, except for hydrogen and lithium atoms, *ab-initio* theoretical potentials are of little use for the description of cold collisions. The accumulated phase method [7, 8] is an approach that enables one to bypass the insufficiently known potential within an interatomic distance r_0 by means of a boundary condition on the relative wave function at a distance r_0 . The idea is that the boundary condition contains less parameters [actually three; a crucial advantage of the accumulated phase method compared to multichannel quantum defect (MQDT) methods is that it specifies the needed number of parameters uniquely] than the detailed potential within r_0 .

The only conditions that need to be fulfilled for the method to be applicable are:

1. r_0 should be so small that the energy difference of the lowest $S = 1$ and $S = 0$ two-atom electron states (see figures 2.2 and 2.3) is large compared to the atomic hyperfine coupling, so that the singlet-triplet coupling due to $V^{\text{hf-}}$ can be neglected.
2. On the other hand r_0 has to be so large that the singlet and triplet potentials for atomic distances $r > r_0$ are known or can be expressed in a small set of (dispersion and exchange) parameters to be determined from experiment.
3. For interatomic distances smaller than r_0 the WKB approximation should be valid enabling one to specify the boundary condition as a phase of the real-valued oscillating radial wave function.
4. The energy E relative to threshold and the angular momentum l value that play a role in the collision are so small that a rapidly converging expansion of the $S = 1$ and $S = 0$ WKB phases in powers of E and $l(l + 1)$ is possible, thus containing a small number of parameters.

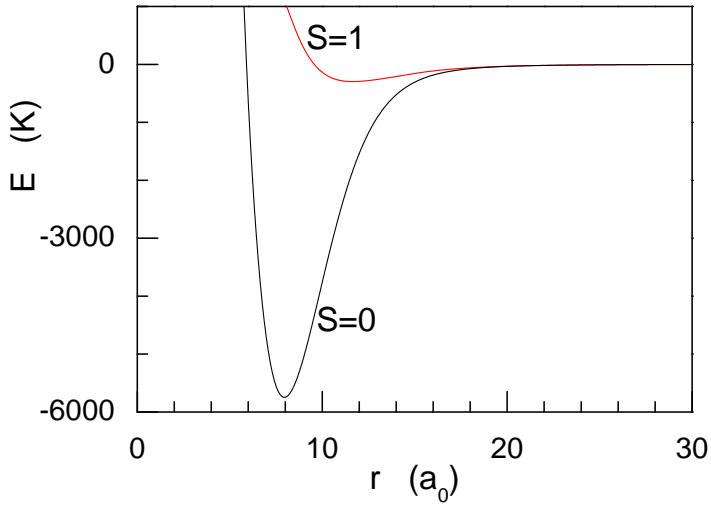


Figure 2.2 Singlet ($S = 0$) and triplet ($S=1$) potentials of ground-state rubidium .

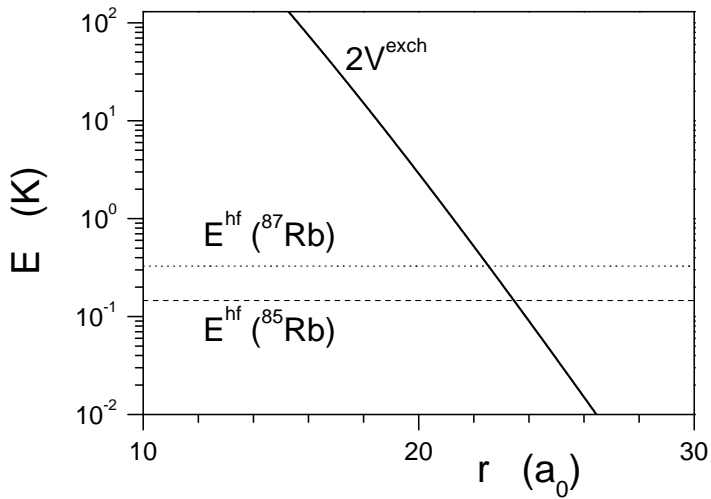


Figure 2.3 The $S = 0 \leftrightarrow 1$ energy splitting of two ground-state rubidium atoms (equal to twice V^{exch}) versus the interatomic separation. The hyperfine energies for both the 85 and 87 isotopes of rubidium are also indicated.

In view of the possibility that conditions 1 and 2 are contradictory, it is far from obvious that a suitable r_0 value can be found. In the nineties when three U.S. experimental groups made a vigorous attempt to create a BEC in an alkali atomic gas, our group was able to predict the signs and rough magnitude of the scattering lengths for almost all alkali species, determining the stability ($a > 0$) or instability ($a < 0$) of a BEC. This essential information could be obtained using the accumulated phase method using a value 19 and even $20a_0$ for r_0 . These values were still reconcilable with condition 1. For example, a predicted negative a for spin-up ^{85}Rb atoms and a positive a for ^{87}Rb led Wieman and Cornell in 1995 to switch from ^{85}Rb to ^{87}Rb leading to the first successful realization of BEC in an ultracold atomic gas [9].

The excessive theoretical precision needed for the present “state of the art” BEC experiments force us to shift r_0 to much smaller distances. Even $16a_0$ would not be small enough to avoid a detrimental hyperfine coupling. Note that V^{hf} has the order of magnitude of an atomic hyperfine splitting, i.e. 0.1K. For instance ^{87}Rb has an atomic hyperfine splitting of 0.33K and ^{85}Rb 0.15K, which should be compared to the $S = 0 \leftrightarrow 1$ energy splitting at $16a_0$ of 75K. A new insight, combined with recently published spectroscopic data, shedding a new light on the singlet potential allowed us to use the $r_0 = 16a_0$ value with a new approach. We will come back this more sophisticated variant of the accumulated phase method in section 2.5.

2.4 Mass scaling

We note that the influence of E, l and the isotopic mass difference on the local phase $\phi(E, l)$ at r_0 comes only from the radial range, where the WKB approximation is valid, so that up to a constant

$$\phi(E, l) = \frac{1}{\hbar} \int^r p(r) dr = \int^r \left[\frac{2\mu}{\hbar^2} (E - V) - \frac{l(l+1)}{r^2} \right]^{\frac{1}{2}} dr. \quad (2.14)$$

Furthermore, with respect to conditions 3 and 4 above, we point out that for the (ultra)cold colliding atoms ($T \lesssim 1\mu\text{K}$) and near-dissociation bound states we are most often considering, E is close to 0 (compared to the depth of the potential at r_0) and l is at most 4. The small E and l ranges then allow a first order Taylor expansion for $\phi(E, l)$ (see figure 2.4) yielding

$$\phi(E, L) = \phi_0 + E\phi^{\text{E}} + l(l+1)\phi^{\text{l}}, \quad (2.15)$$

with

$$\phi^{\text{E}} \equiv \left. \frac{\partial \phi}{\partial E} \right|_{l=0} = \int \frac{\mu dr}{\hbar^2 k} \propto \sqrt{\mu} \quad (2.16)$$

and

$$\phi^{\text{l}} \equiv \left. \frac{\partial \phi}{\partial l(l+1)} \right|_{E=0} = \int \frac{dr}{2kr^2} \propto \frac{1}{\sqrt{\mu}}, \quad (2.17)$$

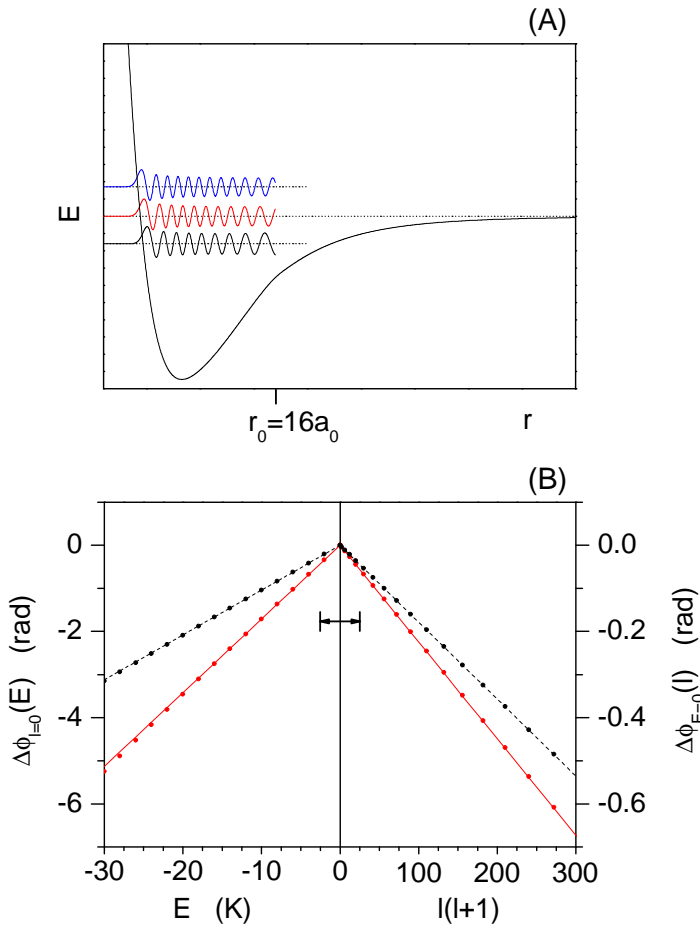


Figure 2.4 Part A illustrates the development of the wavefunction's phase at r_0 for three different energies. A comparison between the true accumulated phase (dots) and a first order approximation (solid lines for triplet, dashed lines for singlet) is shown in part B. The graph depicts as a function of E and $l(l+1)$, the difference in the accumulated phase at $r = r_0$ as compared to the $E = 0, l = 0$ situation: $\Delta\phi(E, l) = \phi(E, l) - \phi(E = 0, l = 0)$. The horizontal arrow indicates the typical E and l range for which we apply the first order approximation. Typical rubidium potentials are used for the calculation. Note that for clarity the energies referred to in part A exceed the energies used in practice by more than an order of magnitude.

with $k = k(r)$ the local wave number.

By making use of this method we introduce two ($S=0,1$) times three (ϕ_0 , ϕ^E , and ϕ^1) parameters which have to be determined by comparison of theoretically predicted to experimentally determined properties of cold collisions or weakly bound states.

As can be seen from Eqns (2.14) and (2.16,2.17) the phase parameters are mass dependent, implying we would need a total of six parameters (three for singlet and three for triplet) for the description of each isotope of a species. However, Seto *et al.* [10] have been able to describe 12148 observed transition frequencies between singlet states of the $^{85}\text{Rb}_2$, $^{87}\text{Rb}_2$, and $^{85}\text{Rb}^{87}\text{Rb}$ molecules with a common potential up to $r=25a_0$, without any sign of a Born-Oppenheimer breakdown. The analysis by Seto *et al.* uses a pure C_6 dispersion tail at r values where our analysis shows higher dispersion terms to be significant. We were able to conclude that this affects the derived singlet potential up to radii of about $23.5a_0$ to a negligible extent. It is also important to point out that any analysis based on transition frequencies such as that of Seto *et al.* can yield relative potential values only, i.e. the absolute energy position of the resulting V_S curve can be shifted arbitrarily. On the basis of this result, we were able to conclude that the singlet part of $^{85}\text{Rb}+^{85}\text{Rb}$ and $^{87}\text{Rb}+^{87}\text{Rb}$ systems can be described with a common potential V_S up to a radius $r=23.5a_0$. This implies that we can relate the parameters for these different isotopes by mass scaling, expecting no signs of break-down effects for the Born-Oppenheimer approximation within the contemporary experimental precision.

From Eqns (2.16,2.17) it is clear that ϕ^E and ϕ^1 should be mass scaled as

$$^{85}\phi^E = \mathcal{R} \ ^{87}\phi^E \quad \text{and} \quad ^{85}\phi^1 = \mathcal{R}^{-1} \ ^{87}\phi^1, \quad (2.18)$$

with $\mathcal{R} = \sqrt{m_{85}/m_{87}}$, in which m_x is the atomic mass of ^xRb .

The mass scaling for ϕ_0 deviates a little from the above equations due to the well-known mass independent contribution of approximately $\pi/4$ to the accumulated phase due to the quantum mechanical penetration into the inner wall of the potential [11](Ch.VI-9). Whereas for the boundary condition on the radial wave function the accumulated phase ϕ_0 may be given modulo π , it is of importance for the mass scaling to know the total phase. Since each “modulo- π phase-cycle” corresponds to one additional (vibrational) bound state in the potential we can express the total accumulated phase as $\phi_0 = n'_b\pi + \phi_{0,\pi}$, with n'_b the number of zero-energy s -wave vibrational nodes up to the radius of interest (r_0) and $\phi_{0,\pi}$ the modulo- π part of the total phase. Given the $k \propto \sqrt{m}$ behavior, the scaled $^{85}\phi_{0,\pi}$ becomes

$$^{85}\phi_{0,\pi} = \mathcal{R} \ ^{87}\phi_{0,\pi} + (1 - \mathcal{R}) \frac{\pi}{4} - \ ^{85}n'_b\pi + \mathcal{R} \ ^{87}n'_b\pi. \quad (2.19)$$

The last term gives rise to a number of discrete values for the mass-scaled phase depending on the number of nodes (up to r_0) contained in the potential. The interval

between these discrete values is approximately $(1 - \mathcal{R})\pi \approx 0.012\pi \approx 0.036$ (for Rb). This discretisation can be exploited when trying to extract information from experimental data of multiple isotopes (see figure 2.5). An implication is that one is able to deduce the number of nodes contained in the potential up to r_0 and thereby the total numbers of bound states contained in the complete singlet and triplet potentials, since additional nodes beyond r_0 can be calculated using the potential derived. For the case of ^{87}Rb we thus find 41 triplet bound states. For ^{85}Rb this number is 40.

For lithium the situation is different in the sense that *ab initio* potentials for the short range part of the potential are a lot more reliable. Although more reliable, they are not accurate enough to predict scattering properties with the precision needed nowadays. In our analysis of the lithium interactions we base the calculations on a combination of the *ab initio* potentials and the accumulated phase method. Theoretical potentials are used for calculation of the wavefunction up to r_0 and at this radius we apply an adjustment of the phase, a *phase jump* $\Delta\phi_0(E, l) = \Delta\phi_0$, which is added to or subtracted from the accumulated phase derived from the *ab initio* potential. The energy and relative angular momentum dependence of the accumulated phase is expected to be accounted for to a sufficient degree of accuracy by the *ab initio* potentials.

2.5 Adiabatic accumulated phase method

In this section we come back to the new variant of the accumulated phase method that we introduced in chapter 3 [published as Phys. Rev. Lett. **88**, 93201 (2002)] and enables us to achieve an unprecedented precision. To begin with we consider the sum V^{hf} of the single-atom hyperfine interactions, Eq. (2.8). Its part $V^{\text{hf}+}$ is diagonal in S (and I), and therefore commutes with the central interaction (2.3). At r_0 it can therefore be included effectively in the Hamiltonian as a constant:

$$\frac{a^{\text{hf}}}{2\hbar^2} \vec{S} \cdot \vec{I} = \frac{a^{\text{hf}}}{4\hbar^2} \{\vec{F}^2 - \vec{S}^2 - \vec{I}^2\} \rightarrow \frac{a^{\text{hf}}}{4\hbar^2} \{F(F+1) - S(S+1) - I(I+1)\}, \quad (2.20)$$

that can simply be added to the triplet potential. It thus leads to a splitting according to I and F (it vanishes for $S = 0$ in which case $F = I$). This splitting was already included in the conventional accumulated phase method.

The new insight concerns the role of $V^{\text{hf}-}$ and the realization that the above condition 1 (section 2.3) for the applicability of the accumulated phase method can be relaxed to some extent, making it possible to shift r_0 to larger atom-atom distances. In the thesis of previous Ph.D. candidates in our group the range of smaller interatomic distances was subdivided in two intervals [see Fig. 2.6(A)]. In one interval V^{hf} is so small compared to V^{exch} , i.e. to the $S = 0$ to $S = 1$ splitting of potential curves that the coupling due to $V^{\text{hf}-}$ can be neglected. Going to larger r this is followed by a range in which V^{hf} and V^{exch} are comparable. It was thought that r_0 should preferably be

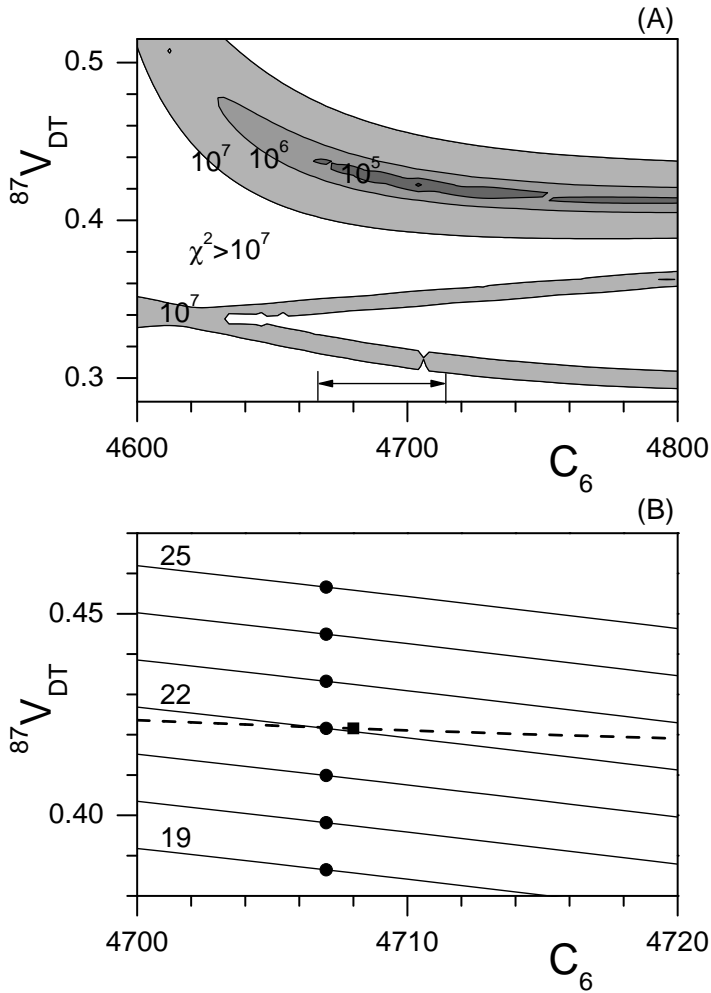


Figure 2.5 (A) Contour plot of the reduced χ^2 as a function of ${}^{87}\nu_{DT}$ and C_6 for ${}^{87}\text{Rb}$ data only. The dispersion coefficient C_6 is expected to be within the interval indicated by the horizontal arrow [12]. (B) The dashed line indicates the bottom of the “deepest trench” in the χ^2 surface of part (A), with the overall minimum indicated by the square. The solid lines indicate equivalent ‘trenches’ in the χ^2 surface for ${}^{85}\text{Rb}$ data only, with the minimum (of each ‘trench’) indicated by a solid circle, making use of mass scaling to translate ${}^{87}\nu_{DT}$ into ${}^{85}\phi_{0,T}$. Different solid lines correspond to a different number ${}^{87}n'_b$ of nodes assumed to be contained by the triplet potential for ${}^{87}\text{Rb}$ up to r_0 : ${}^{87}n'_b=19,\dots,25$. Note that this plot is generated without optimizing ϕ^E , ϕ^I , J , and C_8 .

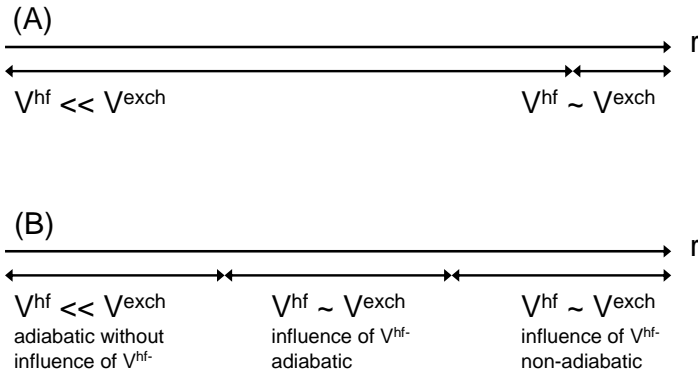


Figure 2.6 Part (A) illustrates the conception of the radial ranges in the traditional accumulated phase method. Part (B) shows the radial intervals as thought of in the “adiabatic accumulated phase method”.

chosen as far right as possible in the $V^{\text{hf}} \ll V^{\text{exch}}$ interval in view of condition 2, which requires pure decoupled singlet and triplet radial waves. However, as long as the WKB is valid in this interval, as is generally the case, a change of phase of a decoupled $S = 0$ or 1 radial wave at one point is equivalent to the same change at another point. This implies that r_0 can be chosen arbitrarily in the $V^{\text{hf}} \ll V^{\text{exch}}$ range. Now consider what happens when we move into the region where $V^{\text{hf}} \sim V^{\text{exch}}$. One will first pass through an interval where the $V^{\text{hf-}}$ coupling is not negligible but still takes place adiabatically, i.e. $V^{\text{hf-}}$ mixes the $S = 0$ and 1 states, but the radial waves are still decoupled when expressed in a new local basis of mixed spin states [see Fig. 2.6(B)]. This enables us to move r_0 into this left-hand part of the $V^{\text{hf}} \sim V^{\text{exch}}$ interval. Changing the phase of a (predominantly) $S = 0$ or 1 radial wave at such a point is still completely equivalent to an equal phase change at an r_0 point chosen in the $V^{\text{hf}} \ll V^{\text{exch}}$ interval. An r_0 choice in this “ $V^{\text{hf}} \sim V^{\text{exch}}$ with adiabatic $V^{\text{hf-}}$ influence” interval is still allowed as long as the local spin mixing due to $V^{\text{hf-}}$ is included in the boundary condition together with pure singlet and triplet phases for the radial waves, for the coupled radial integration further to the right. Note that the l centrifugal splitting and the SIF splitting according to Eq. (2.20) is included in the boundary condition via ϕ^l and ϕ^E terms. Note also that we generally use the vibrational “quantum numbers” at dissociation, ν_D at the dissociation energy of the singlet and triplet potentials (ν_{DS} and ν_{DT}) as model independent quantities to characterize the singlet and triplet phases ϕ_S and ϕ_T in order to avoid the r_0 dependence of these phases [13]. As a third remark we point out that the spin mixing at r_0 depends only on the local energy spacing between the $S = 0$ and 1 potentials, i.e. on V^{exch} . It is independent of the “past history” of the

collision left of r_0 , which depends also on the absolute depth of the potential.

To illustrate the advantages of this “adiabatic accumulated phase method” we compare a calculation including the adiabatic spin mixing at r_0 to one without, i.e. the conventional approach. In both cases we consider the optimization of the potential parameters given a set of ^{87}Rb experimental data. For simplicity we show how one of the parameters, the coefficient J in the exchange interaction (2.6), depends on r_0 . In Fig. 2.7 each of the curves shows the behavior of the relative deviation $\Delta J/J_{\text{th}}$ of the optimal J value from the value J_{th} estimated by Smirnov and Chibisov [1]. The curve with squares shows the result of a calculation along conventional lines. Each point indicated on the curve represents the outcome of a separate χ^2 optimization. The oscillations may be interpreted as a “switch on” effect due to the sudden switch on of the spin mixing during the coupled integration right of r_0 . Switching on the spin mixing adiabatically at r_0 gives rise to the curve with filled circles. Clearly, the oscillation is strongly reduced. Even shifting r_0 to $15a_0$ keeps the oscillation amplitude to below the 12% level¹. Figure 2.7 suggests that one might just as well select a small value for r_0 near $11a_0$ in order to avoid the spin mixing issue altogether. If we would have done that from the beginning, however, we would have missed a key message from the calculation: the fact that the final results are highly independent of the central potentials within an interatomic distance of $16a_0$. This applies in particular to the exchange potential V^{exch} for which the Smirnov-Chibisov radial dependance (2.6) is valid for larger interatomic distances. The same applies to the asymptotic expression (2.5) for the dispersion potential. Note that for rubidium we make use of the singlet potential derived by Seto *et al.* [10] for $r < 23.5a_0$ and are therefore only limited by V^{exch} .

2.6 Resonances

The possibility to change the effective interaction between scattering atoms was mentioned in chapter 1. In this section we will take a closer look at the physics underlying one of the methods mentioned, the magnetically tunable Feshbach resonance. First shape resonances will be discussed after which Feshbach resonances will be explained. This section will be concluded with a brief discussion on the interplay of both, which is of importance when studying relatively high energy (but still s -wave) scattering of atoms in the situation that the scattering length has an anomalously large value away from the resonance (like for ^6Li).

Scattering resonances are continuations of bound states in the continuum. A difference with bound states is that their definition is not unique. Quite a number of

¹When we restrict ourselves to the experimental data available at the time of publishing chapter 3, we can stay within 10% for $r_0 = 16a_0$

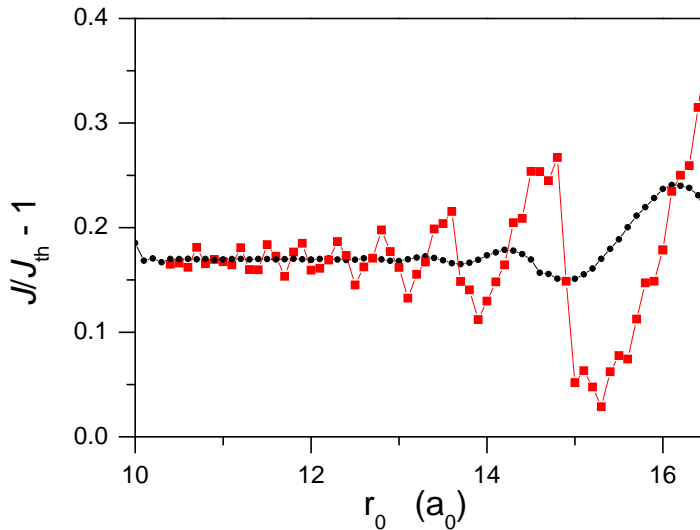


Figure 2.7 Fractional correction to the literature value J_{th} for the strength of the exchange energy versus r_0 (see text). The line with squares corresponds to calculations with the traditional accumulated phase method, while the curve with the solid circles corresponds to calculations performed with the “adiabatic accumulated phase method”. Note that this graph is generated using the most recent experimental data available. For the analysis described in chapter 3, the amplitude of the oscillation was within 10% for $r = 16a_0$ (for the adiabatic variant).

resonance theories have been proposed in the literature since the forties of the previous century. A very elegant definition makes use of poles of the scattering matrix S (some references discussing poles of the S -matrix and scattering resonances are [14–17]). Shape resonances were a well-known phenomenon in nuclear physics, before the first shape resonance was discovered in the scattering of cold atoms by Boesten *et al.* [18].

Let us consider the s-wave scattering of two ^{87}Rb atoms in the spin stretched state, with interaction potential $V(r)$. Introducing a scaling parameter λ , ($\lambda \approx 1$), the interactions between two atoms can be scaled yielding the scaled interaction potential $V'(r) = \lambda V(r)$. By varying λ slightly we can introduce additional bound states or expel them by increasing or decreasing λ , because the potential is made more respectively less attractive. As mentioned before, the (almost) bound state closest to threshold plays a profound role in the interaction between two atoms and its position is closely related to the exact details of the potential. Figure 2.8 shows how the scattering length changes as λ varies. The general pattern is a slowly varying background value with singularities at almost regular intervals. The singularities occur whenever a “bound” state is exactly at threshold.

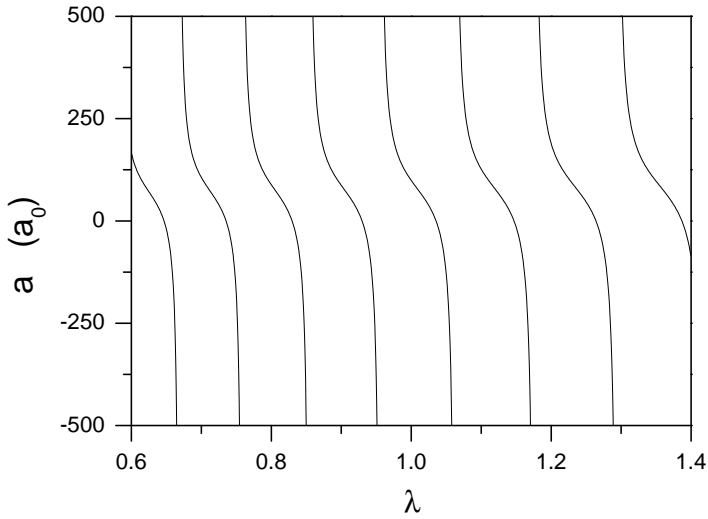


Figure 2.8 Scattering length as a function of the potential depth. The interaction potential is multiplied by λ .

To understand this it is illustrative to see what happens to the bound states, i.e. the single channel S -matrix poles in the complex k -plane, when λ is lowered, i.e. the potential is made less attractive. Figure 2.9(A) depicts the trajectory of a bound state in the complex k -plane, represented by a pole in the S -matrix (a 1×1 matrix in this case) for positive pure imaginary values of k . An initially bound state becomes more weakly bound as λ becomes smaller, i.e. the pole moves down along the imaginary axis and will be located at the origin for a specific potential depth. When the potential is weakened more, the pole crosses the real k axis and moves further down in the complex k -plane, along the negative imaginary axis.

Translating the trajectory in the complex k -plane to a trajectory in the E -plane [see figure 2.9(B)] it must be realized that the k to E mapping is a two-to-one mapping, since $E = \hbar^2 k^2 / 2m$. This ambiguity is reflected in the existence of a physical and a non-physical complex E -plane (a two-sheeted Riemann surface), which are connected via the positive real E axis, which is a branch-cut. When the pole enters the non-physical sheet (i.e. for negative imaginary k), it no longer represents a bound state, but a virtual state, although it is still on the negative E axis.

The scattering matrix changes as a function of the potential depth. With one bound state, i.e. one pole of the S -matrix, close to threshold it is natural to write $S = S^{\text{bgP}} S^{\text{resP}}$ in which S^{resP} describes the resonant influence of the close-to-threshold pole and S^{bgP} summarizes the influence of all other poles (the additional ‘‘P’’ in the superscript is to avoid confusion with S^{bg} and S^{res} which will be introduced below; the

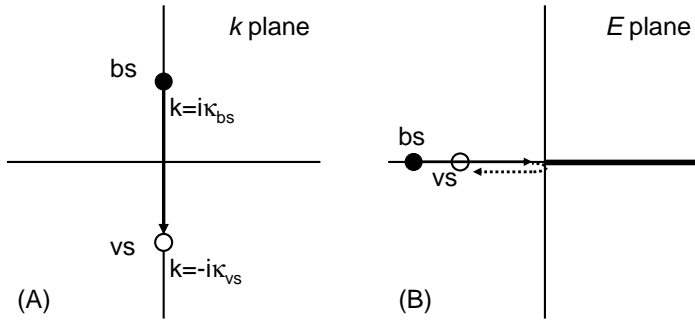


Figure 2.9 Path of the pole in the S -matrix, corresponding to the s -wave bound state (bs) closest to threshold, resulting from making the interaction potential less attractive (i.e. by making λ smaller, see text). Part (A) indicates the path in the complex k -plane, part (B) indicates the equivalent path in the complex E -plane. Note the branch-cut symbolized by the bold positive real E -axis. The pole moves from the physical to the non-physical sheet and becomes a virtual state (vs).

choice for the letter “P” will then also become apparent). We will write the position of a pole in the S -matrix on the positive imaginary axis as $k = i\kappa_b$ and on the negative imaginary axis as $k = -i\kappa_{vs}$ (note that $\kappa_{vs} > 0$). The resonant part of the S -matrix can be obtained by writing $S = \mathcal{F}^*(k)/\mathcal{F}(k)$, with the Jost-function given by [15, 19]

$$\mathcal{F}(k) = \left(1 - \frac{k}{i\kappa_b}\right)g(k) \quad \text{or} \quad \left(1 + \frac{k}{i\kappa_{vs}}\right)g(k), \quad (2.21)$$

where we have to use the first term on the right-hand side if we have a bound state at hand, or the second term if we have a virtual state; $g(k)$ is a smooth function of k summarizing the influence of all distant background poles. Therefore we find

$$S = \left(\frac{i\kappa_b + k}{i\kappa_b - k}\right) \frac{g(k)^*}{g(k)} \quad \text{or} \quad \left(\frac{i\kappa_{vs} - k}{i\kappa_{vs} + k}\right) \frac{g(k)^*}{g(k)} \equiv e^{2i\delta^{\text{resp}}} e^{2i\delta^{\text{bgP}}}, \quad (2.22)$$

with the resonance phase shift $\delta^{\text{resp}} = -\arctan \frac{k}{\kappa_b}$ (or $\delta^{\text{resp}} = +\arctan \frac{k}{\kappa_{vs}}$) and the background phase shift $\delta^{\text{bgP}} = -\arg[g(k)]$. A background scattering length can be defined in terms of the low energy behavior of the total scattering phase shift $\delta(k) = \delta^{\text{bgP}}(k) + \delta^{\text{resp}}(k)$:

$$\delta(k) = -ka^{\text{bgP}} - \arctan\left(\frac{k}{\kappa_b}\right) + \mathcal{O}(k^3) \quad \text{or} \quad -ka^{\text{bgP}} + \arctan\left(\frac{k}{\kappa_{vs}}\right) + \mathcal{O}(k^3), \quad (2.23)$$

with a^{bgP} a background value related to the range of the potential [19, 20] and the arctangent term a resonant part.

The resonance described above is a shape resonance and has a single channel character, meaning that this type of resonance can occur in single channel scattering. An

example is the scattering of triplet ^{85}Rb atoms with $a_T^{85\text{Rb}} = -388a_0$ (see chapter 3), which deviates largely from the range of the potential which is in the order of $100a_0$ for rubidium. To exploit these resonances experimentally one would need to change the depth or shape of the interaction potential, but there are other ways to change the effective interactions between scattering atoms, e.g. with magnetically tunable Feshbach resonances. Their character, however, is different from the resonances described above.

Feshbach resonances

In general the scattering of two atoms involves more than just one channel. In the range where the hyperfine interaction has the same order of magnitude as the exchange interaction, mixing between different channels can take place giving rise to multi-channel resonances. Feshbach resonances are such resonances.

Consider two atoms whose internal + relative angular eigenstate we label by $|\alpha\rangle$. When these two atoms undergo a scattering process they may change their state to a different one, e.g. $|\beta\rangle$, during the scattering. The collection of all states to which coupling may take place can be divided into two spaces. One space, \mathcal{P} , containing all open channels (including the incoming channel) and a space \mathcal{Q} containing the remaining, closed, channels. A channel is open whenever the total energy of the two atoms is higher than the asymptotic (threshold) energy of that channel, i.e. if the atoms can “separate to infinity” in the channel. Now suppose the afore-mentioned atoms in state $|\alpha\rangle$ are put in a magnetic field B . Then their energy will be Zeeman shifted by an amount $\mu_\alpha B$, with μ_α the appropriate magnetic moment (see figure 2.1). Since the asymptotic energy of a channel equals the sum of the internal energies of the two separate atoms in the corresponding states, it is easy to understand that thresholds of the different channels can be shifted relative to one another by applying a magnetic field. Likewise, the energies of bound states contained in channels other than the incoming channel can be shifted, relative to the energy of the two scattering atoms. This is illustrated in figure 2.10, part (A) and (B), and the magnetic field strength for which the energy of a bound state in channel $|\beta\rangle$ is degenerate with the threshold energy of the scattering atoms in channel $|\alpha\rangle$ is indicated by B_0 . For scattering in a magnetic field $B = B_0$ the atoms will resonantly couple to the bound state in the channel $|\beta\rangle$, which has a profound influence on the phase shift and hence on the scattering length $a(B)$ as is shown in figure 2.10(C).

Introducing the projection operator P with the property $P^2 = P$ which projects onto the subspace \mathcal{P} and the equivalent operator Q for projection onto \mathcal{Q} (obeying $P + Q = 1$), we can write the Schrödinger equation as

$$(E - H_{PP})|\Psi_P\rangle = H_{PQ}|\Psi_Q\rangle \quad (2.24)$$

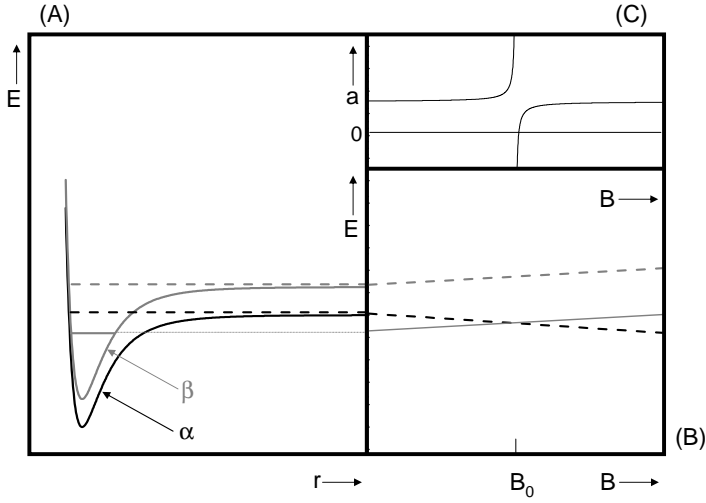


Figure 2.10 Principle of a Feshbach resonance. Part (A) illustrates the potentials corresponding to two different channels with threshold energies indicated by the dashed lines. The solid line within the potential indicates a bound state in the channel with the higher potential. (B) shows how the threshold energies and the energy of the bound state depend on the magnetic field B . At $B = B_0$ the energy of the bound state crosses the threshold energy of the black channel, causing the scattering length associated with the black channel to diverge, as is indicated by part (C).

$$(E - H_{QQ})|\Psi_Q\rangle = H_{QP}|\Psi_P\rangle. \quad (2.25)$$

Here the notation $H_{PP} = PHP$, $H_{PQ} = PHQ$, $|\Psi_P\rangle = P|\Psi\rangle$, etc. is used. We can formally solve these equations by making use of the Green operator $[E^+ - H_{QQ}]^{-1}$ (with $E^+ = E + i0$), inserting $|\Psi_Q\rangle = \frac{1}{E^+ - H_{QQ}}H_{QP}|\Psi_P\rangle$ into Eq. (2.24) yielding the equation for the \mathcal{P} subspace

$$(E - H^{\text{eff}})|\Psi_P\rangle = 0, \quad (2.26)$$

with the effective hamiltonian

$$H^{\text{eff}} = H_{PP} + H_{PQ} \frac{1}{E^+ - H_{QQ}} H_{QP}, \quad (2.27)$$

which can be interpreted as the sum of a direct effect and an indirect effect: coupling from \mathcal{P} space to \mathcal{Q} space, propagation in \mathcal{Q} space and re-emission into \mathcal{P} space. Expanding the Green operator in discrete eigenstates and continuum eigenstates of H_{QQ}

$$\frac{1}{E^+ - H_{QQ}} = \sum_i \frac{|\phi_i\rangle\langle\phi_i|}{E - \varepsilon_i} + \int \frac{|\phi(\varepsilon)\rangle\langle\phi(\varepsilon)|}{E^+ - \varepsilon} d\varepsilon \quad (2.28)$$

and assuming there is only one discrete bound state of H_{QQ} with an energy close to E and neglecting the continuum part of H_{QQ} , Eq. (2.26) can be simplified to

$$(E - H_{PP})|\Psi_P\rangle = H_{PQ} \frac{|\phi_b\rangle\langle\phi_b|H_{QP}|\Psi_P\rangle}{E - \varepsilon_b} \quad (2.29)$$

with the formal solution

$$|\Psi_P\rangle = |\Psi_P^+\rangle + \frac{1}{E^+ - H_{PP}} H_{PQ} \frac{|\phi_b\rangle\langle\phi_b|H_{QP}|\Psi_P\rangle}{E - \varepsilon_b}, \quad (2.30)$$

in which $|\Psi_P^+\rangle$ is an eigenstate of H_{PP} satisfying the outgoing wave boundary conditions, i.e., a solution of the homogeneous part of Eq. (2.29). Multiplication from the left with $\langle\phi_b|H_{QP}$ leads to the solution

$$|\Psi_P\rangle = |\Psi_P^+\rangle + \frac{1}{E^+ - H_{PP}} H_{PQ} |\phi_b\rangle \frac{\langle\phi_b|H_{QP}|\Psi_P^+\rangle}{E - \varepsilon_b - \langle\phi_b|H_{QP} \frac{1}{E^+ - H_{PP}} H_{PQ} |\phi_b\rangle}, \quad (2.31)$$

and hence the expression for the S matrix

$$S_{ji} = S_{ji}^{\text{bg}} - 2\pi i \frac{\langle\Psi_j^-|H_{PQ}|\phi_b\rangle\langle\phi_b|H_{QP}|\Psi_i^+\rangle}{E - \varepsilon_b - \langle\phi_b|H_{QP} \frac{1}{E^+ - H_{PP}} H_{PQ} |\phi_b\rangle}, \quad (2.32)$$

which exhibits a resonant character. By writing the complex energy shift as [11](App. AII)

$$\langle\phi_b|H_{QP} \frac{1}{E^+ - H_{PP}} H_{PQ} |\phi_b\rangle = \Delta^{\text{res}} - \frac{1}{2} i\Gamma^{\text{res}}, \quad (2.33)$$

$$\Delta^{\text{res}} = \langle\phi_b|H_{QP} \frac{\text{c.p.v.}}{E - H_{PP}} H_{PQ} |\phi_b\rangle, \quad (2.34)$$

$$-\frac{1}{2} i\Gamma^{\text{res}} = -i\pi \langle\phi_b|H_{QP} \delta(E - H_{PP}) H_{PQ} |\phi_b\rangle, \quad (2.35)$$

in which c.p.v. refers to the Cauchy principal value, a resonance shift and width can be distinguished. With appropriate phases $\phi_{\text{bn}}^{\text{R}}$ the numerator of Eq. (2.32) can be written as $(2\pi)^{-1} e^{i(\phi_{\text{bj}}^{\text{R}} + \phi_{\text{bi}}^{\text{R}})} \Gamma_{\text{bj}}^{1/2} \Gamma_{\text{bi}}^{1/2}$, defining real positive partial width amplitudes $\Gamma_{\text{bn}}^{1/2}$ by

$$e^{i\phi_{\text{bn}}^{\text{R}}} \Gamma_{\text{bn}}^{1/2} = (2\pi)^{1/2} \langle\phi_b|H_{QP}|\Psi_n^+\rangle = (2\pi)^{1/2} \langle\Psi_n^-|H_{PQ}|\phi_b\rangle \quad (2.36)$$

and the corresponding partial widths

$$\Gamma_{\text{bn}} = 2\pi \left| \langle\phi_b|H_{QP}|\Psi_n^+\rangle \right|^2 = 2\pi \left| \langle\Psi_n^-|H_{PQ}|\phi_b\rangle \right|^2 \quad (2.37)$$

for the formation and decay of the bound state b from and into the open channel n. Eq. (2.32) thus gets the form

$$S_{ji} = S_{ji}^{\text{bg}} - i \frac{e^{i(\phi_{\text{bj}}^{\text{R}} + \phi_{\text{bi}}^{\text{R}})} \Gamma_{\text{bj}}^{1/2} \Gamma_{\text{bi}}^{1/2}}{E - \varepsilon_b - \Delta^{\text{res}} + \frac{1}{2} i\Gamma^{\text{res}}}. \quad (2.38)$$

We now define a resonance energy ε^{res} in terms of the real part of the denominator:

$$\varepsilon^{\text{res}} = \varepsilon_{\text{b}} + \Re \left(\Delta^{\text{res}} - \frac{1}{2} i \Gamma^{\text{res}} \right) \quad (2.39)$$

We are especially interested in the elastic S -matrix element S_{ii} for the channel i with the higher threshold in the case of more than one open channel. Referring the energy E to the threshold of this channel we have

$$S_{ii} = S_{ii}^{\text{bg}} - i e^{2i\phi_{\text{bi}}^{\text{R}}} \frac{\Gamma_{\text{bi}}}{E - \varepsilon^{\text{res}} + i \Im \left(-\Delta^{\text{res}} + \frac{1}{2} i \Gamma^{\text{res}} \right)}. \quad (2.40)$$

The various quantities in the right-hand side are functions of E and B . For small positive E one can show that Γ_{bi} can be written as $2Ck_i$, whereas

$$\varepsilon^{\text{res}} = \Delta\mu(B - B_0) \quad (2.41)$$

not far from resonance, with B_0 the field strength where the resonance energy ε^{res} crosses the threshold of channel i and $\Delta\mu$ the difference in magnetic moment between the bound and free states of the two atom system. We thus obtain

$$S_{ii} = S_{ii}^{\text{bg}} - i e^{2i\phi_{\text{bi}}^{\text{R}}} \frac{\Gamma_{\text{bi}}}{-\Delta\mu(B - B_0) + i \Im \left(-\Delta^{\text{res}} + \frac{1}{2} i \Gamma^{\text{res}} \right)} \quad (2.42)$$

$$= S_{ii}^{\text{bg}} - i e^{2i\phi_{\text{bi}}^{\text{R}}} \frac{2Ck_i}{-\Delta\mu(B - B_0) + i \Im \left(-\Delta^{\text{res}} + \frac{1}{2} i \Gamma^{\text{res}} \right)}. \quad (2.43)$$

To first order in k this equation reads

$$1 - 2ik_i a = 1 - 2ik_i a^{\text{bg}} + 2ik_i e^{2i\phi_{\text{bi}}^{\text{R}}} \frac{C/\Delta\mu}{(B - B_0) - i \Im \left(-\Delta^{\text{res}} + \frac{1}{2} i \Gamma^{\text{res}} \right) / \Delta\mu}, \quad (2.44)$$

so that the total (complex) scattering amplitude a is given by

$$a = a^{\text{bg}} \left(1 - e^{2i\phi_R} \frac{\Delta_{\text{el}}}{B - B_0 + \frac{1}{2} i \Delta_{\text{inel}}} \right) \quad (2.45)$$

in terms of the scattering length a^{bg} for the background scattering and a Feshbach resonance part, the latter containing a “resonance mixing phase” ϕ_R and positive real (in)elastic field widths $\Delta_{\text{el}}(\Delta_{\text{inel}})$ defined by

$$\Delta_{\text{el}} e^{2i\phi_R} \equiv \frac{C}{a^{\text{bg}} \Delta\mu} e^{2i\phi_{\text{bi}}^{\text{R}}} \quad (2.46)$$

$$\Delta_{\text{inel}} \frac{1}{2} \Delta\mu \equiv \Im \left(\Delta^{\text{res}} - \frac{1}{2} i \Gamma^{\text{res}} \right)_{E=0}. \quad (2.47)$$

The case of one open channel has been considered before [21]. In that situation Eq. (2.40) reduces to

$$S_{ii} = S_{ii}^{\text{bg}} - i \frac{\Gamma_{\text{bi}}}{E - \varepsilon_{\text{b}} - \Delta^{\text{res}} + \frac{1}{2} i \Gamma_{\text{bi}}} \quad (2.48)$$

and (2.45) to

$$a = a^{\text{bg}} \left(1 - \frac{\Delta_B}{B - B_0} \right), \quad (2.49)$$

due to a vanishing ϕ_R and ϕ_{inel} . The quantity Δ_B is the magnetic field width over which the scattering length a changes sign with respect to the background value (see figure 2.10).

Interplay

Two sections earlier it was mentioned that some atoms have an anomalously large background scattering length, e.g. ^{85}Rb . When the scattering of this species is studied at relatively high (but still s -wave) energies, in a magnetic field which is tuned near a Feshbach resonance, two resonances are important: a shape resonance in addition to this Feshbach resonance. Their mutual interplay has been studied by Marcelis [19] and it was shown that the energy shift and width of Eq. (2.48) becomes

$$\Delta^{\text{res}}(E) = \frac{-\frac{1}{2}A_{\text{vs}}}{k^2 + \kappa_{\text{vs}}^2} \quad (2.50)$$

$$\Gamma(E) = \frac{A_{\text{vs}}k}{\kappa_{\text{vs}}(k^2 + \kappa_{\text{vs}}^2)}, \quad (2.51)$$

with $A_{\text{vs}} > 0$ and for k real and positive (i.e. for real and positive energies on the physical Riemann sheet) if a virtual state causes the anomalously large scattering length, or

$$\Delta^{\text{res}}(E) = \frac{\frac{1}{2}A_{\text{b}}}{k^2 + \kappa_{\text{b}}^2} \quad (2.52)$$

$$\Gamma(E) = \frac{A_{\text{b}}k}{\kappa_{\text{b}}(k^2 + \kappa_{\text{b}}^2)}, \quad (2.53)$$

if a bound state is the cause, with $A_{\text{b}} > 0$.

References

- [1] B.M. Smirnov and M.S. Chibisov, “*Electron exchange and changes in the hyperfine state of colliding alkaline metal atoms*”, Zh. Eksp. Teor. Fiz. **48**, 939 (1965) [Sov. Phys. JETP **21**, 624 (1965)].
- [2] M. Mizushima, *The theory of rotating diatomic molecules* (Wiley, New York, 1975) p. 233; P.S. Julienne et al. (priv. commun.).
- [3] A.C. den Boer, *Internal report, Theoretical Physics group*, [Eindhoven University of Technology, 1992 (unpublished)].
- [4] F.H. Mies, C.J. Williams, P.S. Julienne, and M. Krauss, “*Estimating Bounds on the Collisional Relaxation Rates of Spin-Polarized ^{87}Rb Atoms at Ultracold Temperatures*”, J. Res. Natl. Inst. Stand. Technol. **101**, 521 (1996).

- [5] Cheng Chin, Vladan Vuletić, Andrew J. Kerman, and Steven Chu, "High Resolution Feshbach Spectroscopy of Cesium", *Phys. Rev. Lett.* **85**, 2717 (2000); Paul J. Leo, Carl J. Williams, and Paul S. Julienne, "*Collision Properties of Ultracold ^{133}Cs Atoms*", *Phys. Rev. Lett.* **85**, 2721 (2000); Cheng Chin, Andrew J. Kerman, Vladan Vuletić, Steven Chu, "*Sensitive Detection of Cold Cesium Molecules by Radiative Feshbach Spectroscopy*", (cond-mat/0207092).
- [6] A. Marte, T. Volz, J. Schuster, S. Dürr, G. Rempe, E.G.M. van Kempen, and B.J. Verhaar, "*Feshbach resonances in rubidium 87: Precision measurement and analysis*", *Phys. Rev. Lett.* **89**, 283202 (2002).
- [7] A. J. Moerdijk and B. J. Verhaar, "*Prospects for Bose-Einstein Condensation in Atomic ^7Li and ^{23}Na* ", *Phys. Rev. Lett.* **73**, 518 (1994).
- [8] A. J. Moerdijk, W. C. Stwalley, R. G. Hulet, and B. J. Verhaar, "*Negative scattering length of ultracold ^7Li gas*", *Phys. Rev. Lett.* **72**, 40 (1994).
- [9] M.H. Anderson, J.R. Ensher, M.R. Matthews, C.E. Wieman, and E.A. Cornell, "*Observation of Bose-Einstein Condensation in a Dilute Atomic Vapor.*", *Science* **269**,198 (1995).
- [10] J.Y. Seto, R.J. Le Roy, J. Vergés, and C. Amiot, "*Direct potential fit analysis of the $X^1\Sigma_g^+$ state of Rb_2 : Nothing else will do!*", *J. Chem. Phys.* **113**, 3067 (2000).
- [11] Albert Messiah, *Quantum Mechanics (two volumes bound as one)*, (Dover, New York, 1999).
- [12] A. Derevianko, W. R. Johnson, M. S. Safronova, and J. F. Babb, "*High-Precision Calculations of Dispersion Coefficients, Static Dipole Polarizabilities, and Atom-Wall Interaction Constants for Alkali-Metal Atoms*", *Phys. Rev. Lett.* **82**, 3589 (1999).
- [13] Boudewijn Verhaar, Kurt Gibble, and Steven Chu, "*Cold-collision properties derived from frequency shifts in a cesium fountain*", *Phys. Rev. A* **48**, R3429 (1993).
- [14] David J. Griffiths, *Introduction to quantum mechanics (second edition)*, (Prentice-Hall, Englewood Cliffs NJ, 1995).
- [15] Roger G. Newton, *Scattering Theory of Waves and Particles (second edition)*, (Springer-Verlag, Berlin, 1982).
- [16] John R. Taylor, *Scattering Theory*, (John Wiley and sons, New York, 1972).
- [17] Charles J. Joachain, *Quantum Collision Theory*, (North-Holland Publishing Company, Amsterdam, 1975).
- [18] H. M. J. M. Boesten, C. C. Tsai, B. J. Verhaar, and D. J. Heinzen, "*Observation of a Shape Resonance in Cold-Atom Scattering by Pulsed Photoassociation*", *Phys. Rev. Lett.* **77**, 5194 (1996); H. M. J. M. Boesten, C. C. Tsai, J. R. Gardner, D. J. Heinzen, and B. J. Verhaar, "*Observation of a shape resonance in the collision of two cold ^{87}Rb atoms*", *Phys. Rev. A* **55**, 636 (1997).
- [19] B. Marcelis, *M.Sc. thesis, Resonances in ultracold collisions*, [Eindhoven University of Technology, 2003 (unpublished)]; B. Marcelis et al., "*Feshbach resonances with large background scattering length: Interplay with open-channel resonances*", *Phys. Rev. A*, **70**, 12701 (2004).

-
- [20] G.F. Gibrakin and V.V. Flambaum, “*Calculation of the scattering length in atomic collisions using the semiclassical approximation*”, Phys. Rev. A **48**, 546 (1993).
- [21] A. J. Moerdijk, B. J. Verhaar, and A. Axelsson, “*Resonances in ultracold collisions of ${}^6\text{Li}$, ${}^7\text{Li}$, and ${}^{23}\text{Na}$* ”, Phys. Rev. A **51**, 4852 (1995)

Inter-isotope determination of ultracold rubidium interactions from three high-precision experiments

E.G.M. van Kempen, S.J.J.M.F. Kokkelmans, D.J. Heinzen, and B.J. Verhaar

Published in Phys. Rev. Lett. **88**, 93201 (2002)

Combining the measured binding energies of four of the most weakly bound rovibrational levels of the $^{87}\text{Rb}_2$ molecule with results of two other recent high-precision rubidium experiments, we obtain exceptionally strong constraints on the atomic interaction parameters in a highly model independent analysis. The comparison of ^{85}Rb and ^{87}Rb data, where the two isotopes are related by a mass scaling procedure, plays a crucial role. We predict scattering lengths, clock shifts, and Feshbach resonances with an unprecedented level of accuracy. Two of the Feshbach resonances occur at easily accessible magnetic fields in mixed-spin channels. One is related to a d -wave shape resonance.

3.1 Introduction

After the first realization of Bose-Einstein condensation (BEC) in a dilute ultracold gas of rubidium atoms [1], experiments with the two isotopes ^{87}Rb and ^{85}Rb further led to an amazingly rich variety of BEC phenomena, ranging from the controlled collapse of a condensate with tunable attractive interactions [2] to the realization of an atomic matter wave on a microchip [3]. Because of the large number of groups that have started doing experiments with these atomic species and the growing complexity and subtlety of the planned experiments, there is a clear need for a more precise knowledge of the interactions between ultracold rubidium atoms in the electronic ground state, since these determine most of the properties of the condensate. For instance, despite a widespread interest, to our knowledge, not until now has any experimental group been able to locate the predicted [4] magnetic-field induced Feshbach resonances that can be used to tune the interactions between ultracold ^{87}Rb atoms. Being able to switch on or off these interactions at will by a mere change of magnetic field may well be one of the main assets of matter waves compared to light waves in the new matter wave devices. In an atomic interferometry device, in particular, a nonlinear interaction

between interfering waves may be introduced or eliminated by changing a field applied at the intersection point.

In this Letter, combining the results of three very recent high-precision observations, we come close to a complete and model-independent specification of the interaction properties of ultracold rubidium atoms. The fact that two isotopes ^{85}Rb and ^{87}Rb are involved in the measurements makes the constraints exceptionally strong and also increases the predictive power: the interaction properties of any other fermionic or bosonic isotope with mass number 82, 83, 84, or 86 are now known with about the same precision. Using mass scaling to relate the different isotopes we are able for the first time to deduce for each of the isotopes the exact numbers of bound Rb_2 states with total spin $S = 0$ (singlet) and 1 (triplet). As an illustration of the predictive power we predict two Feshbach resonances in mixed-spin scattering channels for ^{87}Rb at easily accessible fields that could lead to new time dependent phenomena in coherent spin oscillations and spin waves. There are numerous effects, such as spinor condensate energy differences, which are proportional to differences of scattering lengths. Because these differences are unusually small in Rb, the potentials must be very accurate to calculate them to reasonable accuracy.

3.2 Analysis of recent high-precision experiments

The first of the three high-precision experiments is the recent measurement of four of the highest bound rovibrational levels of the $^{87}\text{Rb}_2$ molecule with 10 kHz precision [5]. The second experiment is the improved characterization [6] of the elastic scattering near a Feshbach resonance in ^{85}Rb , leading to a more precise determination of the resonance field $B_0 = 154.9(4)$ G and the nearby field strength $B'_0 \equiv B_0 + \Delta = 165.85(5)$ G, where the scattering length goes through zero [Δ is the (elastic) resonance width]. The third experimental ingredient going into our analysis is the measurement [7] of 12148 transition frequencies between $X^1\Sigma_g^+$ vibrational levels of the $(^{85}\text{Rb})_2$, $(^{87}\text{Rb})_2$, and $^{85}\text{Rb}^{87}\text{Rb}$ molecules, leading to a highly accurate singlet Rb + Rb potential [8]. Moreover, within the accuracy of this experiment a comparison of levels for the three studied isotopomers shows no sign of Born-Oppenheimer break-down effects, i.e., the observed levels agree with a simple radial Schrödinger equation containing a common singlet potential $V_S(r)$ and the reduced atomic mass. Calculation shows [9] that this justifies neglecting such effects also in our analysis.

This set of extremely precise measurements calls for a very careful construction of the interatomic total spin $S = 0$ and 1 potentials, depending on the interatomic separation r . We combine the singlet potential of Ref. [7] with a long-range part equal to the difference $V_{disp} - V_{exch}$ of a dispersion term and an exchange term, starting at a variable radius r_S between 21 and 23.5 a_0 ($1 a_0 = 0.529\text{Å}$). The part $V_{disp}(r)$

includes C_6, C_8, C_{10} terms and retardation, while $V_{exch}(r)$ is assumed to be given by the asymptotic form $\frac{1}{2}Jr^{7/2\alpha-1}\exp(-2\alpha r)$, derived by Smirnov and Chibisov [10] for r values where the overlap of the electron clouds is sufficiently small [$\alpha = 0.554a_0^{-1}$, following from the ionization potential $\frac{1}{2}\alpha^2$ of the Rb atom in atomic units (au)].

The triplet potential is subject to a larger uncertainty. For its short range part an *ab initio* potential is usually taken. To get rid of this model dependence, we use the accumulated phase method [11]: the “history” of the atom-atom motion is summarized by a boundary condition at an interatomic distance r_0 , in the form of the phase $\phi_T(E, l)$ of the oscillating triplet radial wave function ψ depending on energy E and angular momentum l . Specifying $\phi_T(E, l)$ is equivalent to giving the logarithmic derivative ψ'/ψ at $r = r_0$. In all of our previous work we neglected the singlet-triplet mixing by the hyperfine interaction V_{hf} of the nuclear and electronic spins in the range $r < r_0$, in order to deal with pure singlet and triplet radial waves until the boundary. Here, however, we introduce a new variant that allows us to choose a larger r_0 than would otherwise be possible: we include the adiabatic mixing by V_{hf} in the two-atom spin states but still neglect its influence on the radial wave functions to avoid dependence on the history other than via the pure triplet phase. Model calculations show that in this form the scattering calculations have the required accuracy for r_0 values up to $16 a_0$. The experimental data for either ultracold or weakly bound atoms that we analyze comprise a small E and l range near $E = l = 0$. In this range a first order Taylor expansion $\phi_T(E, l) = \phi_T^0 + E\phi_T^E + l(l+1)\phi_T^l$ is adequate, which reduces the information contained in $V_T(r)$ for $r < r_0$ to three phase parameters only. In principle, these would be needed for both the ^{85}Rb and ^{87}Rb systems. However, since we expect Born-Oppenheimer breakdown effects to be negligible also for the triplet channel in the distance range $r < r_0$, we use mass scaling to express $\phi_T^0, \phi_T^E, \phi_T^l$ for ^{85}Rb in terms of the three phase parameters for ^{87}Rb . Beyond r_0 we construct $V_T(r)$ from $V_S(r)$ by adding $2V_{exch}(r)$.

Applying this method we carry out a full quantum scattering calculation for a set of eight experimentally measured quantities. This set consists of five quantities for ^{87}Rb and three for ^{85}Rb . The ^{87}Rb data are the four bound state energies and the ratio of scattering lengths $a_{1-1}/a_{21} = 1.062(12)$ for atomic scattering in condensates of ^{87}Rb atoms in the hyperfine states $(f, m_f) = (1, -1)$ and $(2, 1)$ [12]. For ^{85}Rb we include the Feshbach resonance fields B_0 and B'_0 , as well as the energy $0.7(1)$ mK of the g-wave shape resonance observed in the scattering of a pair of cold atoms in the total spin $S = 1$ state [13].

With a least-squares search routine we determine optimal values for the parameters $C_6, C_8, J, \phi_T^0(^{87}\text{Rb}), \phi_T^E(^{87}\text{Rb}), \phi_T^l(^{87}\text{Rb})$. C_{10} is kept fixed at the value calculated by Marinescu *et al.* [14], but the effect of $\pm 10\%$ variations around this value and an estimated upper bound for the influence of higher dispersion terms are included in the

Table 3.1 Interaction parameters (au) derived from experiments without (column A) and including (column B) the requirement $V_S = V_{disp} - V_{exch}$ for $r_0 < r < r_S$.

Quantity	A	B
$C_6/10^3$	4.703(9)	4.698(4)
$C_8/10^5$	5.79(49)	6.09(7)
$C_{10}/10^7$	7.665(Ref. [14])	7.80(6)
$C_{11}/10^9$...	-0.86(17)
$C_{12}/10^9$...	11.9(Ref. [22])
$J.10^2$	0.45(6)	0.42(2)
$a_T(^{87}\text{Rb})$	+98.98(4)	+98.99(2)
$a_S(^{87}\text{Rb})$	+90.4(2)	+90.0(2)
$a_T(^{85}\text{Rb})$	-388(3)	-387(1)
$a_S(^{85}\text{Rb})$	+2795 ⁺⁴²⁰ ₋₂₉₀	+2400 ⁺³⁷⁰ ₋₁₅₀
$v_{DT}(\text{mod } 1), n_{bT}(^{87}\text{Rb})$	0.4215(3), 41	0.4214(2), 41
$v_{DS}(\text{mod } 1), n_{bS}(^{87}\text{Rb})$	0.455(1), 125	0.456(1), 125
$v_{DT}(\text{mod } 1), n_{bT}(^{85}\text{Rb})$	0.9471(2), 40	0.9470(1), 40
$v_{DS}(\text{mod } 1), n_{bS}(^{85}\text{Rb})$	0.009(1), 124	0.011(1), 124

final error bars. Column A of Table 3.1 summarizes the main results of the calculations. We find a value for C_6 in agreement with the theoretical value 4691(23) obtained by Derevianko *et al.* [15]. The C_8 value agrees with that calculated by Marinescu *et al.* [14]. To our knowledge this is the first experimental determination of C_8 from a combined set of cold-atom + bound state data. Our analysis also yields the first experimental value of the strength of V_{exch} from such data. The coefficient J agrees with the most recent theoretical value in Ref. [16]. Table 3.1 also gives the values of the pure singlet and triplet scattering lengths for both ^{85}Rb and ^{87}Rb , following from $C_6, C_8, J, \phi_T^0(^{87}\text{Rb})$, as well as the fractional vibrational quantum numbers at dissociation $v_D(\text{mod. } 1)$ [11] and the numbers of bound states n_b . The reduced minimum χ^2 value is 0.5.

3.3 Predictions of Rb scattering properties

The foregoing makes clear that a major step forward has been made possible by the new experiments, two of which make use of a Bose-Einstein condensate. This is a firm basis for making a variety of interesting predictions. As a first example we predict the ^{87}Rb $f = 1$ spinor condensate to be ferromagnetic, i.e., it is favorable for two $f = 1$ atoms to have their spins parallel, because the mean field interaction is more repulsive for total $F = 0$ than for $F = 2$: The calculated scattering lengths are $a_{F=2} = +100.4(1)a_0$ and $a_{F=0} = +101.8(2)a_0$. In a recent preprint Klausen *et al.* [17] independently came

Table 3.2 Predictions of collisional frequency shifts for the ^{87}Rb fountain clock, compared to two recent experiments.

$\left(\frac{1}{n} \frac{\Delta\nu}{\nu}\right)_{exp}$ (10^{-24}cm^3)	Ref.	Present theory (10^{-24}cm^3)
-56_{-21}^{+84}	[18]	-72.5 ± 3.3
$-50(10)_{-34}^{+22}$	[19]	-32.8 ± 0.7
$-60(16)_{-46}^{+29}$	[19]	-41.5 ± 2.9

Table 3.3 Resonance fields B_0 and widths Δ for ^{87}Rb .

$B_0(\text{G})$	403(2)	680(2)	899(4)	1004(3)
$\Delta(\text{mG})$	< 1	15	< 5	216

to this conclusion of a ferromagnetic spinor condensate by calculating the scattering lengths for several assumed numbers of triplet bound states.

We are also able to predict collisional frequency shifts in an ^{87}Rb fountain clock for arbitrary choices of partial densities of atomic hyperfine states. Table 3.2 compares our calculated fractional frequency shifts normalized to total atom density n for two recent experiments [18, 19]. We find good agreement with the three measured shifts.

For various applications there is widespread interest for predictions of magnetic-field values at which Feshbach resonances are to be expected in the scattering of two ^{87}Rb atoms in the $(f, m_f) = (1, +1)$ state. With our interaction parameters we expect them at the four resonance field values B_0 given in Table 3.3 together with the widths Δ . The B_0 values are to be compared with the values 383, 643, 850, and 1018 G predicted in 1997 [4]. It is interesting that the broadest resonance at 1004 G shows a doublet structure [9].

Figure 3.1 shows Feshbach resonances that we predict to occur in the mixed spin channels $(2, +1) + (1, -1)$ and $(2, -1) + (1, +1)$ at easily accessible field values of 1.9 and 9.1G, respectively. The graphs show the predicted field-dependent scattering lengths $a(B)$, which are complex functions due to the presence of exothermal inelastic decay channels. The generalized analytic expression for the field dependence in this case is [9]:

$$a(B) = a_\infty \left(1 - e^{2i\phi_R} \frac{\Delta_{el}}{B - B_0 + \frac{1}{2}i\Delta_{inel}} \right), \quad (3.1)$$

with Δ_{el} and Δ_{inel} the (in)elastic resonance widths and ϕ_R a resonance phase constant, arising due to inelasticity. Note that the real part of the scattering length does not go through infinity. It turns out that the 1.9G resonance is an $l = 2$ resonance, which couples via the spin-spin interaction V_{ss} to the s-wave incident channel. Actually, this

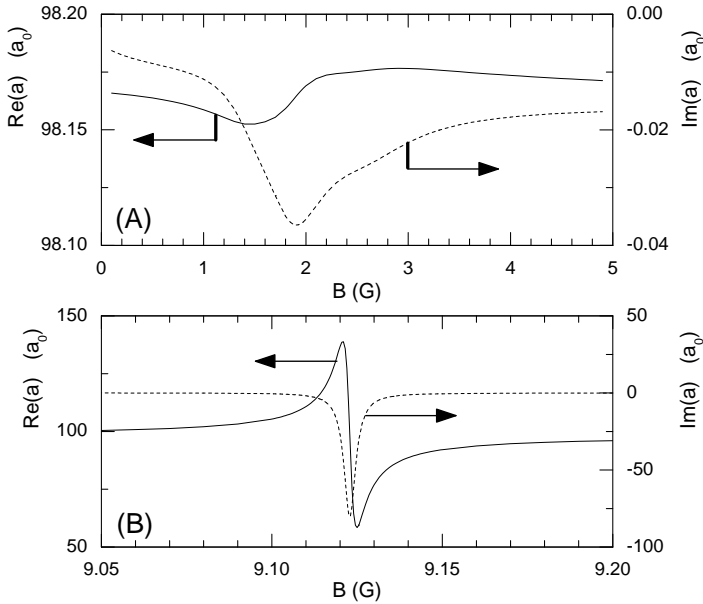


Figure 3.1 (A) Real (solid line) and imaginary (dashed line) parts of the scattering length $a(B)$ in s-wave ^{87}Rb (2,+1)+(1,-1) mixed spin scattering channel, showing the presence of a Feshbach resonance at 1.9G. The imaginary part is proportional to summed rate coefficient G for decay into all open channels. (B) Same for Feshbach resonance in (2,-1)+(1,+1) channel at 9.1G.

resonance is the “hyperfine analog state” [9] in the (2,+1)+(1,-1) scattering channel of the d-wave shape resonance of ^{87}Rb occurring in the spin-stretched (2,+2)+(2,+2) spin channel [13], i.e., a state with essentially the same spatial dependence and differing only in its hyperfine spin structure [20]. It is located at a comparable low energy above threshold. In a similar way the $l = 0$ resonance at 9.1G is the hyperfine analog state of two of the $l = 0$ bound states observed [5] at roughly 25MHz below threshold in the (2,+2)+(2,+2) and (1,-1)+(1,-1) channels, belonging to the same rotational band as the d-wave shape resonance. They might play a role in the damping of coherent spin oscillations of the type which are being observed in experiments at JILA [21].

3.4 Extended analysis

Until now we assumed the expression for V_{disp} to be valid for interatomic distances larger than r_S . We now extend V_{disp} with C_{11} and C_{12} terms and assume it to be valid also between $18 a_0$ and r_S . This leads us to a more ambitious approach that allows us to determine C_{10} and C_{11} as two more free parameters in the least squares search: we take into account the additional constraint arising from the equality $V_S(r) =$

$V_{disp}(r) - V_{exch}(r)$ by imposing this equality at five r points as additional “experimental data” with a standard deviation of 0.5%. We thus effectively include the bound states of Ref. [7] with outer turning points in the range considered. In the search we take C_{12} equal to the theoretical value 11.9×10^9 of Ref. [22]. In column B of Table 3.1 the resulting optimal parameter values are given together with error bars based on a 25 % uncertainty in C_{12} . We find a value for C_{10} differing from the theoretical value 7.665×10^7 au [14] by only 1.8%. While the above attractive C_n terms with even n arise from the interatomic multipole-multipole interaction in second order, a C_{11} term is expected [23] as a repulsive third order dispersion term arising from the mutual dipole excitation and deexcitation of the atoms with an intermediate quadrupole transition between excited states in each of the atoms. Note that the ratio $C_{11}/C_{12} = -0.072$ is comparable to the rigorous value -0.028 for H atoms [24] and the *ab initio* ratio -0.041 for Cs atoms [25]. The remaining residue of the fit, concentrated at the smallest radii in the radial interval may well be due to the summed contributions of further (attractive and repulsive) dispersion terms beyond the C_{12} contribution plus correction terms to the Smirnov-Chibisov exchange expression. Note that the values of the lower dispersion coefficients are dominated by the close-to-threshold measurements, whereas the higher ones are determined primarily by the Seto potential in the middle range $r_0 < r < r_S$. We expect that experiment will prove the value of this more ambitious approach.

For completeness we point out that a weak contribution to the total atom-atom force is still missing in the above picture: the interatomic spin-spin interaction V_{ss} . One component of V_{ss} is the well-known magnetic dipole interaction between the valence electron spins of the interacting atoms. An additional contribution, which arises from the electronic spin-orbit coupling as a second-order effect, has been experimentally determined for the first time for rubidium atoms by Freeland *et al.* [5]. Calculation shows that V_{ss} has a negligible influence on the previous analysis.

3.5 Conclusions

In summary, combining the results of three recent high-precision experiments we have come close to a complete and model independent specification of the interaction properties of cold rubidium atoms. We have determined the van der Waals coefficients C_6 , C_8 , C_{10} , C_{11} , and the strength J of the exchange interaction. We have thus reached a consistent picture of the interactions, with which it is possible to predict essentially all parameters needed for a complete description of a rubidium Bose-Einstein condensate or thermal gas of any isotope in an arbitrary spin state. New experimental data, in particular on the Feshbach resonances, will undoubtedly be helpful to confirm the above consistent picture and to further narrow down the error limits. We believe that our approach sets an example for similar experimental and theoretical work for other

(combinations of) atomic species. From a theoretical point of view, it is fascinating that it is possible to achieve a level of precision for the interaction properties approaching that for collisions of cold hydrogen atoms, based on a combination of experimental results and a sound framework of collision physics.

Acknowledgement

We gratefully acknowledge the support of the work at Texas by the R.A. Welch Foundation, the US National Science Foundation, and the NASA Microgravity Research Division. The work at Eindhoven is part of the research program of the Stichting FOM, which is financially supported by NWO.

References

- [1] M.H. Anderson *et al.*, *Science* **269**, 133 (1995); Press release Nobel prize in physics 2001 (www.nobel.se/physics/laureates/2001).
- [2] J.L. Roberts *et al.*, *Phys. Rev. Lett.* **86**, 4211 (2001).
- [3] W. Hänsel, P. Hommelhoff, T.W. Hänsch, and J. Reichel, *Nature* **413**, 498 (2001).
- [4] J.M. Vogels *et al.*, *Phys. Rev. A* **56**, R1067 (1997).
- [5] R. Wynar *et al.*, *Science* **287**, 1016 (2000); R.S. Freeland, D.Comparat, R. Wynar, C. Ryu, D.J. Heinzen, S.J.J.M.F. Kokkelmans, E.G.M. van Kempen, and B.J. Verhaar (to be published).
- [6] J.L. Roberts *et al.*, *Phys. Rev. A* **64**, 024702 (2001).
- [7] J.Y. Seto, R.J. Le Roy, J. Vergés, and C. Amiot, *J. Chem. Phys.* **113**, 3067 (2000).
- [8] The analysis in Ref. [7] uses a pure C_6 dispersion tail at r values where our analysis shows higher dispersion terms to be significant. Calculation shows that this affects the derived singlet potential up to radii of about $23.5 a_0$ to a negligible extent. Note that the transition frequencies define relative potential values only.
- [9] E.G.M. van Kempen *et al.* (to be published).
- [10] B.M. Smirnov and M.S. Chibisov, *Zh. Eksp. Teor. Fiz.* **48**, 939 (1965) [*Sov. Phys. JETP* **21**, 624 (1965)].
- [11] A.J. Moerdijk, W.C. Stwalley, R.G. Hulet, and B.J. Verhaar, *Phys. Rev. Lett.* **72**, 40 (1994); J.R. Gardner *et al.*, *Phys. Rev. Lett.* **74**, 3764 (1995).
- [12] M.R. Matthews *et al.*, *Phys. Rev. Lett.* **81**, 243 (1998).
- [13] H.M.J.M. Boesten, C.C. Tsai, B.J. Verhaar, and D.J. Heinzen, *Phys. Rev. Lett.* **77**, 5194 (1996).
- [14] M. Marinescu, H.R. Sadeghpour, and A. Dalgarno, *Phys. Rev. A* **49**, 982 (1994).
- [15] A. Derevianko, W.R. Johnson, M.S. Safronova, and J.F. Babb, *Phys. Rev. Lett.* **82**, 3589 (1999).

-
- [16] G. Hadinger and G. Hadinger, *J. Mol. Spectr.* **175**, 441 (1996).
 - [17] N.N. Klausen, J.L. Bohn, and C.H. Greene, preprint arXiv:physics/0104013.
 - [18] C. Fertig and K. Gibble, *Phys. Rev. Lett.* **85**, 1622 (2000).
 - [19] Y. Sortais *et al.*, *Phys. Rev. Lett.* **85**, 3117 (2000).
 - [20] A relation to the d-wave shape resonance was suggested to us by Eric Cornell.
 - [21] E.A. Cornell (priv. commun.)
 - [22] S.H. Patil and K.T. Tang, *J. Chem. Phys.* **106**, 2298 (1996).
 - [23] Y.M. Chan and A. Dalgarno, *Mol. Phys.* **14**, 101 (1968).
 - [24] J.F. Bukta and W.J. Meath, *Mol. Phys.* **27**, 1235 (1974).
 - [25] W. Weickenmeier *et al.*, *J. Chem. Phys.* **82**, 5354 (1985).

Feshbach resonances in rubidium 87: Precision measurement and analysis

A. Marte, T. Volz, J. Schuster, S. Dürr, G. Rempe, E. G. M. van Kempen, and B. J. Verhaar

Published in Phys. Rev. Lett. **89**, 283202 (2002)

More than 40 Feshbach resonances in rubidium 87 are observed in the magnetic-field range between 0.5 and 1260 gauss for various spin mixtures in the lower hyperfine ground state. The Feshbach resonances are observed by monitoring the atom loss, and their positions are determined with an accuracy of 30 mG. In a detailed analysis, the resonances are identified and an improved set of model parameters for the rubidium interatomic potential is deduced. The elastic width of the broadest resonance at 1007 G is predicted to be significantly larger than the magnetic-field resolution of the apparatus. This demonstrates the potential for applications based on tuning the scattering length.

4.1 Introduction

A Feshbach resonance is an exciting tool for controlling the atom-atom interaction in ultracold atomic gases. The elastic s -wave scattering length a can be tuned over orders of magnitude simply by applying a magnetic field. Feshbach resonances have been observed in various alkali atoms [1–7]. They have been used to induce a controlled implosion of a Bose-Einstein condensate (BEC) [8], to create a coherent superposition of an atomic BEC and a molecular state [9], and to realize a bright soliton in a BEC [6, 7]. Future applications could include experiments with the Mott-insulator phase transition [10], a Tonks gas [11], effects beyond the mean-field theory [12], and the creation of a molecular BEC [13]. In addition, the binding energies of ro-vibrational molecular states close to the dissociation threshold can be determined with high accuracy from the position of Feshbach resonances leading to a precise knowledge of the interatomic potential [14]. A Feshbach resonance showing up in elastic collisions is often accompanied by strong changes in the inelastic collision properties [15, 16]. This offers a strategy for searching for new Feshbach resonances by monitoring the resulting atom loss.

Surprisingly, no Feshbach resonance has been observed in ^{87}Rb , which is the isotope used in most of today's BEC experiments. In 1995, a search with atoms in the $|f, m_f\rangle = |1, -1\rangle$ state was carried out, but no resonances were found [17]. Meanwhile various experiments [18–21] greatly improved the knowledge of the Rb interatomic potential. Recent models based on this [22, 23] are consistent with the observations of Ref. [17]. But these models predict four Feshbach resonances in the $|1, 1\rangle$ state.

This letter reports the observation of more than 40 Feshbach resonances in ^{87}Rb with most (but not all) atoms prepared in the $|1, 1\rangle$ ground state. The theoretical model is extended to various spin mixtures and to bound states with rotational quantum number $l \leq 3$. Thus, all except one of the resonances can be clearly identified. Moreover, the measured position of one Feshbach resonance is used for an improved fit of the model parameters. The relative deviation between the predicted and observed positions is 1.6×10^{-3} (rms). The observed loss might be due to two- or three-body inelastic collisions, but should be purely three body for those resonances which involve only the $|1, 1\rangle$ state. The broadest resonance at 1007 G offers the possibility to tune the scattering length and investigate its loss mechanism.

4.2 Experimental method

The experiment is performed with a new setup similar to our previous one [24], but with all relevant components significantly improved. In particular, atoms are captured in a vapor-cell magneto-optical trap (MOT) at a loading rate of $7 \times 10^{10} \text{ s}^{-1}$. The atoms are transferred to a second MOT, in which 6×10^9 atoms are accumulated by multiple transfer within 2 s. The atoms are then loaded into a Ioffe-Pritchard magnetic trap with a lifetime of 170 s. The measured bias-field drift of less than 1 mG/h illustrates the excellent stability of the magnetic trap. After 26 s of evaporative cooling, a BEC with up to 3.6×10^6 atoms is formed in the $|1, -1\rangle$ state.

The $|1, 1\rangle$ state, in which the resonances are predicted, cannot be held in a magnetic trap. Therefore the atoms are now loaded into an optical dipole trap made of a single beam from an Yb:YAG laser at a wavelength of 1030 nm. A laser power of 45 mW is focused to a waist of 15 μm , resulting in measured trap frequencies of 930 Hz and 11 Hz, and an estimated trap depth of $k_B \times 20 \mu\text{K}$.

Once the atoms are in the optical trap, a radio-frequency field is used to transfer the atoms to the desired $|1, 1\rangle$ state. With a Stern-Gerlach method, the fraction of atoms that end up in the $|1, 1\rangle$ state is determined to be roughly 90%. Almost all other atoms are in the $|1, 0\rangle$ state. Next, a homogeneous magnetic field is applied in order to observe a Feshbach resonance. The field is created using the compensation coils of the magnetic trap which are in near-perfect Helmholtz configuration. Up to 1760 A of current are stabilized with a home-built servo to a few ppm. The magnetic field is

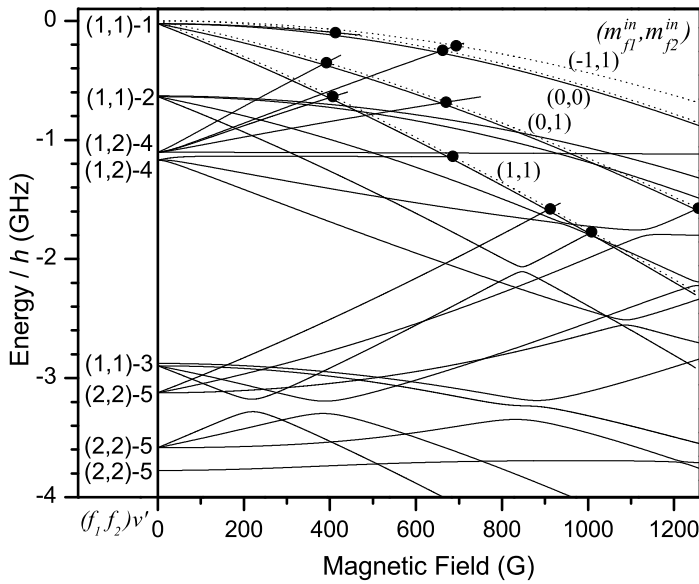


Figure 4.1 $l = 0$ Feshbach resonances in a coupled-channel calculation. Bound-state energies (solid lines) are shown as a function of magnetic field with quantum numbers $(f_1, f_2)v'$ assigned at $B = 0$. Additionally, dissociation threshold energies (dotted lines) are shown for four different entrance channels $(m_{f_1}^{in}, m_{f_2}^{in})$. A Feshbach resonance (●) occurs, when a bound state with quantum number m_F crosses a dissociation threshold with the same m_F .

held at a fixed value for typically 50 ms and then quickly switched off. Although many Feshbach resonances are rapidly crossed when the magnetic field is turned on or off, no significant loss of atoms is observed from these rapid crossings. After switching off the magnetic field, the atoms are released from the optical trap, and 14 ms later an absorption image of the expanded cloud is taken.

The search for Feshbach resonances was typically performed with a purely thermal cloud of 4×10^6 atoms in the optical trap at a temperature of $2 \mu\text{K}$, corresponding to a peak density of $2 \times 10^{14} \text{ cm}^{-3}$. The magnetic-field range between 0.5 and 1260 G was scanned and 43 Feshbach resonances were found. The magnetic-field values of these resonances B_{exp} are listed in Tabs. 4.1 and 4.2. The fields were calibrated with 30 mG precision using microwave spectroscopy in the vicinity of each resonance.

4.3 Theoretical perspective on the 43 Feshbach resonances

In order to analyze these results theoretically, both continuum and bound-state calculations are carried out using an accurate description of the atomic interaction between

two Rb atoms [23]. An introduction to the theory of Feshbach resonances can be found in Refs. [25, 26]. The strong central part of the interaction, consisting of singlet and triplet potentials, conserves the orbital quantum numbers l, m_l and the total-spin magnetic quantum number m_F separately. (In bound-state spectroscopy, l is often called N .) In the ultracold regime, with this part of the interaction included, Feshbach resonances are expected to occur only when an $l = 0$ bound state with a certain value of m_F crosses the dissociation threshold of an entrance channel with the same m_F . Figure 4.1 shows these crossings in the E - B plane as solid dots along various $(m_{f_1}^{in}, m_{f_2}^{in})$ thresholds. The resonance fields obtained from these bound-state calculations are listed in Tabs. 4.1 and 4.2 ($l = 0$ quantum number). The same field values also follow from the B -dependence of the elastic S -matrix element, as obtained in a continuum calculation.

In Fig. 4.1, the bound states are labelled $(f_1, f_2)v'$, with the vibrational quantum number $v' = -1, -2, -3, \dots$ counting from the corresponding (f_1, f_2) threshold. At $B = 0$, the exchange interaction couples the atomic spins f_1, f_2 to a total molecular spin F and causes a splitting between states with the same $(f_1, f_2)v'$ but different F . In the presence of a strong external magnetic field, however, m_{f_1} and m_{f_2} become good quantum numbers instead of F , while m_F is always a good quantum number. What constitutes a strong field in this sense depends on the size of the F -splitting at $B = 0$. For small $|v'|$, the F -splitting is hardly visible in Fig. 4.1.

The much weaker spin-spin interaction V_{ss} consists of the magnetic dipole-dipole interaction of the valence electrons together with a second-order spin-orbit term [27]. Because of its tensor form it breaks the spatial spherical symmetry and allows a redistribution between the angular momenta of the spin and spatial degrees of freedom so that the sum $m_l + m_F$ is the only conserved quantum number. V_{ss} admixes an $l = 0$ component in otherwise pure $l = 2$ bound states and therefore induces additional s -wave Feshbach resonances in the ultracold regime. Resonances of this type have previously been observed in Cs [14], but up to now never in ^{85}Rb or ^{87}Rb . The resulting resonance fields are again listed in the tables ($l = 2$ resonances). For clarity, the $l = 2$ bound states and resonances have been left out in Fig. 4.1. For mixed species resonances, such as $|1, 0\rangle \otimes |1, 1\rangle$, the $l = 1$ partial wave can be populated in the entrance channel, thus opening up the possibility to observe resonances due to $l = 1$ or $l = 3$ bound states.

4.4 Fine-tuning the interaction parameters

The set of potential parameters used in this calculation is obtained as follows. The field value 911.74 G of one resonance is added to the set of eight experimental data already included in the analysis of Ref. [23]. This particular resonance was chosen, because the corresponding bound state is a pure triplet state and the previous experimental constraints on the singlet potential [20] are much stronger than those on the triplet

potential. Then, a least-squares analysis is applied with the column A parameters of Tab. I in Ref. [23] as starting values. This leads to an adjusted set of parameter values differing from the starting values by less than 1σ ; in atomic units: $C_6 = 4.707 \times 10^3$, $C_8 = 5.73 \times 10^5$, $C_{10} = 7.665 \times 10^7$ (Ref. [28]), $J = 0.486 \times 10^{-2}$, $a_S(^{87}\text{Rb}) = +90.6$, $a_T(^{87}\text{Rb}) = +98.96$, $v_{DS}(^{87}\text{Rb}) = 0.454$, and $v_{DT}(^{87}\text{Rb}) = 0.4215$. Coupled-channel calculations [25,26] based on these fine-tuned parameters then yield theoretical resonance fields B_{th} . The relative deviation of all these positions from the observations is 1.6×10^{-3} (rms). Compared to the four resonance positions predicted in [23], this is an improvement of a factor of 6. Since only one resonance position was included in the fit, the excellent agreement with all other positions demonstrates the accuracy of the model. Note that the observed position of maximum loss might deviate from the pole of the elastic scattering length [29]. However, such deviations are typically not larger than the elastic widths of the resonances; and they are small as discussed below.

4.5 Discussing the experimental results

Some resonances are so close together that they cannot be identified merely from their positions. In these cases, a Stern-Gerlach method was used to experimentally determine which m_f states incurred the strongest atom loss. Thus the entrance channel could be clearly identified, in particular when additionally varying the initial spin mixture. The entrance channel of the non-identified resonance at 1236.73 G was also determined with this method.

An interesting property of a Feshbach resonance – besides its position – is its strength. The strength of the elastic resonance is proportional to the field width Δ over which the scattering length has opposite sign [26], as listed in Tab. 4.1. The strength of the inelastic scattering properties is quantified by the loss rate. The dominant loss for the resonances in Tab. 4.1 arises from inelastic three-body collisions. This is because for the parameters of the experiment, single-body loss is negligible; and since the $|1, 1\rangle$ entrance channel is the absolute ground state of atomic ^{87}Rb , inelastic two-body collisions cannot occur [15]. (This is not the case for the resonances in Tab. 4.2.) The three-body loss is characterized by the coefficient K_3 in the rate equation $\dot{N} = -K_3 \langle n^2 \rangle N$, where N is the atom number and n the density. The depth d listed in Tab. 4.1 is a nonlinear, yet monotonic function of K_3 . In Tab. 4.1, one finds a clear trend that stronger resonances with larger Δ cause faster loss, i.e. larger d . This is plausible, although the theory of three-body losses is not yet fully understood, especially in the vicinity of Feshbach resonances [26,29].

Interestingly, the widths Δ of the $l = 0$ resonances in Tab. 4.1 are much smaller than for other alkali atoms [4, 5, 15, 21]. This is due to the approximate phase equality of the waves reflected from the short-range singlet and triplet potentials, that is also

responsible for other remarkable ^{87}Rb phenomena: the coexistence of condensates in different hyperfine states [18] and the smallness of the fountain-clock frequency shift [23].

All resonances display a nearly symmetric loss feature. A Gaussian is fit to the atom loss at a 50-ms hold time in order to extract the depth and the width of the atom loss. The Gaussian was chosen for convenience and because it fits well to the data. The obtained rms widths are between 20 and 100 mG for almost all resonances. For small d , this width is identical to the width of the resonance in K_3 (if two-body loss is absent). For large d , however, the nonlinear dependence of d on K_3 broadens the observed width at a given hold time, somewhat similar to saturation broadening of spectral lines. In addition, the finite temperature of the cloud gives rise to a broadening of typically 20 mG and leads to a shift of similar size. The observed rms width of 24(4) mG at 965.96 G sets an experimental upper limit to thermal and technical broadening.

The broadest resonance is centered at 1007 G (see Fig.4.2). The theoretical prediction for its elastic width, $\Delta = 170(30)$ mG, is large compared to the above-mentioned upper bound on the experimental broadening of 24(4) mG. This demonstrates the potential for a controlled variation of the scattering length with the present setup.

For various field values, the decay of the atom number was also measured as a function of time. If one assumes that the loss can be described by a rate equation, three-body loss dominates (see above). Values of K_3 determined from a fit are shown in Fig. 4.2. Note that the value $K_3 = 3.2(1.6) \times 10^{-29} \text{ cm}^6\text{s}^{-1}$ obtained away from the resonance is consistent with the measured value $K_3 = 4.3(1.8) \times 10^{-29} \text{ cm}^6\text{s}^{-1}$ for the $|1, -1\rangle$ state [30]. The absence of two-body loss makes this resonance an ideal candidate for testing theories of three-body loss [29]. The values of K_3 in Fig. 4.2 are much smaller than those for ^{85}Rb [16], where exciting experiments have been performed [8,9]. Three-body loss will therefore not be a substantial problem for applications.

All data obtained here fit well to a three-body decay, but the initial atom number extrapolated from the fit is a factor of up to 2 lower at the 1007 G resonance as compared to the off-resonance value. Since no data were taken for hold times shorter than 10 ms, this observation suggests the existence of an additional loss mechanism acting on much faster timescales. This could be related to molecule formation and dissociation when suddenly switching the magnetic field on and off [31]. Note, however, that here loss from a purely thermal cloud is observed, while loss from a BEC is discussed in Ref. [31].

4.6 Conclusions

To summarize, more than 40 Feshbach resonances have been observed in ^{87}Rb . All except one were identified by theory. After including one of the observed resonances in

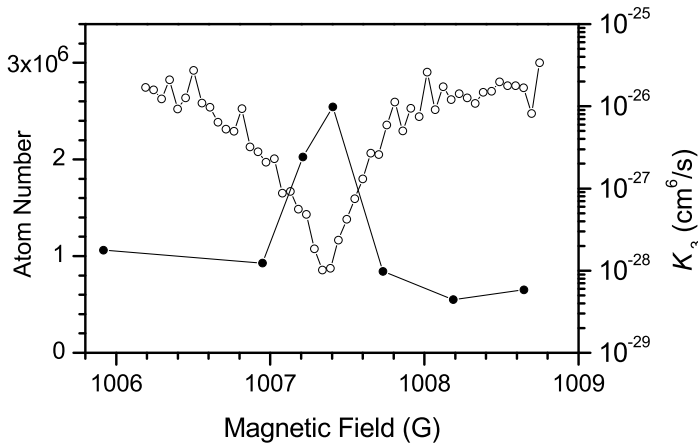


Figure 4.2 Asymmetric shape of the broadest Feshbach resonance. The number of atoms (\circ) remaining in the trap after a 50 ms-hold time is displayed as a function of magnetic field. The three-body loss rate coefficient K_3 is also shown (\bullet).

fitting the model parameters, theory and experiment are in excellent agreement. The magnetic field control is so accurate that it should be possible to resolve changes in the elastic scattering length on the broadest resonance at 1007 G.

Acknowledgement

The work in Garching is supported by the European-Union network “Cold Quantum Gases”, the DFG-Forschergruppe “Quantengase”, and GIF. The work at Eindhoven is part of the research program of the Stichting FOM, which is financially supported by NWO.

References

- [1] S. Inouye *et al.*, Nature (London) **392**, 151 (1998).
- [2] P. Courteille *et al.*, Phys. Rev. Lett. **81**, 69 (1998).
- [3] J. Roberts *et al.*, Phys. Rev. Lett. **81**, 5109 (1998).
- [4] V. Vuletic *et al.*, Phys. Rev. Lett. **82**, 1406 (1999).
- [5] T. Loftus *et al.*, Phys. Rev. Lett. **88**, 173201 (2002).
- [6] L. Khaykovich *et al.*, Science **296**, 1290 (2002).
- [7] K. Strecker *et al.*, Nature (London) **417**, 150 (2002).
- [8] E. Donley *et al.*, Nature (London) **412**, 295 (2001).
- [9] E. Donley *et al.*, Nature (London) **417**, 529 (2002).

- [10] M. Greiner *et al.*, Nature (London) **415**, 39 (2002).
- [11] M. Girardeau and E. Wright, Laser Physics **12**, 8 (2002).
- [12] F. Dalfovo *et al.*, Rev. Mod. Phys. **71**, 463 (1999).
- [13] S. Kokkelmans, H. Visser, and B. Verhaar, Phys. Rev. A **63**, 31601 (2001); M. Mackie physics/0202041.
- [14] C. Chin *et al.*, Phys. Rev. Lett. **85**, 2717 (2000); P. Leo, C. Williams, and P. Julienne, *ibid.* **85**, 2721 (2000).
- [15] J. Stenger *et al.*, Phys. Rev. Lett. **82**, 2422 (1999).
- [16] J. Roberts *et al.*, Phys. Rev. Lett. **85**, 728 (2000).
- [17] N. Newbury, C. Myatt, and C. Wieman, Phys. Rev. A **51**, 2680 (1995).
- [18] C. Myatt *et al.*, Phys. Rev. Lett. **78**, 586 (1997).
- [19] R. Wynar *et al.*, Science **287**, 1016 (2000).
- [20] J. Seto *et al.*, J. Chem. Phys. **113**, 3067 (2000).
- [21] J. Roberts *et al.*, Phys. Rev. A **64**, 24702 (2001).
- [22] J. Vogels *et al.*, Phys. Rev. A **56**, 1067 (1997).
- [23] E. van Kempen *et al.*, Phys. Rev. Lett. **88**, 93201 (2002).
- [24] U. Ernst *et al.*, Europhys. Lett. **41**, 1 (1998).
- [25] D. Heinzen, in *Proceedings of the International School of Physics "Enrico Fermi", Course CXL*, edited by M. Inguscio *et al.* IOS Press, Amsterdam, (1999), p. 351.
- [26] J. Burke, Ph.D. thesis, University of Colorado, 1999, available at <http://amo.phy.gasou.edu/bec.html/bibliography.html>.
- [27] M. Mizushima, *The theory of rotating diatomic molecules* Wiley, New York, (1975), p. 223; F. Mies *et al.*, J. Res. Natl. Inst. Stand. Technol. **101**, 521 (1996).
- [28] M. Marinescu, H. Sadeghpour, and A. Dalgarno, Phys. Rev. A **49**, 982 (1994).
- [29] P. Fedichev, M. Reynolds, and G. Shlyapnikov, Phys. Rev. Lett. **77**, 2921 (1996); F. van Abeelen and B. Verhaar, *ibid.* **83**, 1550 (1999); E. Nielsen and J. Macek, *ibid.* **83**, 1566 (1999); B. Esry, C. Greene, and J. Burke, *ibid.* **83**, 1751 (1999); E. Braaten and H. Hammer, *ibid.* **87**, 160407 (2001).
- [30] E. Burt *et al.*, Phys. Rev. Lett. **79**, 337 (1997).
- [31] N. Claussen *et al.*, Phys. Rev. Lett. **89**, 10401 (2002); S. Kokkelmans and M. Holland cond-mat/0204504; R. Duine and H. Stoof cond-mat/0204529; M. Mackie, K. Suominen, and J. Javanainen cond-mat/0205535.

Table 4.1 Feshbach resonances in the $|1, 1\rangle \otimes |1, 1\rangle$ entrance channel. The experimentally observed positions B_{exp} are compared with the theoretical predictions B_{th} calculated at $2 \mu\text{K}$. Also shown are the observed depths d , defined as the fraction of atoms lost during a 50 ms-hold time. Note that the presence of atoms in spin states other than $|1, 1\rangle$ prevents d from reaching 100%. For comparison, theoretical results for the elastic widths Δ of the resonances are listed. The last columns list the quantum numbers of the (quasi) bound state that gives rise to the resonance. Some very weak $l = 2$ resonances could not be detected experimentally.

$B_{\text{exp}}(\text{G})$	$B_{\text{th}}(\text{G})$	$d(\%)$	$\Delta(\text{mG})$	$l(f_1, f_2)v', m_F$	F	m_{f_1}, m_{f_2}
406.23	406.6	57	0.4	0(1,2)-4, 2		0,2
685.43	685.8	78	17	0(1,2)-4, 2		1,1
911.74	911.7	72	1.3	0(2,2)-5, 2	4	
1007.34	1008.5	64	170	0(2,2)-5, 2	2	
...	377.2	...	$\ll 0.1$	2(1,1)-2, 0		-1,1
...	395.0	...	$\ll 0.1$	2(1,1)-2, 0		0,0
856.85	857.6	< 10	$\ll 0.1$	2(1,1)-2, 1	2	0,1
...	249.1	...	$\ll 0.1$	2(1,2)-4, 1		-1,2
306.94	306.2	34	$\ll 0.1$	2(1,2)-4, 0		-1,1
319.30	319.7	54	< 0.1	2(1,2)-4, 2		0,2
387.25	388.5	53	< 0.1	2(1,2)-4, 1		0,1
391.49	392.9	63	0.3	2(1,2)-4, 3	3	1,2
532.48	534.2	57	< 0.1	2(1,2)-4, 0		0,0
551.47	552.0	66	0.2	2(1,2)-4, 2		1,1
819.38	819.3	29	< 0.1	2(1,2)-4, 1		1,0
632.45	632.5	77	1.5	2(2,2)-5, 4	4	2,2
719.48	719.5	77	0.5	2(2,2)-5, 3	4	1,2
831.29	831.3	67	0.2	2(2,2)-5, 2	4	
930.02	930.9	78	< 0.1	2(2,2)-5, 2	2	
978.55	978.3	36	< 0.1	2(2,2)-5, 1	4	
1139.91	1140.9	10	$\ll 0.1$	2(2,2)-5, 1	2	
...	1176.1	...	$\ll 0.1$	2(2,2)-5, 0	4	

Table 4.2 Experimentally observed Feshbach resonances in other entrance channels $|1, m_{f1}^{in}\rangle \otimes |1, m_{f2}^{in}\rangle$.

$B_{\text{exp}}(\text{G})$	$B_{\text{th}}(\text{G})$	$l(m_{f1}^{in}, m_{f2}^{in})$	$B_{\text{exp}}(\text{G})$	$B_{\text{th}}(\text{G})$	$l(m_{f1}^{in}, m_{f2}^{in})$
391.08	391.7	0(0,1)	825.11	825.1	3(0,1)
417.20	417.7	2(0,1)	965.96	966.0	1(0,1)
535.01	536.6	2(0,1)	1137.97	1135.5	1(0,1)
548.60	550.7	2(0,1)	414.34	413.6	0(0,0)
669.19	670.7	0(0,1)	661.43	662.2	0(0,0)
802.94	805.0	2(0,1)	729.43	728.5	2(0,0)
821.04	821.7	2(0,1)	760.73	762.1	2(0,0)
840.95	841.0	2(0,1)	1167.14	1167.1	2(0,0)
981.54	981.7	2(0,1)	1208.69	1209.4	2(0,0)
1162.15	1162.5	2(0,1)	1252.68	1254.9	2(0,0)
1236.73	...	-(0,1)	692.75	693.6	0(-1,1)
1237.19	1238.1	2(0,1)	1216.32	1216.6	2(-1,1)
1256.96	1257.1	0(0,1)			

Radio-Frequency Spectroscopy of Ultracold Fermions

S. Gupta, Z. Hadzibabic, M.W. Zwierlein, C.A. Stan, K. Dieckmann, C.H. Schunck, E.G.M. van Kempen, B.J. Verhaar and W. Ketterle

Published in *Science* **300**, 1726 (2003)

Radio-frequency techniques were used to study ultracold fermions. We observed the absence of mean-field “clock” shifts, the dominant source of systematic error in current atomic clocks based on bosonic atoms. This absence is a direct consequence of fermionic antisymmetry. Resonance shifts proportional to interaction strengths were observed in a three-level system. However, in the strongly interacting regime, these shifts became very small, reflecting the quantum unitarity limit and many-body effects. This insight into an interacting Fermi gas is relevant for the quest to observe superfluidity in this system.

5.1 Introduction

Radio-frequency (RF) spectroscopy of ultracold atoms provides the standard of time. However, the resonance frequencies are sensitive to the interactions between atoms, leading to the so-called clock shifts of the unperturbed resonances [1]. These shifts limit the accuracy of current atomic clocks [2, 3], but can also be used to characterize atomic interactions.

RF spectroscopy has previously been applied to cold atoms to determine the size and temperature of atom clouds [4, 5]. RF methods have also been used for evaporative cooling, for preparing spinor Bose-Einstein condensates (BEC) [6, 7], and as an output coupler for atom lasers [5, 8]. In all these experiments, shifts and broadenings due to atomic interactions were negligible. Recently, density-dependent frequency shifts of RF transitions were observed in rubidium [9] and sodium [10] BECs. These frequency shifts are proportional to the difference in mean-field energies of two internal atomic states and allow scattering lengths to be extracted. Mean field shifts in BECs have been observed also by optical spectroscopy [11, 12].

Here, we apply RF spectroscopy to ultracold clouds of fermions and demonstrate several phenomena: (1) the absence of a clock shift in a two-level system because of

fermionic antisymmetry, (2) the emergence of mean-field shifts in a three-level system after the relaxation of pair correlations, (3) the limitation of mean-field shifts because of the unitarity limit, and (4) the universality of the interaction energy in a dense cloud, independent of the attractive or repulsive nature of the two-particle interactions.

Research in ultracold fermions has advanced rapidly, with six groups now having cooled fermions into quantum degeneracy [13–18]. A major goal of this research is to induce strong interactions by tuning magnetic fields to scattering resonances (called Feshbach resonances). Under these conditions, Cooper pairs of fermions may form, leading to superfluidity. This would establish a model system for studying Bardeen-Cooper-Schrieffer (BCS) pairing at densities nine orders of magnitude lower than in previous realizations in ^3He and superconductors. We show that RF spectroscopy can be used to characterize interactions between fermions in the regime where superfluidity has been predicted [19, 20].

5.2 Experimental techniques

Our experimental technique for preparing ultracold fermions has been considerably improved since our earlier work [17, 21]. Because the Pauli exclusion principle suppresses elastic collisions between identical fermions at low temperatures and prevents evaporative cooling, we cooled fermionic ^6Li sympathetically with bosonic ^{23}Na loaded into the same magnetic trap. In contrast to previous work, we cooled both species in their upper hyperfine states ($^{23}\text{Na}: |F, m_F\rangle = |2, +2\rangle$, $^6\text{Li}: |F, m_F\rangle = |3/2, +3/2\rangle$), where F and m_F are the quantum numbers for the total spin and its z component respectively. This led to a reduction of inelastic loss processes, boosting our final fermion atom numbers by two orders of magnitude. We could produce BECs that contained up to 10 million sodium atoms in the $|2, +2\rangle$ state by evaporatively cooling pure bosonic samples in the magnetic trap. For a Bose-Fermi mixture, the finite heat capacity of the bosons limited the final lithium temperature after the 30 s evaporation cycle to $\sim 0.3 T_F$ for 10 million fermions and $\sim T_F$ for 50 million fermions [22], where T_F is the Fermi temperature.

The spin states of ^6Li of most interest for superfluid pairing are the two lowest states $|1\rangle$ and $|2\rangle$ ($|1/2, +1/2\rangle$ and $|1/2, -1/2\rangle$ at low field), which are predicted to have an inter-state s-wave Feshbach resonance at ~ 800 G [24, 25]. However, both states are high-field seeking at these fields, which makes them unsuitable for magnetic trapping. We therefore transferred the atoms into an optical trap. For these experiments, 6 to 8 million $|3/2, +3/2\rangle$ lithium atoms were loaded into the optical trap at $T \sim T_F \sim 35 \mu\text{K}$ [26]. The atoms were then transferred to the lowest energy state $|1\rangle$, with an adiabatic frequency sweep around the lithium hyperfine splitting of 228 MHz. Magnetic fields of up to ~ 900 G were applied, a range encompassing the $|1\rangle - |2\rangle$ Feshbach resonance.

Using RF-induced transitions near 80 MHz, we could create mixtures of states $|1\rangle$, $|2\rangle$ and $|3\rangle$ ($|3/2, -3/2\rangle$ at low field), and explore interactions between fermions in these states.

5.3 Absence of clock shift

Collisions between atoms cause a shift of their energy, which is usually described by the mean-field effect of all the other atoms on the atom of interest. For example, atoms in state $|2\rangle$ experience an energy shift $\frac{4\pi\hbar^2}{m}n_1a_{12}$ due to the presence of atoms in state $|1\rangle$. Here \hbar is Planck's constant divided by 2π , m is the mass of the atom, n_1 is the density of $|1\rangle$ atoms and a_{12} is the interstate scattering length. We use the convention that positive scattering length corresponds to a repulsive interaction. Density-dependent shifts of the resonance frequency for the transition that connects two states have been observed in laser-cooled $[1]$ and Bose-condensed clouds $[9,10]$.

In the case of ultracold fermions, only interactions between different internal states are allowed. For a system of density n , let us compare the energy of a gas prepared purely in state $|1\rangle$, to a gas in which one atom is transferred into state $|2\rangle$. The energy difference is $h\nu_{12} + \frac{4\pi\hbar^2}{m}na_{12}$, where ν_{12} is the resonance frequency of the non-interacting system. Similarly, the energy difference between a gas prepared purely in state $|2\rangle$, and a gas in which one atom is transferred into state $|1\rangle$ is $h\nu_{12} - \frac{4\pi\hbar^2}{m}na_{12}$.

However, these energy shifts should not affect the resonance for a coherent transfer out of a pure state. For fermions in the initial pure state, the pair-correlation function vanishes at zero distance because of the antisymmetry of the wavefunction. During any coherent transfer process, the state vectors of all the atoms rotate "in parallel" in Hilbert space, i.e. the superposition of the two spin states has the same relative phase for all atoms. Thus, the atoms remain identical and cannot interact in the s-wave regime. The mean-field energy is thus established only after the coherence of the superposition state is lost and the pair correlations have relaxed, forming a purely statistical mixture of the two states.

It is a consequence of Fermi statistics that spectroscopic methods do not measure the equilibrium energy difference between the initial and final state of the system, but rather measure the unperturbed resonance frequency. The expected absence of the clock shift has led to suggestions for the use of fermions in future atomic clocks $[27]$. Our work presents an experimental demonstration of this phenomenon.

We determined the transition frequency between states $|1\rangle$ and $|2\rangle$, first starting with a pure state $|1\rangle$, and then with a pure state $|2\rangle$ sample. The absence of a splitting between these two lines proves the suppression of the clock shift. Fig. 5.1 shows an example of such measurements. The magnetic field was ramped up to 570 G with the cloud in state $|1\rangle$. At this field, $a_{12} \sim 150a_0$. Therefore, the expected equilibrium

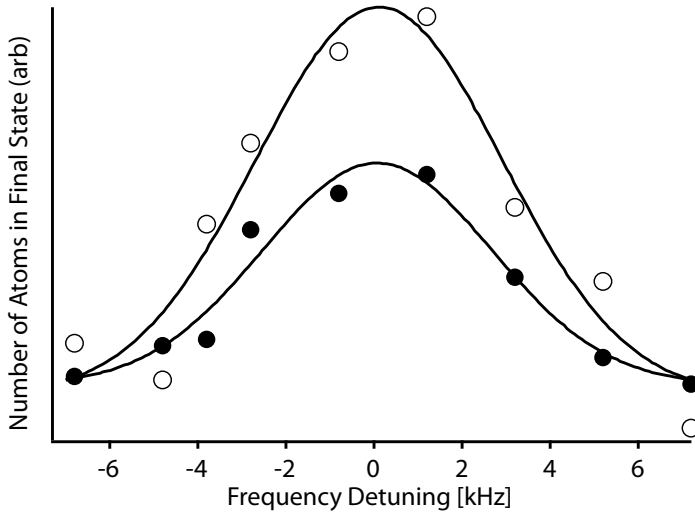


Figure 5.1 Absence of the clock shift. RF transitions were driven between states $|1\rangle$ and $|2\rangle$ on a system prepared purely in state $|1\rangle$ (solid circles), and purely in state $|2\rangle$ (open circles). Mean-field interactions would have resulted in 5 kHz shifts for the two curves in opposite directions. Gaussian fits (solid lines) to the data are separated by 0.04 ± 0.35 kHz. This gives a clock-shift suppression factor of 30. Arb., arbitrary units.

mean-field shifts were $\Delta\nu = \pm 5$ kHz for our mean density of $3 \times 10^{13} \text{ cm}^{-3}$ [28]. The interaction between states $|1\rangle$ and $|2\rangle$ at this magnetic field was also observed in the mutual evaporative cooling of the two states in the optical trap. RF pulses of $140 \mu\text{s}$ duration were applied at frequencies near the unperturbed resonance $\nu_{12} \sim 76$ MHz. Atoms in states $|1\rangle$ and $|2\rangle$ could be monitored separately by absorption imaging, because they are optically resolved at this field. We observed a suppression of the clock shift by a factor of 30 (Fig. 5.1). Using the same method, we observed the absence of the clock shift at several other magnetic fields. In particular, we observed a suppression of more than three orders of magnitude at ~ 860 G [29].

P-wave interactions [23] could lead to a nonvanishing clock shift. However, at these low temperatures, they are proportional to T or T_F , whichever is higher, and are therefore strongly suppressed.

5.4 Measurement of $a_{12} - a_{13}$

We can measure mean-field shifts and scattering lengths spectroscopically by driving transitions from a statistical mixture of two states to a third energy level. (While this work was in progress, use of a similar method to measure scattering lengths in fermionic ^{40}K was reported [30].) Specifically, we recorded the difference between the RF spectra

for the $|2\rangle \rightarrow |3\rangle$ transition in the presence and in the absence of state $|1\rangle$ atoms. The presence of atoms in state $|1\rangle$ is then expected to shift the resonance by [31]:

$$\Delta\nu = \frac{2\hbar}{m}n_1(a_{13} - a_{12}) \quad (5.1)$$

In our experimental scheme to determine the interaction energy at different magnetic fields (Fig. 5.2), the system was prepared by ramping up the magnetic field to 500 G with the atoms in state $|1\rangle$. Either partial or complete RF transfer to state $|2\rangle$ was then performed. The number of atoms in state $|1\rangle$ was controlled by adjusting the speed of a frequency sweep around the $|1\rangle \rightarrow |2\rangle$ resonance. A fast, non-adiabatic sweep created a superposition of the two states, whereas a slow, adiabatic sweep prepared the sample purely in state $|2\rangle$. A wait time of 200 ms was allowed for the coherence between states $|1\rangle$ and $|2\rangle$ to decay and the system to equilibrate.

Typical parameters for the decohered $|1\rangle - |2\rangle$ mixture were mean-density $n_1 \sim 2.4 \times 10^{13} \text{ cm}^{-3}$ and $T \sim 0.7 T_F$. The magnetic field was then changed to the desired value, and the transition from state $|2\rangle$ to state $|3\rangle$ was driven with $140 \mu\text{s}$ RF pulses [Fig. 5.2(C)]. We monitored the appearance of atoms in state $|3\rangle$ and the disappearance of atoms from state $|2\rangle$, using simultaneous absorption imaging. Fig. 5.2(D) shows the unperturbed and perturbed resonances at the magnetic field $B = 480 \text{ G}$. The position of the unperturbed resonance ν_{23} also determines the magnetic field to an accuracy of $< 0.1 \text{ G}$. Fig. 5.2(E) shows absorption images of atoms in state $|3\rangle$, obtained for different values of the applied radio-frequency. One can clearly see the spatial dependence and thus the density dependence of the mean-field shift: Close to the unperturbed resonance, the low density wings of the cloud are predominantly transferred, whereas the high-density central part of the cloud is transferred only at sufficient detuning. To suppress spurious effects from this spatial dependence, only a small central part of the images was used to extract the transferred atomic fraction.

To ensure that our mean-field measurements were performed on a statistical mixture, we measured the timescale for decoherence in our system. The decay of the $|1\rangle - |2\rangle$ coherence at 500 G was observed by monitoring the $|2\rangle \rightarrow |3\rangle$ transfer at the measured unperturbed resonance ν_{23} , as a function of wait time (Fig. 5.3). For wait times that are small compared to the decoherence time of the $|1\rangle - |2\rangle$ superposition, the $|2\rangle \rightarrow |3\rangle$ RF drive places each atom in an identical three-state superposition. All mean-field shifts are then absent and the resulting transfer is unchanged from the unperturbed case. For longer wait times, the $|1\rangle - |2\rangle$ superposition decoheres and mean-field interactions set in. This shifts the resonance frequency of the $|2\rangle \rightarrow |3\rangle$ transition, reducing the transferred fraction at ν_{23} . The measured decoherence time of $\sim 12 \text{ ms}$ was attributed mainly to the sensitivity of ν_{12} to magnetic field variations across the cloud. These inhomogeneities cause the relative phase of the $|1\rangle - |2\rangle$

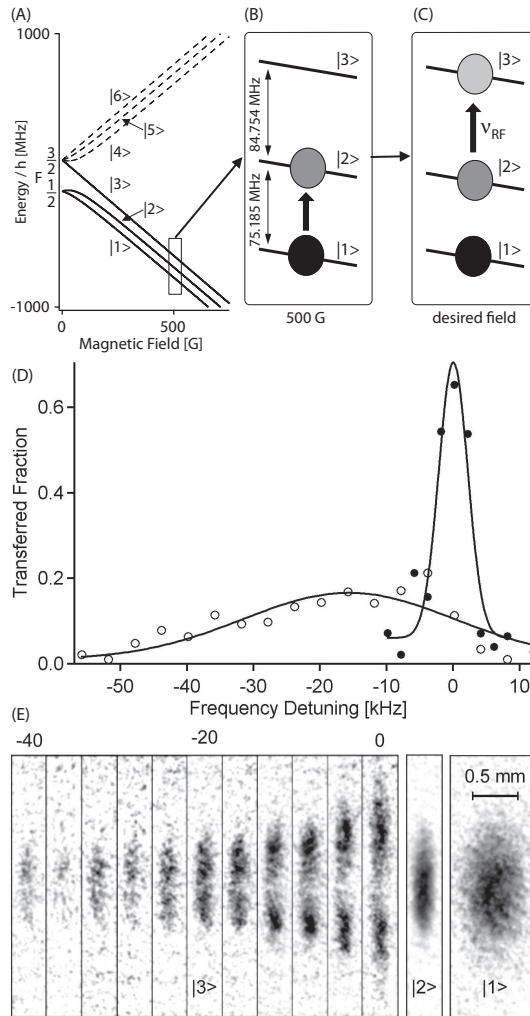


Figure 5.2 Schematic of the mean-field measurement and representative spectra at 480G. (A) Hyperfine structure of the ground state of ${}^6\text{Li}$. (B and C) Experimental scheme: (B) preparation of a mixture of atoms in states $|1\rangle$ and $|2\rangle$, and (C) RF spectroscopy of the $|2\rangle \rightarrow |3\rangle$ transition using a variable radio frequency (ν_{RF}). (D) The fraction of atoms transferred from $|2\rangle$ to $|3\rangle$, with $|1\rangle$ atoms absent (solid circles), and present (open circles). The mean-field shift is computed from gaussian fits to the data (solid lines). (E) Spatial images of state $|3\rangle$ for the perturbed resonance. The optical trap was turned off immediately after the RF pulse and absorption images of the atoms were taken after $120 \mu\text{s}$ expansion time. The central section of $\sim 150 \mu\text{m}$ vertical extent was used to extract the transferred fractions in (D). (E) also shows images of states $|2\rangle$ and $|1\rangle$ for zero RF detuning. States $|3\rangle$ and $|2\rangle$ were imaged simultaneously to observe their complementary spatial structure. State $|1\rangle$ was imaged after $760 \mu\text{s}$ expansion time to record its density for normalization purposes.

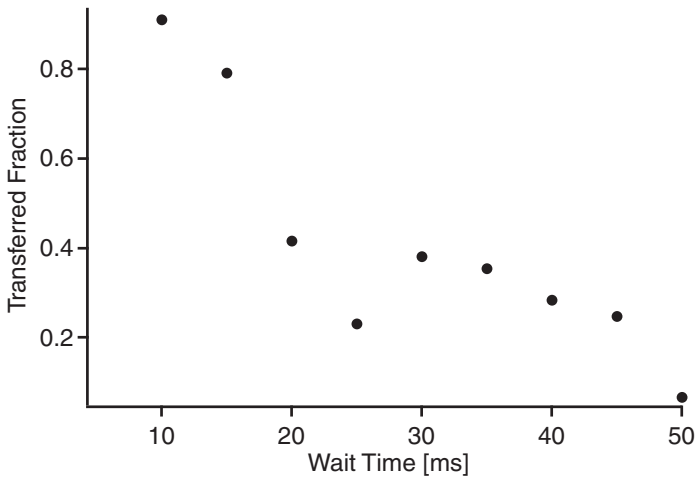


Figure 5.3 Emergence of mean-field shifts due to decoherence at 500 G. Decoherence leads to a reduction of the $|2\rangle \rightarrow |3\rangle$ transfer at the unperturbed resonance ν_{23} . An exponential fit to the data (solid line) gives a time constant of 12 ms.

superposition in different parts of the trap to evolve at different rates, given by the local ν_{12} . Atoms that travel along different paths within the trap therefore acquire different phases between their $|1\rangle$ and $|2\rangle$ components. Being no longer in identical states, s-wave interactions between them are allowed. The inhomogeneities scale with B , whereas the sensitivity of the transition scales with $\partial\nu_{12}/\partial B$. We would thus expect the decoherence time to vary inversely with the product of these two quantities. Our hypothesis is supported by our observation of longer decoherence times at higher fields, where $B \times \partial\nu_{12}/\partial B$ is lower.

Fig. 5.4(A) summarizes the results of our mean-field measurements for a wide range of magnetic fields up to 750 G. For magnetic fields up to 630 G, our data can be explained fairly well using Eq. 5.1 with the theoretical calculations of the scattering lengths shown in Fig. 5.4(B), and an effective density of $n_1 = 2.2 \times 10^{13} \text{ cm}^{-3}$, which is consistent with the initial preparation of the system at 500 G. A narrow resonance of a_{12} at ~ 550 G [21, 25, 32] is indicated by the data, but was not fully resolved. We also see additional structure near 470 G, which is not predicted by theory and deserves further study.

For fields above 630 G, the measured shifts strongly deviate from the predictions of Eq. 5.1, indicating a different regime of interactions. In the region between 630 G and 680 G, the two scattering lengths are expected to be large and positive, with $a_{13} \gg a_{12}$ [Fig. 5.4(B)]. Eq. 5.1 would thus predict large positive mean-field shifts. In contrast, we observe very small shifts, indicating almost perfect cancellation of the

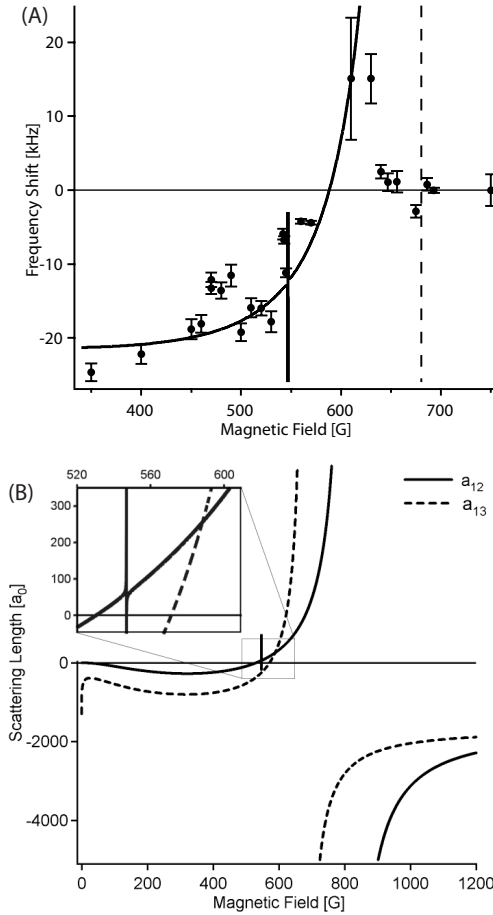


Figure 5.4 Spectroscopic measurement of interaction energy. (A) Frequency shift versus magnetic field for the $|2\rangle \rightarrow |3\rangle$ resonance due to atoms in state $|1\rangle$. The shifts are computed by monitoring the arrival fraction in state $|3\rangle$ for $140\mu\text{s}$ RF pulses, except at 750 G. At 750G, because of strong inelastic losses between $|3\rangle$ and $|1\rangle$ atoms, we monitored the loss of atoms in state $|2\rangle$ after applying RF sweeps of 3 ms duration and 2 kHz width. All the data points are normalized to the same atom number in state $|1\rangle$. The fit at low fields (solid line) uses Eq. 5.1 with $n_1 = 2.2 \times 10^{13} \text{ cm}^{-3}$ and the theoretical calculations of the scattering lengths. The error bars reflect uncertainty in the state $|1\rangle$ atom number, and the uncertainty in the gaussian fits to the spectra. The dashed line indicates the position of the predicted a_{13} resonance. (B) S -wave scattering lengths a_{12} and a_{13} as a function of magnetic field, obtained from a highly model-independent quantum scattering calculation. The calculation makes use of the presently available ${}^6\text{Li}$ experimental data [40] in a coupled channel approach to deduce accumulated phases that characterize the less well-known, short-range parts of the ${}^6\text{Li} + {}^6\text{Li}$ scattering potential [32]. a_{12} has a narrow Feshbach resonance at 550 G and a wide one at 810 G. a_{13} has a wide Feshbach resonance at 680 G.

two contributions. We also observe essentially no mean-field shifts between 680 G and 750 G, where the two scattering lengths are predicted to be very large in magnitude and of opposite signs, and in a simple picture should add up to a huge negative shift. These results are evidence for new phenomena in a strongly interacting system, where the scattering length becomes comparable to either the inverse wavevector of interacting particles, or the interatomic separation.

5.5 Role of unitarity

Eq. 5.1 is valid only for low energies and weak interactions, where the wave vector of the two particles, k , satisfies $k \ll 1/|a|$. For arbitrary values of ka , the s-wave interaction between two atoms is described by replacing the scattering length a with the complex scattering amplitude:

$$f = \frac{-a}{1 + k^2 a^2} (1 - ika) \quad (5.2)$$

The real part of f , $\text{Re}(f)$ determines energy shifts, and hence the ground state properties of an interacting many-body system. The imaginary part, $\text{Im}(f)$ determines the (inverse) lifetime for elastic scattering out of a momentum state, and hence the dynamic properties of the system such as thermalization rates. For $k|a| \rightarrow \infty$, the elastic cross-section $\sigma = 4\pi\text{Im}(f)/k$ monotonically approaches the well known “unitarity limited” value of $4\pi/k^2$. On the other hand, the two particle contribution to the mean-field energy, proportional to $-\text{Re}(f) = a/(1 + k^2 a^2)$, peaks at $|a| = 1/k$, and then, counter-intuitively, decreases as $1/|a|$ for increasing $|a|$. Averaging $\text{Re}(f)$ over a zero-temperature Fermi distribution with Fermi momentum $\hbar k_F$, limits its absolute value to $1.05/k_F$, and markedly weakens its dependence on the exact value of a in the $k_F|a| > 1$ regime [33]. This results in a prediction for the mean-field energy that is sensitive to the sign of the scattering length, remains finite for $k_F|a| \gg 1$, and never exceeds $0.45E_F$, where E_F is the Fermi energy. Hence, this approach could qualitatively explain our results in the 630 – 680 G region, but it is in clear contradiction with negligible resonance shifts in the 680 – 750 G region [34].

We suggest that these discrepancies might be due to the fact that we are in the high density regime, where $n|a|^3$ approaches unity. In a degenerate Fermi gas, the interparticle spacing is comparable to the inverse Fermi wavevector, $k_F^3 = 6\pi^2 n$. Hence, the unitarity limit coincides with the breakdown of the low-density approximation ($n|a|^3 \ll 1$) and higher-order many-body effects can become important. Some recent many-body calculations [35–37] suggest that in the regime $k_F|a| \gg 1$ (or $n|a|^3 \gg 1$), the interaction energy is always negative and independent of both sign and magnitude of a . This suggests that whenever the scattering length is large, either positive or negative, the interaction energy is a universal fraction of the Fermi energy [33]. This is

a possible explanation for the small line shifts that we observed for fields above 630 G, where the interactions are strong in both states.

This picture is consistent with other recent experimental observations [30,33,38,39]. Expansion energy measurements in a mixture of states $|1\rangle$ and $|2\rangle$ of ${}^6\text{Li}$ [39], showed a negative interaction energy at 720 G, which is on the repulsive side of the predicted Feshbach resonance. RF spectroscopy in ${}^{40}\text{K}$ [30] has also shown some saturation of the mean-field in the vicinity of a Feshbach resonance, which may reflect the unitarity limit.

5.6 Conclusions

In characterizing an interacting Fermi gas by RF spectroscopy, we have demonstrated absence of clock shifts in a two-level system, and introduced a three-level method for measuring mean-field shifts. For strong interactions, we have found only small line shifts that may reflect both the unitarity limit of binary collisions and many-body effects. It would be very important to distinguish between two-body and many-body effects by studying the gas over a broad range of temperatures and densities. In a very dilute and very cold gas, the weakly interacting limit could be extended to very large values of $|a|$, thus allowing for direct verification of molecular calculations. This presents experimental challenges, because cooling changes the density and the temperature together. It would also be interesting to study similar phenomena in bosonic gases, in order to distinguish to what extent the high density many-body effects depend on quantum statistics. This new insight into the physics of strongly interacting Fermi gases must be taken into account in the search for superfluidity in these systems.

References

- [1] K. Gibble and S. Chu, Phys. Rev. Lett. **70**, 1771 (1993).
- [2] C. Fertig and K. Gibble, Phys. Rev. Lett. **85**, 1622 (2000).
- [3] Y. Sortais, *et al.*, Physica Scripta **T95**, 50 (2001).
- [4] A. G. Martin, *et al.*, Phys. Rev. Lett. **61**, 2431 (1988).
- [5] I. Bloch, T. W. Hüsich, and T. Esslinger, Phys. Rev. Lett. **82**, 3008 (1999).
- [6] M. R. Matthews, *et al.*, Phys. Rev. Lett. **81**, 243 (1998).
- [7] J. Stenger, *et al.*, Nature **396**, 345 (1998).
- [8] M. O. Mewes, *et al.*, Phys. Rev. Lett. **78**, 582 (1997).
- [9] D.M. Harber, H.J. Lewandowski, J.M. McGuirk, E.A. Cornell, Phys. Rev. A, **66**, 053616 (2002).
- [10] A. Görlitz, *et al.*, Phys. Rev. Lett. **90**, 090401 (2003).

- [11] T.C. Killian *et al.*, Phys. Rev. Lett. **81**, 3807 (1998).
- [12] J. Stenger *et al.*, Phys. Rev. Lett. **82**, 4569 (1999).
- [13] B. DeMarco and D. S. Jin, Science **285**, 1703 (1999).
- [14] A. G. Truscott, *et al.*, Science **291**, 2570 (2001).
- [15] F. Schreck, *et al.*, Phys. Rev. Lett. **87**, 080403 (2001).
- [16] S. R. Granade, M. E. Gehm, K. M. O'Hara, and J. E. Thomas, Phys. Rev. Lett. **88**, 120405 (2002).
- [17] Z. Hadzibabic, *et al.*, Phys. Rev. Lett. **88**, 160401 (2002).
- [18] G. Roati, F. Riboli, G. Modugno, and M. Inguscio, Phys. Rev. Lett. **88**, 160401 (2002).
- [19] M. Houbiers and H. T. C. Stoof, Phys. Rev. A **59**, 1556 (1999).
- [20] M. Holland, S. J. J. M. F. Kokkelmans, M. L. Chiofalo, and R. Walser, Phys. Rev. Lett. **87**, 120406 (2001).
- [21] K. Dieckmann *et al.*, Phys. Rev. Lett. **89**, 203201 (2002).
- [22] Z. Hadzibabic *et al.*, arXiv:cond-mat/0306050 (2003).
- [23] *S*-wave and *p*-wave interactions refer to two-body interactions with relative angular momentum 0 and \hbar , respectively.
- [24] M. Houbiers, H. T. C. Stoof, W. I. McAlexander, and R. G. Hulet, Phys. Rev. A **57**, R1497 (1998).
- [25] K. M. O'Hara, *et al.*, Phys. Rev. A **66**, 041401 (2002).
- [26] The transfer efficiency is limited by finite optical trap depth and residual heating during the transfer.
- [27] K. Gibble and B. J. Verhaar, Phys. Rev. A **52**, 3370 (1995).
- [28] For our modest degeneracy, we can use a gaussian approximation for the density distribution. The mean density is then lower than the peak density by a factor of $2\sqrt{2}$.
- [29] Our estimate uses the direct mean-field measurement of Bourdel *et al.* [39] scaled to our parameters .
- [30] C.A. Regal, D.S. Jin, Phys. Rev. Lett. **90**, 230404 (2003).
- [31] Note that due to fermionic antisymmetry, there is no clock shift from interactions between atoms in states $|2\rangle$ and $|3\rangle$. Mean field shifts only arise during a decoherence time (see later in the text), but are negligible if the population of atoms in state $|3\rangle$ is small.
- [32] E. G. M. van Kempen *et al.*, in preparation (2003).
- [33] M.E. Gehm, S.L. Hemmer, S.R. Granade, K.M. O'Hara, J.E. Thomas, Phys. Rev. A, **68**, 011401(R) (2003).
- [34] We note that for fields above 630 G, number losses generally reduced n_1 , and all the shifts in this region were scaled up by a factor of 1.1 – 2.7, but still remained negligible.
- [35] J. V. Steele, arXiv:nucl-th/0010066 (2000).
- [36] H. Heiselberg, Phys. Rev. A **63**, 043606 (2001).

- [37] R. Combescot, arXiv:cond-mat/0302209 (2003).
- [38] K.M. O'Hara, S.L. Hemmer, M.E. Gehm, S.R. Granade, J. E. Thomas, *Science*, **298**, 2179 (2002).
- [39] T. Bourdel, *et al.*, arXiv:cond-mat/0303079 (2003).
- [40] This includes the recent measurement of 800 ± 40 G for the resonance in a_{12} [39].
- [41] The work at MIT was supported by the NSF, ONR, ARO, and NASA. The work at Eindhoven was supported by FOM (NWO).

P-wave Feshbach resonances of ultracold ${}^6\text{Li}$

J. Zhang, E. G. M. van Kempen, T. Bourdel, L. Khaykovich, J. Cubizolles, F. Chevy,
M. Teichmann, L. Tarruell, S. J. J. M. F. Kokkelmans, and C. Salomon

Published in Phys. Rev. A **70**, 030702 (2004)

We report the observation of three p -wave Feshbach resonances of ${}^6\text{Li}$ atoms in the lowest hyperfine state $f = 1/2$. The positions of the resonances are in good agreement with theory. We study the lifetime of the cloud in the vicinity of the Feshbach resonances and show that, depending on the spin states, two- or three-body mechanisms are at play. In the case of dipolar losses, we observe a nontrivial temperature dependence that is well explained by a simple model.

6.1 Introduction

In the presence of a magnetic field, it is possible to obtain a quasidegeneracy between the relative energy of two colliding atoms and that of a weakly bound molecular state. This effect, known as a Feshbach resonance, is usually associated with the divergence of the scattering length and is the key ingredient that led to the recent observation of superfluids from fermion atom pairs of ${}^6\text{Li}$ [1–4] and ${}^{40}\text{K}$ [5]. Up to now these pairs were formed in s -wave channels but it is known from condensed matter physics that fermionic superfluidity can arise through higher angular momentum pairing: p -wave Cooper pairs have been observed in ${}^3\text{He}$ [6] and d -wave in high- T_c superconductivity [7]. Although Feshbach resonances involving p or higher partial waves have been found in cold atom systems [8–10], p -wave atom pairs have never been directly observed.

In this paper we report the observation of three narrow p -wave Feshbach resonances of ${}^6\text{Li}$ in the lowest hyperfine state $f = 1/2$. We measure the position of the resonance as well as the lifetime of the atomic sample for all combinations $|f = 1/2, m_f\rangle + |f = 1/2, m'_f\rangle$, henceforth denoted (m_f, m'_f) . We show that the position of the resonances are in good agreement with theory. In the case of atoms polarized in the ground state $(1/2, 1/2)$, the atom losses are due to three-body processes. We show that the temperature dependence of the losses at resonance cannot be described by the threshold law predicted by [11] on the basis of the symmetrization principle for identical particles.

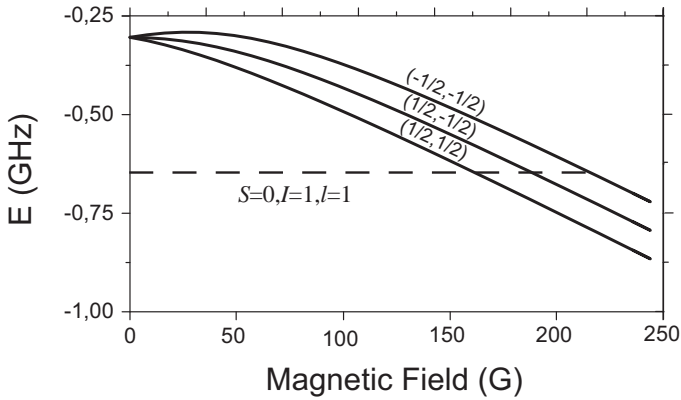


Figure 6.1 Coupled channels calculation of p -wave binding energies, which give rise to Feshbach resonances at threshold. The two-atom states (full line) are indicated by their quantum number (m_{f_1}, m_{f_2}) , while the bound state (dashed line) is labelled by the molecular quantum numbers S, I , and l .

In the case of atoms polarized in $(-1/2, -1/2)$ or that of a mixture $(1/2, -1/2)$, the losses are mainly due to two-body dipolar losses. These losses show a nontrivial temperature dependence that can nevertheless be understood by a simple theoretical model with only one adjustable parameter. In the $(1/2, -1/2)$ channel, we take advantage of a sharp decrease of the two-body loss rate below the Feshbach resonance to present a first evidence for the generation of p -wave molecules.

6.2 Identification of the resonance-inducing state

The p -wave resonances described in these paper have their origin in the same singlet ($S = 0$) bound state that leads to the s -wave Feshbach resonances located at 543 G and ~ 830 G. The latter has been used to generate stable molecular Bose-Einstein condensates [1–4]. In order to discuss the origin of these resonances, it is useful to introduce the molecular basis quantum numbers S, I , and l , which correspond to the total electron spin $\mathbf{S} = \mathbf{s}_1 + \mathbf{s}_2$, total nuclear spin $\mathbf{I} = \mathbf{i}_1 + \mathbf{i}_2$, and orbital angular momentum l . Furthermore, the quantum numbers must fulfill the selection rule

$$S + I + l = \text{even}, \quad (6.1)$$

which is a result of the symmetrization requirements of the two-body wave-function. Since the atomic nuclear spin quantum numbers are $i_1 = i_2 = 1$, and $S = 0$, there are two possibilities for the total nuclear spin in combination with an s -wave ($l = 0$) collision: $I = 0$ and $I = 2$. These two states give rise to the two aforementioned s -wave Feshbach resonances. For p -wave ($l = 1$) collisions only $I = 1$ is possible. This bound

Table 6.1 Theoretical and experimental values of the magnetic field B_F at the p -wave Feshbach resonance for ${}^6\text{Li}$ atoms in $|f_1 = 1/2, m_{f_1}\rangle$ and $|f_1 = 1/2, m_{f_2}\rangle$.

(m_{f_1}, m_{f_2})	Theory (G)	Experiment (G)
(1/2,1/2)	159	160.2(6)
(1/2,-1/2)	185	186.2(6)
(-1/2,-1/2)	215	215.2(6)

state may then give rise to the three p -wave Feshbach resonances of Fig. 6.1. This threshold state does not suffer from exchange decay, and is therefore relatively stable. Our predicted resonance field values B_F (Tab. 6.1) result from an analysis which takes into account the most recent experimental data available for ${}^6\text{Li}$. The calculation has been performed for all spin channels (m_f, m'_f) and a typical collision energy of $15 \mu\text{K}$. A more detailed analysis will be published elsewhere [12].

6.3 Experimental method

Experimentally, we probe these p -wave resonances using the setup described in previous papers [13, 14]. After evaporative cooling in the magnetic trap, we transfer $\sim 5 \times 10^5$ atoms of ${}^6\text{Li}$ in $|f = 3/2, m_f = 3/2\rangle$ in a far-detuned crossed optical trap at low magnetic field. The maximum power in each arm is $P_h^0 = 2 \text{ W}$ and $P_v^0 = 3.3 \text{ W}$ in the horizontal and vertical beam respectively and corresponds to a trap depth of $\sim 80 \mu\text{K}$. The oscillation frequencies measured by parametric excitation are respectively $\omega_x = 2\pi \times 2.4(2) \text{ kHz}$, $\omega_y = 2\pi \times 5.0(3) \text{ kHz}$, $\omega_z = 2\pi \times 5.5(4) \text{ kHz}$, where the x (y) direction is chosen along the horizontal (vertical) beam. A first radio-frequency (rf) sweep brings the atoms to $|f = 1/2, m_f = 1/2\rangle$ and, if necessary, we perform a second rf transfer to prepare the mixture $(1/2, -1/2)$ or the pure $(-1/2, -1/2)$. The variable magnetic field B is the sum of two independent fields B_0 and B_1 . B_0 offers a wide range of magnetic field while B_1 can be switched off rapidly. After the radio-frequency transfer stage, we ramp the magnetic field to $B_0 \sim 220 \text{ G}$ with $B_1 \sim 8 \text{ G}$ in 100 ms. When needed, we reduce in 100 ms the power of the trapping beams to further cool the atoms. For the coldest samples, we obtain at the end of this evaporation sequence $N \sim 10^5$ atoms at a temperature $\sim 5 \mu\text{K}$. This corresponds to a ratio $T/T_F \sim 0.5$, where $k_B T_F = \hbar(6N\omega_x\omega_y\omega_z)^{1/3}$ is the Fermi energy of the system. To reach the Feshbach resonance, we reduce B_0 in 4 ms to its final value $B_{0,f} \sim B_F$, near the Feshbach resonance. At this stage, we abruptly switch off B_1 so that the total magnetic field is now close to resonance. After a waiting time in the trap $t_{\text{wait}} = 50 \text{ ms}$, we switch off the trapping and the magnetic field and we measure the remaining atom number after a 0.35 ms time of flight.

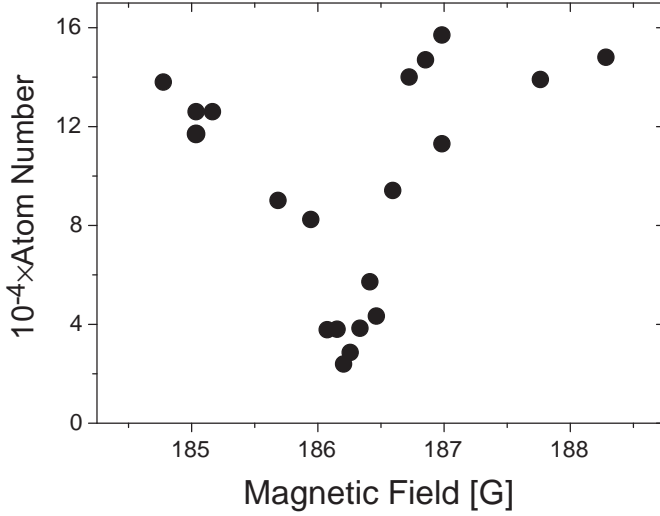


Figure 6.2 Atom number vs magnetic field $B_{0,f}$ after a 50 ms wait for atoms in the spin mixture $(1/2, -1/2)$ at $T \sim 14\mu\text{K}$. The sharp drop close to $B_0 \sim 186$ G over a range $\simeq 0.5$ G is the signature of the p -wave Feshbach resonance predicted by theory.

We show in Fig. 6.2 the dependence of the atom number on the final value of $B_{0,f}$ in the case of the spin mixture $(1/2, -1/2)$ at a temperature $T \sim 14 \mu\text{K}$. As expected from theory, we observe a sharp drop of the atom number for values of the magnetic field close to 186 G. The other two p -wave Feshbach resonances have a similar loss signature and Tab. 6.1 shows that for all spin channels, the resonance positions are in good agreement with predictions. Note that in table 6.1, the uncertainty is mainly due to the magnetic field calibration while the short term stability is $\lesssim 50$ mG.

6.4 Trap losses

To evaluate the possibility of keeping p -wave molecules in our trap, we have studied the lifetime of the gas sample at the three Feshbach resonances. We have measured the number N of atoms remaining in the trap after a variable time t_{wait} . Accounting for two- and three-body processes only, N should follow the rate equation

$$\frac{\dot{N}}{N} = -G_2\langle n \rangle - L_3\langle n^2 \rangle, \quad (6.2)$$

where n is the atom density and $\langle n^a \rangle = \int d^3r n^{a+1}/N$ ($a = 1, 2$) is calculated from the classical Boltzman distribution. In this equation, we can safely omit one-body losses since the measured decay time is ~ 100 ms, much smaller than the one-body lifetime

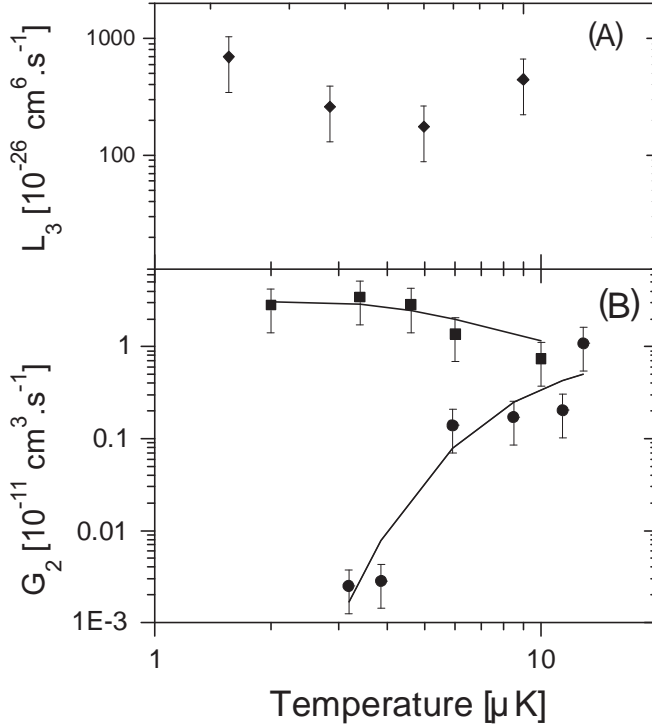


Figure 6.3 Variations of (A) three-body and (B) two-body loss rates vs temperature at the Feshbach resonance. (A): \blacklozenge : atoms in the Zeeman ground state $|f = 1/2, m_f = 1/2\rangle$, $B_{0,f} \sim 159$ G. (B): \blacksquare : atoms polarized in $|f = 1/2, m_f = -1/2\rangle$, $B_{0,f} \sim 215$ G. \bullet : mixture $|f = 1/2, m_f = 1/2\rangle + |f = 1/2, m_f = -1/2\rangle$, $B_{0,f} \sim 186$ G. In both cases, the full line is a fit to the data using prediction of Eq. 6.4 with the magnetic field as the only fitting parameter.

~ 30 s.

In the $(1/2, 1/2)$ channel, we find that three-body losses are dominant. The dependence of L_3 with temperature is very weak [Fig. 6.3(A)]. A theoretical calculation of the temperature dependence of three-body loss rate has been performed in [11] and it predicts that in the case of indistinguishable fermions L_3 should be proportional to T^λ , with $\lambda \geq 2$. Although this prediction seems in disagreement with our experimental results, the analysis of [11] relies on a Wigner threshold law, *i.e.* a perturbative calculation based on the Fermi golden rule. At the Feshbach resonance where the scattering cross-section is expected to diverge, this simplified treatment is not sufficient. This suggests that three-body processes must be described by a more refined formalism, analogous to the unitary limited treatment of the s -wave elastic collisions [15]. To

Table 6.2 parameters characterizing the two-body loss rates for $(1/2,-1/2)$ and $(-1/2,-1/2)$ spin channels.

(m_{f_1}, m_{f_2})	K $\text{cm}^3 \cdot \mu\text{K} \cdot \text{s}^{-1}$	γ μK	μ $\mu\text{K} \cdot \text{G}^{-1}$
$(1/2,-1/2)$	1.21×10^{-13}	0.05	117
$(-1/2,-1/2)$	7.33×10^{-13}	0.08	111

confirm this assumption, we have compared the loss-rates at two given temperatures ($T = 2 \mu\text{K}$ and $T = 8 \mu\text{K}$, respectively) for various values of the magnetic field (Fig. 6.4). If the threshold law is valid, then the ratio $L_3(2 \mu\text{K})/L_3(8 \mu\text{K})$ should always be smaller than $(2/8)^2 \sim 0.0625$ (full line of Fig. 6.4). As seen before, experimental data show no significant variation of L_3 with temperature near resonance. However, when the magnetic field is tuned out of resonance we recover a dependence in agreement with [11].

In contrast to s -wave Feshbach resonances where dipolar losses are forbidden in the $f = 1/2$ manifold [16], the losses at resonance are found to be dominantly two-body in the $(1/2,-1/2)$ and $(-1/2,-1/2)$ channels. The variations of the two-body loss rate with temperature are displayed in Fig. 6.3(B). The temperature dependence appears very different in the two cases. We show now that this is the consequence of a strong sensitivity to magnetic field detuning from resonance, rather than a specific property of the states involved. In an extension of the work presented in [17], we describe inelastic collisions by two noninteracting open channels coupled to a single p -wave molecular state [18]. This model leads to an algebra close to the one describing photoassociation phenomena [19] and the two-body loss rate at energy E is given by

$$g_2(E) = \frac{KE}{(E - \delta)^2 + \gamma^2/4}. \quad (6.3)$$

Here $\delta = \mu(B - B_F)$ is the detuning to the Feshbach resonance and K , μ and γ are phenomenological constants depending on the microscopic details of the potential [21]. For each channel, these parameters are estimated from our coupled-channel calculation (Tab. 6.2). To compare with experimental data, Eq. (6.3) is averaged over a thermal distribution and for $\delta > 0$ and $\delta \gg \gamma$ we get

$$G_2 \sim 4\sqrt{\pi} \frac{K}{\gamma} \left(\frac{\delta}{k_B T} \right)^{3/2} e^{-\delta/k_B T}. \quad (6.4)$$

Equation 6.4 is used to fit the data of Fig. 6.3(B), with $B - B_F$ as the only fitting parameter. We get a fairly good agreement if we take $B - B_F = 0.04 \text{ G}$ (resp. 0.3 G) for the $(-1/2,-1/2)$ [resp. $(1/2,-1/2)$] channel, illustrating the extreme sensitivity of G_2

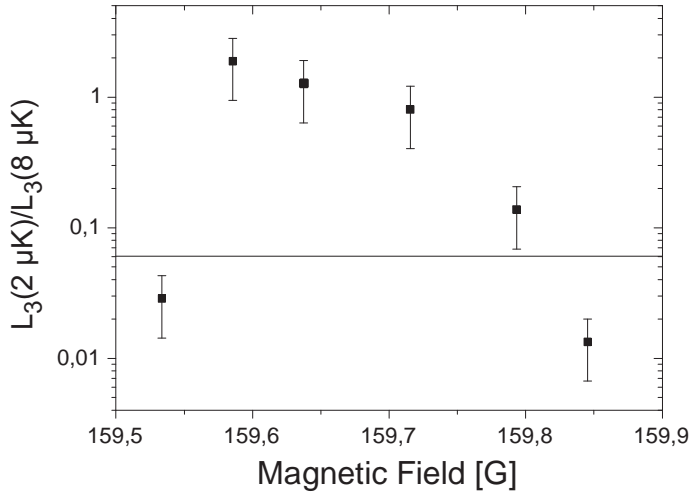


Figure 6.4 Ratio $L_3(T = 2\mu\text{K})/L_3(T = 8 \mu\text{K})$ of the three-body decay rate for two different temperatures for a gas of atoms polarized in $|f = 1/2, m_f = 1/2\rangle$. Full line: threshold law $L_3 \sim T^2$.

to detuning and temperature. This feature was also qualitatively tested by measuring the variations of G_2 with magnetic field at constant temperature. Another interesting feature of Eq. 6.4 is that it predicts that the width δB of the Feshbach resonance, as measured by atom losses, should scale like $k_B T/\mu$. For a typical temperature $T \sim 15 \mu\text{K}$, this yields $\delta B \sim 0.15 \text{ G}$, in agreement with the resonance width shown in Fig. 6.2.

From Eq. 6.4, we see that G_2 nearly vanishes at $\delta = 0$. The thermal average of (6.4) for $\delta = 0$ yields $G_2(\delta = 0) \propto K k_B T$. The ratio between the maximum two-body loss rate ($\delta = 3k_B T/2$) and that at $\delta = 0$ is then $\sim k_B T/\gamma$, $\sim 10^2$ for $\sim 10 \mu\text{K}$. In the region $\delta < 0$ where we expect to form molecules, we benefit from a $1/\delta^2$ further reduction of the two-body losses [see Eq. 6.4].

6.5 Formation of molecules using a Feshbach resonance

We have checked the production of molecules in $(1/2, -1/2)$ by using the scheme presented in [13, 22]. We first generate molecules in $|S = 0, I = 1, l = 1\rangle$ by ramping in 20 ms the magnetic field from $190 \text{ G} > B_F$ to $B_{\text{nuc}} = 185 \text{ G} < B_F$. At this stage, we can follow two paths before detection (Fig. 6.5). Path 1 permits to measure the number N_1 of free atoms: by ramping *down* in 2 ms the magnetic field from 185 G to 176 G, we convert the molecules into deeply bound molecular states that decay rapidly

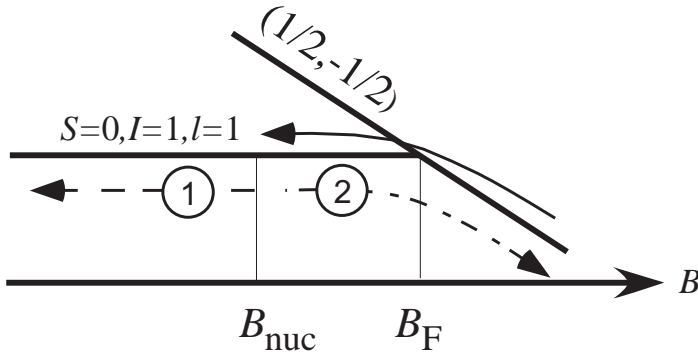


Figure 6.5 Molecules are generated by ramping from a magnetic field higher than B_F to $B_{\text{nuc}} < B_F$. From there, two paths are used. In path 1 (dashed line), the magnetic field is decreased to create tightly bound molecules that will not appear on absorption images. In path 2 (dash dotted line), the magnetic field is ramped up across resonance to dissociate the molecules. The efficiency of the molecule production is simply given by $(1 - N_1/N_2)$ where N_i is the atom number measured after path i .

by two-body collisions. Path 2 gives access to the total atom number N_2 (free atoms + atoms bound in p -wave molecules). It consists in ramping *up* the magnetic field in 2 ms from B_{nuc} to $202 \text{ G} > B_F$ to convert the molecules back into atoms. Since the atoms involved in molecular states appear only in pictures taken in path 2, the number of molecules in the trap is $(N_2 - N_1)/2$. In practice, both sequences are started immediately after reaching B_{nuc} and we average the data of 25 pictures to compensate for atom number fluctuations. We then get $N_1 = 7.1(5) \times 10^4$ and $N_2 = 9.1(7) \times 10^4$ which corresponds to a molecule fraction $1 - N_1/N_2 = 0.2(1)$. Surprisingly, we failed to detect any molecule signal when applying the same method to $(1/2, 1/2)$ atoms.

Since the dramatic reduction of inelastic losses close to a s -wave Feshbach resonance [23] was a key ingredient to the recent observation of fermionic superfluids, the formation of stable atom pairs requires a full understanding of the decay mechanisms at play close to a p -wave resonance. In this paper we have shown that in the particular case of two-body losses, the maximum losses take place when the detuning is positive. Since stable dimers are expected to be generated for negative detuning, dipolar losses should not present a major hindrance to further studies of p -wave molecules.

Acknowledgement

We thank Z. Hadzibabic for very helpful discussions. S.K. acknowledges support from the Netherlands Organisation for Scientific Research (NWO). E.K. acknowledges support from the Stichting FOM, which is financially supported by NWO. This work was

supported by CNRS, and Collège de France. Laboratoire Kastler Brossel is *Unité de recherche de l'École Normale Supérieure et de l'Université Pierre et Marie Curie, associée au CNRS*.

References

- [1] S. Jochim, *et al.*, Science **302**, 2101 (2003).
- [2] M. W. Zwierlein, *et al.*, Phys. Rev. Lett. **91**, 250401 (2003).
- [3] T. Bourdel *et al.*, cond-mat/0403091.
- [4] J. Kinast *et al.*, Phys. Rev. Lett. **92**, 150402 (2004).
- [5] M. Greiner, C. A. Regal, and D. S. Jin, Nature **426**, 537 (2003).
- [6] D. M. Lee, Rev. Mod. Phys. **69**, 645 (1997).
- [7] C.C Tsuei and J.R. Kirtley, Phys. Rev. Lett. **85**,182 (2000).
- [8] C. Chin *et al.* Phys. Rev. Lett. **85**, 2717 (2000).
- [9] C. A. Regal *et al.* Phys. Rev. Lett. **90**, 053201 (2003).
- [10] T. Weber *et al.*, Phys. Rev. Lett. **91**, 123201 (2003).
- [11] B. D. Esry, C. H. Greene, and H. Suno, Phys. Rev. A **65**, 010705 (2002).
- [12] E. G. M. van Kempen *et al.*, cond-mat/0406722.
- [13] J. Cubizolles, *et al.*, Phys. Rev. Lett. **91** 240401 (2003).
- [14] T. Bourdel, *et al.*, Phys. Rev. Lett. **91**, 020402 (2003).
- [15] H. Suno, B. D. Esry, and C. H. Greene, Phys. Rev. Lett. **90**, 053202 (2003).
- [16] K. Dieckmann *et al.*, Phys. Rev. Lett. **89**, 203201 (2002).
- [17] M. Holland, *et al.*, Phys. Rev. Lett. **87**, 120406 (2001).
- [18] We also neglect the splitting between the different m_l predicted by [20].
- [19] R. Napolitano *et al.*, Phys. Rev. Lett. **73**, 1352 (1994)
- [20] C. Ticknor *et al.*, Phys. Rev. A **69**, 042712 (2004).
- [21] Note that in our case μ is positive. This corresponds to molecular states stable at low field.
- [22] C. A. Regal *et al.*, Nature **424**, 47 (2003).
- [23] D. S. Petrov, Phys. rev. A, **67**, 010703 (2003).

Formation of fermionic molecules via interisotope Feshbach resonances

E.G.M. v. Kempen, B. Marcelis, and S.J.J.M.F. Kokkelmans

Published in Phys. Rev. A **70**, 050701 (2004)

We perform an analysis of recent experimental measurements and improve the lithium interaction potentials. For ${}^6\text{Li}$ a consistent description can be given. We discuss theoretical uncertainties for the position of the wide ${}^6\text{Li}$ Feshbach resonance, and we present an analytic scattering model for this resonance, based on the inclusion of a field-dependent virtual open-channel state. We predict new Feshbach resonances for the ${}^6\text{Li}$ - ${}^7\text{Li}$ system, and their importance for different types of crossover superfluidity models is discussed.

7.1 Introduction

Resonances in cold atomic gases offer the key to connections with challenging condensed matter physics. In particular, resonances make lithium atomic systems very versatile. The first Bose-Einstein condensates (BEC) were quite small in number due to a negative scattering length [1], later Feshbach resonances [2] have been used to create condensates with positive scattering length and to generate bright solitons [3, 4] by changing the scattering length a back to negative. Even more interesting is the usability to form molecules, since the Feshbach resonance results from bringing a molecular state on threshold. The connection between fermionic atoms and composite bosons (molecules) has great impact for the study of the well-known crossover problem between BEC and Bardeen-Cooper-Schrieffer (BCS)-type superfluidity [5–7].

In this Rapid Communication, we study several Feshbach resonances in the lithium system. We first review the knowledge of the interatomic interaction potentials, and use experimental data as input to improve these potentials. We discuss the special situation for the wide ${}^6\text{Li}$ resonance, where the background scattering length depends strongly on the magnetic field. This will be interpreted as a field-dependent virtual state (a second resonance) which is situated close to threshold. The full energy-dependent scattering process can be parametrized according to a simple analytical model that encapsulates both field-dependent resonances. Further, we apply our knowledge of

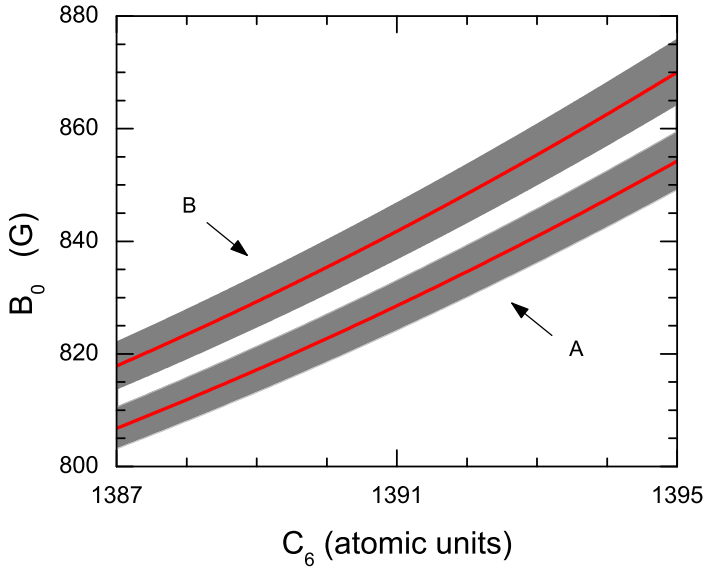


Figure 7.1 (color online) Dependency of the wide-resonance position B_0 on C_6 , according to the second analysis (see text). The shaded area indicates the associated uncertainty. The curve indicated with A (B) is obtained making use of the exchange energy according to [11] ([12]).

the lithium interactions to a system of ${}^6\text{Li}$ - ${}^7\text{Li}$, and find several Feshbach resonances which are accessible in current experimental setups. The underlying molecular state is of a composite fermionic nature, which allows for a new type of crossover physics — the transition of an atomic BEC to a molecular Fermi-type of superfluidity. Recently, Feshbach resonances in a heteronuclear Bose-Fermi mixture have been observed [8,9], where polar fermionic molecules underly the resonance state.

7.2 The interaction model

For an accurate prediction of resonance properties, we need a detailed understanding of the actual interatomic potentials. Here we describe how we improved the precision of existing potentials by using recent experimental measurements as input. The potentials can be divided in two radial intervals. For large interatomic separations r the potential is given by the sum of the dispersive Van der Waals tail $V^{\text{vdw}}(r) = -C_6/r^6 - C_8/r^8 - C_{10}/r^{10}$ and the exchange contribution $V_S^{\text{ex}}(r) = (-1)^{S+1} C^{\text{ex}} r^{7/2\alpha-1} e^{-2\alpha r}$ [10], resulting in two potentials: a singlet ($S = 0$) and a triplet ($S = 1$) potential. The coefficient C^{ex} is taken from Refs. [11,12], α is directly related to the ionization energy $\alpha^2/2$ [13], and C_8 and C_{10} are taken from Refs. [14].

For smaller r we use the model singlet and triplet potentials which have also been used in Refs. [15, 16].

These short-range and long-range potentials are smoothly connected at $r = 18a_0$, with a_0 the Bohr radius. To overcome the inaccuracies of the short-range potentials, we make use of the accumulated phase method [15]. A boundary condition is applied on the partial-wave radial wave functions at $r = 17.5a_0$ in the form of a WKB phase $\phi_{S,T}(E, \ell) = \phi_{S,T}^0(E, \ell) + \Delta\phi_{S,T}$. The first term on the right-hand side is calculated by radial integration of the model potential up to $17.5a_0$ and is expected to account for the energy and angular momentum dependence of the accumulated phase to a sufficient degree of accuracy. The second term is an energy and angular momentum independent shift of the phase, determined from experimental data. These corrections $\Delta\phi_{S,T}$ to the accumulated singlet and triplet phases can be converted to the more physical quantities $\nu_{DS,DT}$, which are the fractional vibrational quantum numbers at dissociation.

We determine the free parameters of our interaction potentials ν_{DS} , ν_{DT} , and C_6 from experimental input by means of a χ^2 minimization. An interisotope analysis in which ${}^7\text{Li}$ is related to ${}^6\text{Li}$ by means of a simple mass-scaling relation failed, yielding inconsistent results for ν_{DS} . This is a strong indication of a breakdown of the Born-Oppenheimer approximation for the singlet potential. Such a breakdown was demonstrated in detailed spectroscopy [17]. We therefore avoid mass scaling of the singlet potential, and we perform two different analyses. In the first analysis, we only take ${}^6\text{Li}$ data into account. In the second analysis we investigate ${}^7\text{Li}$ as well, however, we only do a mass scaling for the triplet potential. Our total set of ${}^6\text{Li}$ experiments comprises 6 data points. The zero crossing of the scattering length of a system in the two lowest hyperfine states [18, 19]; in the same spin state configuration, the positions of the narrow [20] and wide [7] Feshbach resonances; and the measurement of the scattering length in the lowest and third to lowest hyperfine state [21] and the binding energy of the most weakly bound triplet state [22].

7.3 Application of the interaction model

In our first analysis we obtain a minimum in the reduced χ^2 distribution of $\chi^2 = 0.5$. The corresponding parameter values are $\nu_{DS} = 0.3496(5)$, equivalent with a singlet scattering length $a_S = 45.3(1)a_0$ and $\nu_{DT} = 0.9954(2)$, corresponding to $a_T = -2025(70)a_0$. For the leading dispersion coefficient we find $C_6 = 1388(6)$ at. units. This result has been obtained with a C^{ex} of Ref. [12]. When we weaken C^{ex} to the value of Ref. [11], we find that the optimal C_6 is shifted to $C_6 = 1390$ at. units. The scattering lengths found are consistent with previous determinations [16, 22]. Our C_6 coefficient agrees with the values found in *ab initio* calculations [14, 23].

The objective of a second analysis [24] is to reevaluate the position of the wide

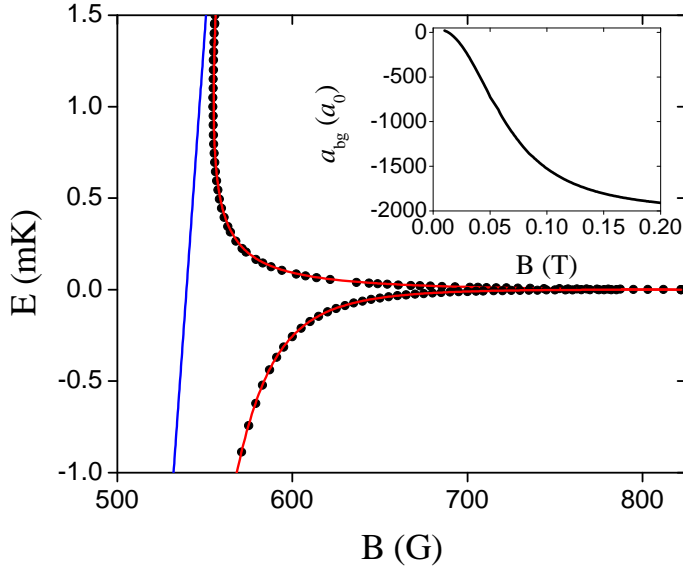


Figure 7.2 (color online) Energy of the dressed (quasi-)molecular state as obtained with a full coupled-channels calculation (dots), with respect to the $|f_1, m_{f_1}\rangle \otimes |f_2, m_{f_2}\rangle = 1/2, 1/2\rangle \otimes 1/2, -1/2\rangle$ threshold. The straight line is the bare closed-channel energy $\epsilon_b(B)$, and the energy of the dressed state according to our model is indicated by the curved line. Inset: corresponding background value of the scattering length as a function of the magnetic field B .

s-wave Feshbach resonance of ${}^6\text{Li}$ in the two lowest hyperfine states, without making use of the experimental result $B_0=822\text{G}$ [7]. Here we want to combine all available cold collision data on lithium, and we add the positions of three p -wave Feshbach resonances, which have been measured recently [25], and experimental data of ${}^7\text{Li}$ [3,26], to the set of experiments. In this combined isotope analysis we perform a mass scaling procedure for the triplet boundary condition only. As explained above, we will not mass-scale the singlet potential but rather optimize the boundary conditions for the singlet potential independently for the two isotopes, by making $\nu_{DS,7}$ a free parameter independent of $\nu_{DS,6}$.

Since the p -wave resonances are measured with high accuracy, we also allow for small corrections of the angular momentum dependence of $\phi_S^0(E, \ell)$ via the parameter $\Delta\phi_S^l$ by means of an addition $\Delta\phi_S^l \cdot l(l+1)$ cf. [27]. By optimizing the interaction parameters ($\nu_{DS,6}$, $\nu_{DS,7}$, $\nu_{DT,6}$, $\Delta\phi_S^l$) for various fixed values of C_6 we are able to obtain a minimum reduced χ^2 of 0.7. The dependency of χ^2 on C_6 is rather weak and therefore the set of experiments does not restrict the C_6 coefficient to an acceptable degree. However, the minimal χ^2 occurs for $C_6 = 1390.6$ at. units close to *ab initio*

values, when using C^{ex} from Ref. [11], positioning the wide Feshbach resonance at $B_0 = 826$ G. We estimate $808 \text{ G} < B_0 < 846 \text{ G}$ for $1388 < C_6 < 1393$ at. units, see Fig. 7.1. For C^{ex} from Ref. [12] we find a minimum $\chi^2 = 0.5$ for $C_6 = 1395.6$.

7.4 Analytic resonance model

From now on, the properties of the Feshbach resonances will be derived from our first analysis. First, we study the wide $B_0 = 822$ G Feshbach resonance in the two lowest hyperfine states of ${}^6\text{Li}$. This resonance is quite remarkable for two reasons: it has a large width of the order of 100 G, and its background scattering length a_{bg} is strongly depending on the magnetic field, which can be seen from the inset of Fig. 7.2. At zero field, a_{bg} is 3 and positive, while for large field values a_{bg} is large and negative, indicating the presence of a nearby virtual state in the open-channel subspace P [28]. Consequently several important quantities, such as the S and T matrices which summarize the collision process, depend nontrivially on the collision energy E . Here we will apply the model discussed in Ref. [28] to this s -wave Feshbach resonance. This model takes the virtual state into account explicitly, and gives an analytical description of all important two-body quantities near the Feshbach resonance.

In general, the relation between the background scattering length a_{bg} , the range of the potential a_{bg}^P , and the virtual state pole κ_{vs} , is given by $a_{\text{bg}} = a_{\text{bg}}^P - 1/\kappa_{\text{vs}}$. The range of the potential is related to the Van der Waals coefficient C_6 , and does not depend on the magnetic field. Therefore, we account for the field dependence of a_{bg} by generalizing the model of Ref. [28] to the case of a field-dependent virtual-state $\kappa_{\text{vs}}(B)$. The complex energy shift is then given by

$$\begin{aligned} A(E, B) &= \Delta_{\text{res}}(E, B) - \frac{i}{2}\Gamma(E, B) \\ &= \frac{-iA_{\text{vs}}(B)}{2\kappa_{\text{vs}}(B)[k + i\kappa_{\text{vs}}(B)]}, \end{aligned} \quad (7.1)$$

where $A_{\text{vs}}(B)$ is related to the coupling matrix element between the open-channel virtual state and the closed-channel bound state responsible for the Feshbach resonance. Our wavenumber units are such that $E = k^2$.

The total scattering length is then given by

$$a(B) = a_{\text{bg}}^P - \frac{1}{\kappa_{\text{vs}}(B)} - \lim_{E \rightarrow 0} \frac{\Gamma(E, B)/2}{k[\epsilon_b(B) + \Delta_{\text{res}}(E, B)]}, \quad (7.2)$$

where $\epsilon_b(B) = \Delta\mu^{\text{mag}}(B - \bar{B}_0)$ is the energy of the bare closed-channel bound state, $\Delta\mu^{\text{mag}} = 2.0\mu_B$ the magnetic moment, μ_B the Bohr magneton, and $\bar{B}_0 = 539.5$ G the field where the bare closed-channel energy crosses threshold. For a fixed B value, the parameters $A_{\text{vs}}(B)$ and $\kappa_{\text{vs}}(B)$ are obtained by fitting Eq. (7.2) to the coupled-channels

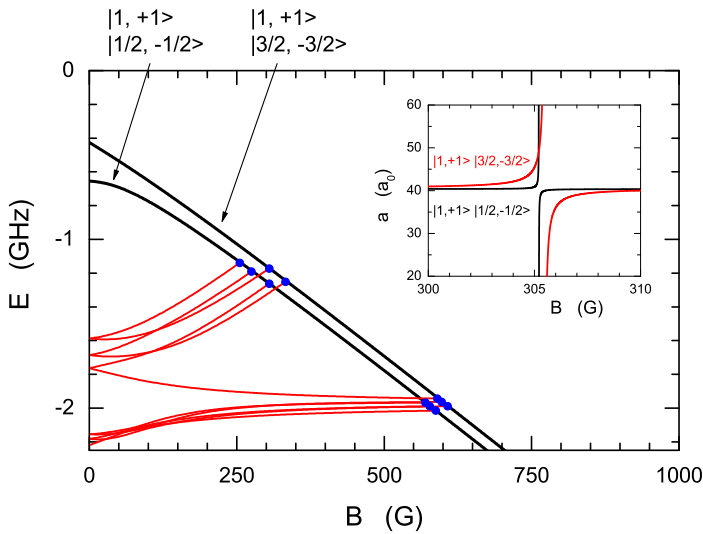


Figure 7.3 (color online) Two thresholds for the ${}^6\text{Li}$ - ${}^7\text{Li}$ system which show the coincidence of two Feshbach resonances. Inset: scattering length as a function of magnetic field, for the two coinciding Feshbach resonances.

result for $a(B)$, using two close-lying data points where we assume A_{vs} and κ_{vs} locally constant. Repeating this for every field value, we obtain explicit expressions for the non-trivial energy dependence of the complex energy shift, using only the zero-energy information contained in $a(B)$. Note that there are only two free parameters, and $a_{\text{bg}}(B)$ is fixed once $\kappa_{\text{vs}}(B)$ is known.

The fit functions are summarized in Table 7.1. In Fig. 7.2 we compare the dressed (quasi-)molecular state calculated by coupled-channels methods and by our analytical model, which agrees excellent. Therefore, this model can be used to analytically describe the S and T matrices [28], scattering phase shifts, etc., with similar precision as a full coupled channels calculation, for a large range of energies and magnetic fields. We note also that the narrow 543 G Feshbach resonance (width of order 0.1 G) can be described by Feshbach theory. Here, however, an easier description is possible based on only one single background part and a single resonance state, since the narrow resonance has a ‘local’ background scattering length of the order of a_{bg}^P . For narrow resonances [29, 30], the typical resonance features in the continuum scattering which depend on the details of the potential, are very important to the BEC-BCS crossover physics, since they are visible for energies less than the Fermi energy, resulting in a nonuniversal crossover picture.

Table 7.1 Parameters of the virtual-state model. For the magnetic fields of interest ($530 \text{ G} \lesssim B \lesssim 830 \text{ G}$), the parameters are given by a third-order polynomial fit, $c_0 + c_1 B + c_2 B^2 + c_3 B^3$. For $A_{\text{vs}}(B)$ the units are given by $[c_n] = K^2 G^{-n}$, and for $\kappa_{\text{vs}}(B)$ the units are given by $[c_n] = K^{1/2} G^{-n}$. The range of the potential is given by $a_{\text{bg}}^P = 45 a_0$.

	c_0	c_1	c_2	c_3
$A_{\text{vs}}(B)$	$1.62 \cdot 10^{-5}$	$-5.10 \cdot 10^{-8}$	$6.07 \cdot 10^{-11}$	$-2.56 \cdot 10^{-14}$
$\kappa_{\text{vs}}(B)$	$4.65 \cdot 10^{-2}$	$-1.54 \cdot 10^{-4}$	$1.92 \cdot 10^{-7}$	$-8.26 \cdot 10^{-11}$

7.5 Creating fermionic molecules

Now we turn to the final topic of this paper, the study of Feshbach resonances in a ${}^6\text{Li}$ fermion - ${}^7\text{Li}$ boson mixture. We use again our first analysis of the interaction parameters for ${}^6\text{Li}$, and perform a simple mass scaling of the accumulated phases for the ${}^6\text{Li}$ - ${}^7\text{Li}$ system. As discussed before, this leads to less accurate predictions for the resonance positions as suggested by the accuracies from the ${}^6\text{Li}$ interaction parameters. We estimate the inaccuracies in the mixed isotope resonance positions to be of order a few Gauss, due to inaccuracies of the mass-scaling relations.

Feshbach resonances in the ${}^6\text{Li}$ - ${}^7\text{Li}$ system have been studied before in Ref. [16], where only the case of magnetically trappable atoms was investigated. Moreover, those resonances are accompanied by large inelastic exchange losses. We investigate only ${}^6\text{Li}$ - ${}^7\text{Li}$ hyperfine state combinations where exchange losses are absent. Within these boundaries, there are still numerous resonances present, and we restrict ourselves to the most interesting results. The ${}^6\text{Li}$ - ${}^7\text{Li}$ $|1/2, 1/2\rangle \otimes |1, 1\rangle$ channel has the lowest energy in the two-body hyperfine diagram. Therefore, this channel will not suffer from magnetic dipolar relaxation. We find five Feshbach resonances at magnetic field values of 218 G, 230 G, 251 G, 551 G, and 559 G. Measurements of these resonances might provide the missing information to exactly locate the position of the wide ${}^6\text{Li}$ resonance, as all mixed resonances arise from the same underlying bound state in the triplet potential.

Feshbach resonances between bosons and fermions give rise to a fundamentally different type of crossover physics. Already some work on the interactions in Bose-Fermi mixtures can be found in the literature [31, 32], however, in order to describe correctly the many-body physics and interactions close to resonance, more research is needed. To make the system feasible, some requirements have to be fulfilled. For a stable BEC, a positive scattering length for the bosons is required. Approaching the resonance from the atomic side, the mixed boson-fermion scattering length will become negative, and stability of the system could become an issue. At the other side of the resonance, it is important that the effective interaction between the fermionic molecules is attractive. Point-like composite fermions do not undergo s -wave collisions. However, close to

resonance the molecules are long stretched, and an effective interaction mediated via the bosons could be possible. An approach similar to Ref. [33] could be conclusive on this and on the expected dependence of the inelastic rate coefficient on the scattering length. Also, the effect of Pauli blocking will not be as strong as in Ref. [33] since a three-body decay process with only one fermion and two bosons involved is possible. However, a reduction with respect to the pure bosonic case could still be expected.

Another interesting situation occurs when two Feshbach resonances coincide. Further away from resonance, where the size of the molecule is comparable to the size of the potential, s -wave collisions are not allowed for these composite fermions. Therefore, in order to preserve superfluid behavior in this region, two different molecular spin configurations are needed to allow for s -wave collisions between molecules. Moreover, it is desirable that the two resonances responsible for the molecule formation coincide. Such a coincidence can be found from Fig. 7.3, where the ${}^6\text{Li}$ - ${}^7\text{Li}$ $|1/2, -1/2\rangle \otimes |1, 1\rangle$ and $|3/2, -3/2\rangle \otimes |1, 1\rangle$ bound states and thresholds are plotted as a function of magnetic field. Every crossing of a bound state with threshold indicates the position of a Feshbach resonance. It can be seen that at $B = 305$ G two Feshbach resonances coincide. These two threshold channels have the same bosonic ${}^7\text{Li}$ state, but a different fermionic ${}^6\text{Li}$ state. This coincidence is systematic, and will not depend on the interaction parameters. The scattering lengths as a function of the magnetic field can be seen in the inset of Fig. 7.3.

In conclusion, we analyzed recent experimental measurements for lithium, and showed that mass scaling between ${}^6\text{Li}$ and ${}^7\text{Li}$ fails for the singlet potential. We investigated uncertainties in the wide ${}^6\text{Li}$ resonance position, and demonstrated an analytical model for this resonance that includes the nearby virtual state. Finally, we showed that ${}^6\text{Li}$ - ${}^7\text{Li}$ mixtures feature accessible Feshbach resonances, giving rise to fermionic molecules, yielding new BCS-BEC crossover physics.

Acknowledgement

We acknowledge discussions with B. Verhaar, M. Holland, J. Zhang, T. Bourdel, F. Chevy and C. Salomon, and we acknowledge the Netherlands Organization for Scientific Research (NWO). E. K. acknowledges support from the Stichting FOM, financially supported by NWO.

References

- [1] C. C. Bradley et al., Phys. Rev. Lett. **75**, 1687 (1995); *ibid.* Phys. Rev. Lett. **79**, 1170 (1997).
- [2] H. Feshbach, Ann. of Phys. (N.Y.) **5**, 357 (1958); *ibid.* **19**, 287 (1962).
- [3] L. Khaykovich et al., Science **296**, 1290 (2002).

-
- [4] K. E. Strecker et al., *Nature* **417**, 150 (2002).
- [5] P. Nozières and S. Schmitt-Rink, *J. Low Temp. Phys.* **59**, 195 (1982); M. Randeria and references in *Bose-Einstein condensation*, Cambridge Un. Press, Cambridge (1995).
- [6] C. A. Regal, M. Greiner, and D. S. Jin, *Phys. Rev. Lett.* **92**, 083201 (2004).
- [7] M. W. Zwierlein et al., *Phys. Rev. Lett.* **92**, 120403 (2004).
- [8] C.A. Stan et al., cond-mat/0406129.
- [9] S. Inouye et al., cond-mat/0406208.
- [10] B.M. Smirnov and M.S. Chibisov, *Zh. Eksp. Teor. Fiz.* **48**, 939 (1965) [*Sov. Phys. JETP* **21**, 624 (1965)].
- [11] W.T. Zemke and W.C. Stwalley, *J. Chem. Phys.* **111**, 4962 (1999).
- [12] M. Marinescu and A. Dalgarno, *Z. Phys. D* **36**, 239 (1996).
- [13] C.J. Lorenzen and K. Niemax, *J. Phys.* **B 15**, L139-L145 (1982).
- [14] Z.-C. Yan et al., *Phys. Rev. A* **54**, 2824 (1996).
- [15] A.J. Moerdijk and B.J. Verhaar, *Phys. Rev. Lett.* **73**, 518 (1994).
- [16] F. A. van Abeelen, B. J. Verhaar, and A. J. Moerdijk, *Phys. Rev. A* **55**, 4377 (1997).
- [17] X. Wang et al., *J. Chem. Phys.* **117**, 9339 (2002).
- [18] K. M. O'Hara et al., *Phys. Rev. A* **66**, 041401(R) (2002).
- [19] S. Jochim et al., *Phys. Rev. Lett.* **89**, 273202 (2002).
- [20] K.E. Strecker, G.B. Partridge, and R.G. Hulet, *Phys. Rev. Lett.* **91**, 080406 (2003).
- [21] K. M. O'Hara et al., *Phys. Rev. Lett.* **85**, 2092 (2000).
- [22] E. R. I. Abraham et al., *Phys. Rev. A* **55**, R3299 (1997).
- [23] A. Derevianko, J. F. Babb, and A. Dalgarno, *Phys. Rev. A* **63**, 052704 (2001).
- [24] Here C^{ex} is taken from ref. [11].
- [25] J. Zhang et al, cond-mat/0406085.
- [26] E.R.I. Abraham et al., *Phys. Rev. Lett.* **74**, 1315 (1995).
- [27] E.v. Kempen et al., *Phys. Rev. Lett.* **88**, 093201 (2002).
- [28] B. Marcelis et al., *Phys. Rev. A* **70**, 012701 (2004).
- [29] S. De Palo et al, cond-mat/0404672.
- [30] D.S. Petrov, cond-mat/0404036.
- [31] L. Viverit, *Phys. Rev. A* **66**, 023605 (2002).
- [32] M. Mackie et al., *Phys. Rev. A* **69**, 053614 (2004).
- [33] D.S. Petrov, C. Salomon, and G.V. Shlyapnikov, cond-mat/0309010.

Summary

The research described in this thesis is part of an international effort with the aim of studying ultracold quantum degenerate gas samples like Bose-Einstein condensates and Fermi degenerate systems, consisting of atoms confined in magnetic or optical traps. The behavior of such samples is governed by the inter-atomic interactions and the resulting properties of the atom-atom scattering. At the relevant temperatures of 1nK to 10 μ K a key property is the atom-atom scattering length a .

In chapter 2 a theoretical method is presented which enables one to describe the interaction and scattering of (ultra)cold atoms to unprecedented precision. It is also unparalleled in comprehensiveness: it allows the prediction of a large and varied set of experimental data for all isotopes of the same element. The method relies on the extraction from experiments of a few (phase) parameters which completely summarize the behavior of the atoms in the (ultra)cold regime. In chapter 3 the method is applied to the “workhorses” of cold-atom physics: the atomic species ^{85}Rb and ^{87}Rb . We extract the foregoing parameters to a very high precision from several recent high precision experiments, allowing us to predict e.g. the ^{87}Rb spinor condensate to be ferromagnetic: a prediction for which the scattering length has to be calculated with a precision better than 1%. We also predict Feshbach resonances at experimentally accessible magnetic field strengths; resonances searched for and found by the experimental group of Rempe. In close collaboration with his group we “fine-tune” the interaction parameters found previously, by making use of only one of the observed resonances. We then obtain agreement with 42 out of the observed 43 resonance field strengths and are able to identify bound states inducing the Feshbach resonances at these locations. Chapter 4 describes the results of this research.

With a thorough understanding of the rubidium interactions, we then switch to lithium which has a fermionic (^6Li) and a bosonic (^7Li) isotope. Both are being used in cold-atom experiments. In chapter 5 we evaluate the interaction parameters for lithium allowing us to predict magnetic field strengths for which a sample of fermionic ^6Li atoms can be regarded as strongly interacting. Furthermore, a three-level method for measuring mean-field shifts, based on radio-frequency techniques, is introduced. For weak interactions we find proportionality of resonance shifts to interaction strengths. In the strongly interacting regime, however, these shifts become very small reflecting the quantum unitarity limit and many-body effects. Most interesting is the fact that in this regime the shifts are small both for large positive a and for large negative a , likely reflecting the universality of the interaction energy.

In chapters 6 and 7 the interactions between lithium atoms are reinvestigated, making use of newly available experimental data and with the updated interaction parameters special attention is paid to locating field strengths at which magnetically tunable Feshbach resonances occur in the scattering of lithium atoms. In chapter 6 scattering events in a gas of (fermionic) ${}^6\text{Li}$ atoms are studied. In chapter 7 we show that a consistent description of the ${}^6\text{Li}+{}^6\text{Li}$ system can be given. We discuss theoretical uncertainties for the position of the wide ${}^6\text{Li}$ Feshbach resonance and present an analytic scattering model for this resonance, based on the inclusion of a field-dependent virtual open-channel state. We predict new Feshbach resonances for the ${}^6\text{Li}-{}^7\text{Li}$ system, and their importance for different types of crossover superfluidity models is discussed. Molecules created by magnetically sweeping over these resonances will have a fermionic character. One magnetic field strength is predicted at which two different fermionic molecules can be created simultaneously.

Samenvatting

Het werk beschreven in dit proefschrift maakt deel uit van een internationale inspanning, gericht op het bestuderen van ultrakoude gedegenereerde quantumgassen, zoals Bose-Einstein condensaten en Fermi gedegenereerde gassen, bestaande uit atomen opgesloten in een magnetische of optische val. Het gedrag van zo'n gaswolkje wordt bepaald door de interatomaire interacties en de daaruit voortvloeiende atoom-atoom verstrooiings-eigenschappen. Bij de in dit proefschrift relevante temperaturen (1nK tot $10\mu\text{K}$) treedt één van die eigenschappen sterk op de voorgrond: de verstrooiingslengte a .

In hoofdstuk 2 wordt een theoretische methode gepresenteerd die ons in staat stelt de verstrooiings-eigenschappen van (ultra)koude atomen met een ongekennde precisie te beschrijven. De methode is ook ongeëvenaard wat betreft het toepassingsgebied: op basis ervan kan een grote en gevarieerde verzameling experimentele gegevens voorspeld worden voor alle isotopen van hetzelfde element. De methode is gebaseerd op het samenvatten van het interatomair gedrag in het ultrakoude regime met slechts een paar (fase-)parameters. In hoofdstuk 3 passen we de methode toe op het “werkpaard” van de koude-atomen fysica: de atomen ^{85}Rb en ^{87}Rb . We bepalen de bovengenoemde parameters met een zeer grote nauwkeurigheid uit een aantal recente hoge-precisie experimenten. Hierdoor zijn we bijvoorbeeld in staat om te voorspellen dat het gedrag van een ^{87}Rb “spinor” condensaat ferromagnetisch zal zijn: een voorspelling waarvoor de verstrooiingslengte met een precisie van ten minste 1% berekend dient te worden. Tevens voorspellen we Feshbach resonanties bij magnetische veldsterkten die experimenteel realiseerbaar zijn; resonanties die na zoekwerk ook zijn waargenomen door de experimentele groep van Rempé. In een nauw samenwerkingsverband met zijn groep hebben we de eerder bepaalde interactie parameters onderworpen aan een fijnafstemming, door gebruik te maken van (slechts) één van de waargenomen resonanties. Na deze fijnafstemming komt onze theorie goed overeen met de experimenten, waardoor we voor 42 van de 43 resonantie veldsterkten in staat waren om de gebonden toestand te kunnen identificeren die de resonantie veroorzaakt. Hoofdstuk 4 beschrijft de resultaten van dit onderzoek.

Met een gedegen begrip van de rubidium interacties concentreren we ons vervolgens op lithium, waarvan een fermionische (^6Li) en een bosonische (^7Li) isotoop bestaat. Beide worden gebruikt in de experimentele koude-atomen fysica. In hoofdstuk 5 evalueren we de interactie parameters van lithium, waardoor we in staat zijn om te voorspellen voor welke magnetische veldsterkten we een gaswolkje ^6Li atomen

kunnen beschouwen als sterk wisselwerkend. Daarnaast introduceren we een, op rf-techniek gebaseerde, drie-niveau methode om “mean-field” verschuivingen te meten. Voor zwakke interacties vinden we proportionaliteit van de resonantie verschuiving met de sterkte van de wisselwerking. In het regime van de sterke wisselwerking, daarentegen, worden deze verschuivingen zeer klein, hetgeen een signaal is van de unitariteits limiet en van veel-deeltjes effecten. Zeer interessant is dat de verschuivingen klein zijn voor zowel zeer grote positieve a als voor zeer grote negatieve a , hetgeen waarschijnlijk een weerspiegeling is van de universaliteit van de interactie energie.

In de hoofdstukken 6 en 7 worden de interacties tussen lithium atomen nogmaals onder de loep genomen, waarbij we gebruik maken van recenter beschikbaar gekomen experimentele data. Met een volledig aangepaste set parameters zoeken we veldsterkten waarbij Feshbach resonanties optreden bij de verstrooiing van lithium atomen. In hoofdstuk 6 bestuderen we verstrooiings-verschijnselen in een gaswolkje van (fermionische) ${}^6\text{Li}$ atomen. In hoofdstuk 7 laten we zien dat het mogelijk is een consistente beschrijving te geven van het ${}^6\text{Li}+{}^6\text{Li}$ systeem. We beschouwen de theoretische onzekerheid in de positie van de brede ${}^6\text{Li}$ Feshbach resonantie. Tevens presenteren we een analytisch verstrooiingsmodel voor deze resonantie, gebaseerd op het meenemen van een veld-afhankelijke virtuele toestand in het open kanaal. We voorspellen nieuwe Feshbach resonanties in het ${}^6\text{Li}+{}^7\text{Li}$ systeem en beschouwen het belang hiervan voor de verschillende typen van “crossover” fysica. Fermionische moleculen kunnen worden gemaakt door het magnetische veld te variëren over een bereik waarbij een Feshbach resonantie wordt gepasseerd. We voorspellen één resonantie veldsterkte waarbij het mogelijk is om simultaan twee verschillende fermionische moleculen te maken.

Dankwoord

Graag wil ik tot slot een aantal mensen noemen die een enorme steun zijn geweest bij de totstandkoming van dit proefschrift. Allereerst natuurlijk Boudewijn Verhaar voor de enthousiaste en stimulerende begeleiding. Ook mijn tweede promotor Herman Beijerinck wil ik bedanken voor de stimulerende begeleiding en copromotor Servaas Kokkelmans voor de prettige samenwerking.

Binnen de vakgroep AQT wil ik iedereen dank zeggen voor de plezierige contacten gedurende de promotie en bij de theoretische groep wil ik Leon, Johan, Maikel en Bout bedanken voor de gezellige tijd. Bij de experimentele groep gaat mijn dank uit naar Edgar Vredenburg die de gave heeft om problemen met apparatuur in het lab te verhelpen door ernaast te gaan staan en er enkel naar te kijken. Ik ben ook Frank, Jan-Pieter en Karin erkentelijk voor hun hulp bij het experimentele deel van mijn promotie. Louis van Moll en Jolanda van de Ven mogen natuurlijk ook niet onvermeld blijven, vanwege hun inventieve hulp bij het aanpassen van de opstelling. Alle waardering heb ik voor Rina Boom. Haar hulp bij het afhandelen van de nodige bureaucratische rompslomp was onmisbaar. De collega promovendi van AQT wil ik bedanken voor de goede sfeer en fijne tijd. Kenian, Maarten, Bert, Bart, Veronique, Bout, Edwin, Gabriel, Alquin, Paul en Simon: Bedankt! And of course the Australian guys, Colin, Luke, Lincoln, Rob and Jonathan: Thanks!

I would also like to thank W. Ketterle, C. Salomon and the members of their research groups for the nice and fruitful collaborations. Also thanks go out to D. Heinzen for the collaboration we had. I am grateful to G. Rempe and the members of his research group, especially Andreas Marte and Stephan Dürr, for contributions to our combined projects.

Phil Gould and Ed Eyster I would like to thank for their hospitality and for giving me the chance to work in their lab at the University of Connecticut. Also the fellow students at UConn I wish to thank for making the work and stay in Storrs an enjoyable experience. Dave, Marco, Han, Erin: Thanks! Court and Andrea, I am also grateful to you for a great time in Storrs.

Tenslotte wil ik ook nog mijn ouders en de rest van mijn familie danken voor alle steun die ik altijd van hen heb mogen ontvangen.

Curriculum Vitae

8 november 1975	Geboren te Sittard
1988–1994	Atheneum, Bisschoppelijk College Echt te Echt
1994–2002	Studie Technische Natuurkunde, Technische Universiteit Eindhoven
2002–2006	Promotieonderzoek, groep Atoomfysica en Quantum Technologie, Faculteit Technische Natuurkunde, Technische Universiteit Eindhoven
juli 2005–nov 2005	Werkbezoek University of Connecticut (UConn) Storrs, CT, USA